Summer 7-10-2019

INTRATYPIC GENETIC VARIABILITY OF HUMAN ADENOVIRUS TYPE 4: IMPLICATION FOR VIRAL PATHOGENESIS

Camden Roy Bair
University of New Mexico

Camden R Bair
Candidate

Biomedical Sciences
Department

This dissertation is approved, and it is acceptable in quality and form for publication:

Approved by the Dissertation Committee:

Bryce Chackerian, Chairperson

Adriana Kajon

Michelle Ozbun

Diane Lidke

INTRATYPIC GENETIC VARIABILITY OF HUMAN ADENOVIRUS TYPE 4: IMPLICATION FOR VIRAL PATHOGENESIS

by

CAMDEN R BAIR

B.S., Molecular Biology, Brigham Young University, 2012

DISSERTATION

Submitted in Partial Fulfillment of the
Requirements for the Degree of

Doctor of Philosophy
Biomedical Sciences

The University of New Mexico
Albuquerque, New Mexico

July 2019

Acknowledgements

I would like to acknowledge and thank the many people who helped me during this journey. First, to my adviser Adriana Kajon, thank you for the opportunity to study and work in your laboratory. I have learned many things from my time spent in your laboratory, the most important being hard work and dedication. Thank you for providing a wonderful experience to learn and grow. Finally, thank you for caring about me as person, and not just as an employee.

To the members of my dissertation Committee on Studies, Bryce Chackerian, Michelle Ozbun, and Diane Lidke, thank you all for holding me to a high standard and always expecting the best out of me. Most especially, thank you for the encouraging words during the many difficult times. Those conversations motivated me to persevere.

To the members of the Kajon laboratory, both past and present, including Susan Core, Amanda Snider, Megan Sartain, Ulrike Galasinski, and Anjie Lewis thank you for your support and help with my projects. Most especially, thank you Poornima Kotha for the many times you sat down with me to plan experiments, troubleshoot, or just listened when things were not going my way. Thank you for your generosity and all that you taught me.

I want to acknowledge our wonderful collaborators and others who supported my graduate studies: Jorge Blanco and his team (Sigmovir Biosystems Inc.) and Bojana Rodic-Polic (Diasorin Molecular LLC) for their contribution of the animal studies; Gabriel Gonzalez, Michael Carr, and Hidemi Watanabe for the collaboration in the genomics studies; and other investigators

at Lovelace Respiratory Research Institute including Steven Belinsky, Carmen Tellez, Yong Lin, Yohannes Tesfaigzi, Marc Wathelet, and Julie Hutt for provided reagents or advice in my experiments. I also want to thank the administration at Lovelace Respiratory Research Institute for supporting my graduate studies at the institute.

I would like to thank my parents and my family. I know you may not have always understood what I was doing, but you were always patient and encouraging during my explanations of my research and always wanted the best for me and my family.

To my children, who didn't like it when I stayed late at work some nights or went on too many trips, thank you for always being ready with a big hug when I came home.

To my best friend and wife, Etta, thank you for sticking with me until the end. Thank you for the constant encouragement, love, and a good kick in the pants when I needed it. Thank you for humoring me while I told you about the progress of my research and for always being there for me, through the good and bad. And most especially, thank you for answering all my math questions, because math is hard.

And finally, thank you to God, for blessing my family and me so much.

Intratypic Genetic Variability of Human Adenovirus Type 4: Implications for Viral Pathogenesis

by

Camden R Bair

B.S., Molecular Biology, Brigham Young University, USA, 2012

Ph.D., Biomedical Sciences, University of New Mexico, USA, 2019

ABSTRACT

Human adenovirus type 4 (HAdV-E4) is a causative agent of acute respiratory disease and conjunctivitis worldwide. Two major lineages of HAdV-E4 genomic variants have been identified by their distinct BamHI restriction profiles: prototype-like (p-like) strains and the a-like genomic variants. Recent molecular epidemiology studies have shown a predominance of a-like genomic variants detected in association with disease which suggests a-like strains have a fitness advantage or they may be more pathogenic. The impact of HAdV-E4 intratypic genetic variability on *in vitro* and *in vivo* phenotypes relevant to pathogenesis is a major gap in knowledge. I hypothesize that HAdV-E4 comprises two distinct evolutionary lineages that differ in their *in vitro* growth and *in vivo* pathogenetic phenotypes. Whole genome sequences (WGS) from 45 HAdV-E4 strains isolated

between 1953 and 2015 clustered into two phylogroups: phylogroup I (PG I) includes the p-like strains and phylogroup II (PG II) comprises the a-like variants. Bioinformatics analysis of WGS identified divergence at multiple genomic loci that may contribute to differences in *in vitro* and *in vivo* pathogenic phenotypes. In cell culture, PG I strains formed larger plaques, exhibited an enhanced cell killing phenotype, and replicated faster compared to PG II strains. Interestingly, infection with a PG II strain resulted in more severe pulmonary pathology in a cotton rat model of HAdV respiratory infection. The results of this study set the foundation for future efforts to elucidate the molecular basis of HAdV-E4 pathogenesis by comparing these *in vitro* and *in vivo* phenotypes using isogenic mutant viruses.

Table of Contents

List of Figures

List of Tables

Chapter 1 – Introduction

1.1 Adenoviruses

Adenoviruses (AdVs) are nonenveloped double-stranded DNA viruses that infect vertebrates. AdVs were first isolated independently by two groups in 1953 and 1954: Rowe and colleagues isolated AdV while attempting to culture adenoids and Hilleman and Werner isolated AdV from a throat washing from a military recruit presenting with acute respiratory disease (ARD) (1, 2).

Human adenovirus (HAdV) infections are associated with a wide variety of diseases among immunocompetent individuals including respiratory disease, ocular disease, and gastrointestinal disease (3). Among immunocompromised individuals, infections can result in renal, myocardial, hepatic, and disseminated disease (3). The more than 60 years of AdV research have contributed to numerous fundamental discoveries of basic biology, including the discovery of mRNA splicing (4, 5). The extensive knowledge of the biology of AdVs has also aided in the development of AdVs as gene delivery tools, platforms for numerous vaccines (including the ChAd3-EBO-Z vaccine against Ebola (6–8), currently in phase I clinical trials in the United States (https://clinicaltrials.gov/ct2/show/NCT03583606?term=chad3-ebo-z&rank=2)), as well as oncolytic agents (9).

1.2 Taxonomy

Adenoviruses belong to Family *Adenoviridae* which currently comprises five genera accepted by the International Committee on Taxonomy of Viruses

(ICTV): *Atadenovirus*, *Aviadenovirus*, *Ichtadenovirus*, *Mastadenovirus*, and *Siadenovirus*. AdVs isolated from mammals belong to the genus M*astadenovirus* or *Atadenovirus*. AdVs that infect birds are classified within the genus *Atadenovirus*, *Aviadenovirus*, or *Siadenovirus*. AdVs that infect reptiles are classified in the genus *Atadenovirus* or *Siadenovirus*. Finally, only one AdV has been isolated from a fish and is classified in the genus *Ichtadenovirus* (10, 11).

The ICTV recognizes 45 species classified within genus *Mastadenovirus*. The known human AdVs (HAdVs) are classified into seven species, designated *Human mastadenovirus* A to G (HAdV-A to HAdV-G) (10, 12). While the ICTV is charged with the responsibility of classifying viruses on the species level, further classification including naming and assigning strains to an existing species is accomplished by the research community by peer review (https://talk.ictvonline.org/taxonomy/w/ictv-taxonomy) (13). Originally, 51 serotypes were identified based on serological criteria including virus neutralization (VN) against reference hyperimmune animal sera and hemagglutination inhibition (HI) assays (14–17). Molecular typing using restriction fragment length polymorphism (RFLP) analysis facilitated the rapid identification and characterization of intratypic genetic variability. While this method continues to be used today, the advent of whole genome sequencing has allowed greater resolution of genomic data at a relatively inexpensive cost. Whole genome sequencing is used to identify differences in intratypic variants, and is now commonly used to identify and characterize new genotypes (18). Genotyping has replaced serotyping in the identification of novel AdVs as VN and

HI have become increasingly uncommon. Whole genome sequencing provides an affordable and reliable method to accurately characterize novel AdVs. Criteria for describing a novel HAdV genotype include phylogenetic analysis of the genome sequence with particular emphasis on the identity of the penton base, hexon, and fiber genes. Recombinant AdVs are also classified as new genotypes as long as sufficient genomic, biological, or pathological differences are demonstrated when compared to related genotypes (18, 19). The HAdV Working Group was formed to establish the criteria for the characterization and naming of novel HAdVs. In addition, they also help coordinate naming of new genotypes to reduce confusion in the literature. This group works with the National Center for Biotechnology Information and is composed of a committee of researchers with expertise in AdV typing (18). Under the new typing system, 35 additional genotypes (HAdV-D53 to HAdV-D90) were described and recognized by the HAdV research community between 2007 and 2018. The reported genotypes are listed in Table 1 (20). The genotype designations include “HAdV-“ followed by the letter referring to the species and their genotype number. As an example, genotype 1 from species *Human mastadenovirus* C is designated as “HAdV-C1”. To avoid confusion, each genotype is assigned a unique sequential number, so there will be not be “HAdV-C1” and an “HAdV-D1”. The complete genome sequences of all types, including the original 51 serotypes are publicly available for reference in the GenBank database (12). Despite the establishment of the HAdV Working Group (18), debate regarding the criteria used to designate new types continues (21, 22).

Table 1: Taxonomy and Tropism of HAdVs

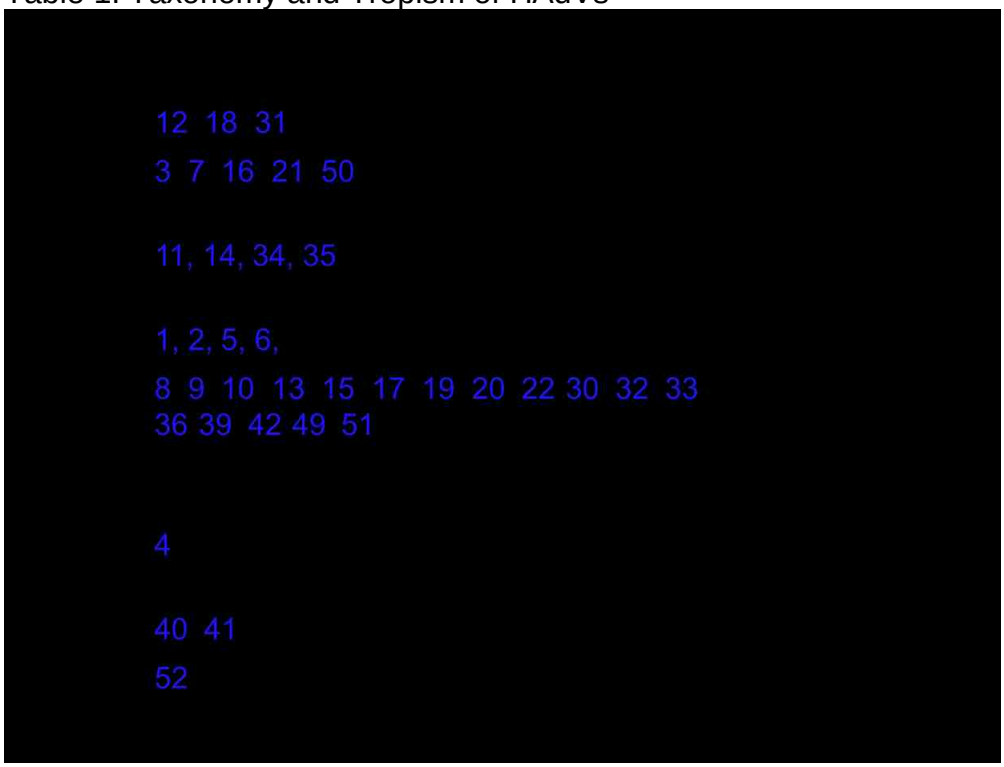

1.3 Structure

HAdVs are nonenveloped viruses with an icosahedral capsid symmetry. The capsid is formed from 240 hexon capsomers and 12 penton capsomers with a pseudo T = 25 triangulation number (23, 24). A trimeric fiber protrusion is associated with each penton base with an approximate length of 300 Å (25). Most AdVs encode a single fiber with the notable exceptions of members of HAdV-F, HAdV-G, as well as some simian, fowl, and lizard AdVs which encode two fibers (26–32). The capsid is also composed of four minor capsid proteins: IIIa, VI, VIII, and IX. Proteins V, VII, IVa2, μ, terminal protein (TP), and protease are packaged with the viral genome (23, 25). The virions have an average diameter of 950Å (25).

1.4 Genome Organization of Adenoviruses

AdVs have a linear double-stranded DNA genome that varies in size depending on the species (11). The HAdV genome is approximately 34 kb to 36 kb in length (11). The genome organization varies significantly among the different AdV genera, especially in genes thought to be genus-specific, namely those in early region 1 (E1), early region 3 (E3), and early region 4 (E4) (11). A genome organizational map for HAdV is shown in Figure 1. All AdVs have inverted terminal repeats (ITRs) on the extreme termini of the genome which are important for DNA duplication (11). The expression of genes encoded in the AdV genome is temporarily regulated in three major phases: early, intermediate, and late. The general functions of HAdV-encoded genes are listed in Table 2.

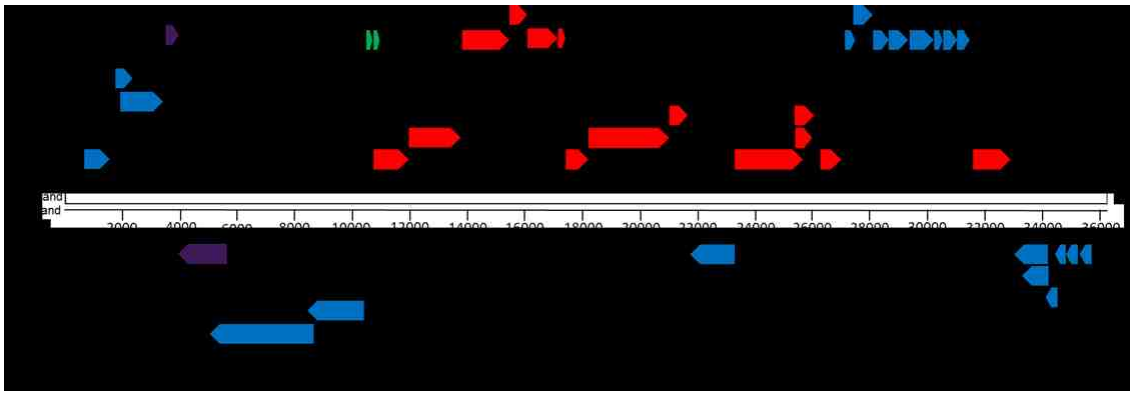

Figure 1: **Genome organization of HAdV-E4**
The 36 kb double stranded genome of HAdV-E4 encodes 13 temporally regulated transcriptional units: early (blue), intermediate (purple), and late (red). L1-L5 comprise the major late transcriptional unit. Forward and reverse arrows indicate transcriptional units encoded on the right (R) or left (L) strands, respectively. The locations and sizes of the CDS for each transcriptional unit are approximate. The noncoding virus-associated (VA) RNAs are shown in green. Adapted from Akusjarvi G, 2008 (33).

Table 2: AdV Gene Products and Functions

Transcriptional Unit	Protein Products	Temporal Expression	General Function and Notes
E1A	Large E1A Small E1A	Early	Activation of S phase, early transcription
E1B	19K, 55K	Early	Inhibition of apoptosis
E2A	DBP	Early/late	Replication
E2B	Pol, pTP,	Early/late	Replication
E3	Various	Early/late	Modulation of the host immune response to infection
E4	ORF1, ORF2, ORF3, ORF 4, ORF 5, ORF6/7	Early	Various functions including inhibition of interferon response, inhibition of DNA Damage response, and induction of apoptosis
IX	IX	Intermediate	Structural protein
IVa2	IVa2	Intermediate	Structural protein, stimulates late transcription
Major Late	L1-L5	Late	Structural Proteins, 14 total protein products

1.5 The Adenovirus Life Cycle

The adenovirus life cycle has been most extensively studied for members of HAdV-C. The life cycle is divided roughly into two phases: early and late. The early phase comprises events that prepare the cellular environment for viral DNA replication following entry of the virus into the cell. The late phase includes viral DNA duplication, expression of structural proteins, assembly of virions, and viral progeny egress from the infected cell. Some HAdV protein products are also produced at intermediate times as noted in Table 2. Figure 2 represents the highlights of the adenovirus replication cycle, which is summarized in sections 1.5.1 and 1.5.2.

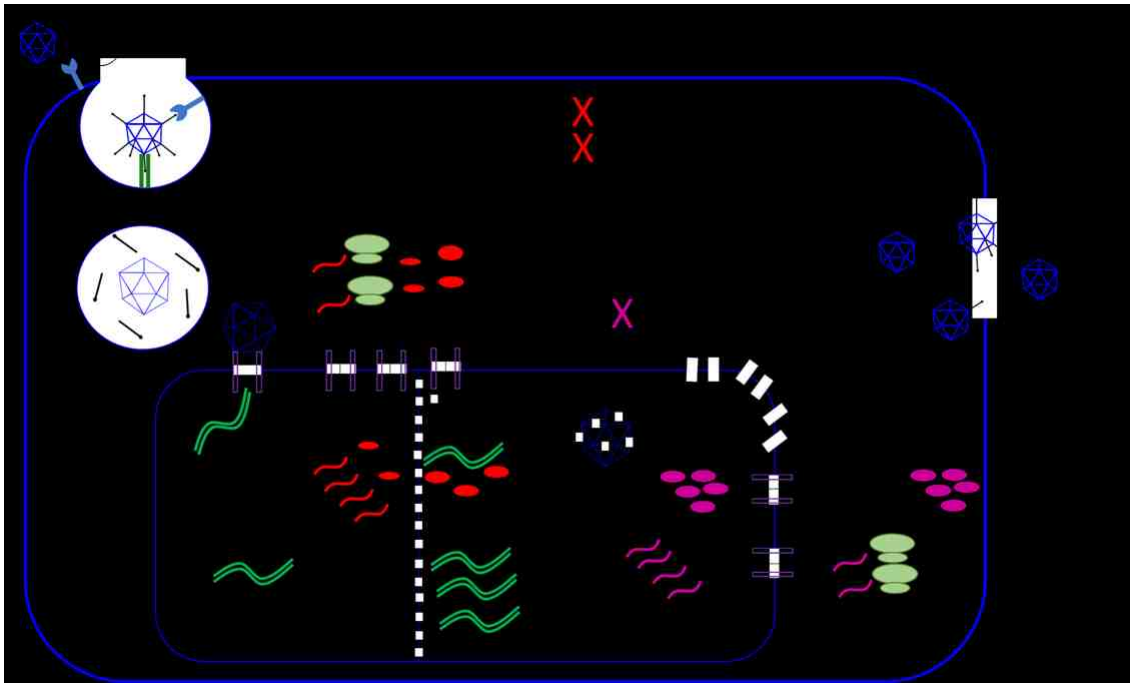

Figure 2: **Summary of the adenovirus Life Cycle**
The adenovirus life cycle is divided into two major phases: early and late. Viral attachment is mediated by a cellular host receptor (1) followed by clathrin-mediated endocytosis. (2). The viral particle undergoes partial disassembly before escaping into the cytosol (3) where it traffics to the nuclear pore complex via the microtubule network (4). The viral genome is released into the nucleus and transcription of the E1 genes commences (5). E1 transcripts are translated (6) and transported into the nucleus where they act as transactivators to assist in driving the expression of other early genes (7). Early gene products have many functions including modulating apoptosis and the host response to infection. Some early gene proteins are transported into the nucleus where they assist in replication of the viral genome using a strand displacement mechanism (9). During viral DNA replication, the major late promoter is activated which drives the expression of all late genes (10). The virus shuts down host cell translation at late times post infection (11). The majority of the late viral transcripts encode structural proteins which are shuttled into the nucleus where viral assembly occurs (12). Progeny virions escape the cell using a lytic mechanism.

1.5.1 Early phase

Viral attachment and entry into the cell is mediated by several different HAdV species-specific surface receptors. The coxsackie and adenovirus receptor (CAR) is used by species A, C, D, E, and F, while CD46 and desmoglein-2 are

used by species B. Studies have demonstrated that some members of HAdV-D have a low affinity for CAR and instead may use sialic acid. Scavenger receptors on Kupffer cells have also been shown to mediate HAdV attachment (34). Interaction between the RGD motif of the HAdV penton base and cellular integrins, including α3β1, α5β1, α_vβ1, and α_vβ1, facilitates receptor-mediated endocytosis in clathrin-coated vesicles (35, 36), and pH changes in the early endosome facilitates partial disassembly of the virion. Protein VI aids in rupture of the endosome and subsequent release of the virion in to the cytoplasm (37). The virion is then transported to the nucleus via dynein motor proteins on the microtubules (38). The viral DNA is then imported into the nucleus (39).

The E1A transcription unit encodes two major proteins which are the first viral protein products detected in infected cells. E1A proteins have two major functions: to stimulate the host cell into S phase (40), and to stimulate the expression of other HAdV early genes (41, 42). E1A transcripts are alternatively spliced into two major mRNAs that give rise to the large and small E1A proteins (43). The large E1A protein has four distinct regions of conservation (CR1 through CR4) shared among all HAdV species (44). The small E1A protein only includes CR1, CR2, and CR4 (see Figure 3). Both the large and small E1A proteins are sufficient to push the cell into S phase through interactions between the CR1 and CR2 regions and the retinoblastoma protein (RB), the p300/CREB-binding protein (CBP) complex, and the RB-like proteins p107 and p130 (45, 46). Stimulation of S phase (particularly the inactivation of RB through interaction with E1A) induces apoptosis (47).

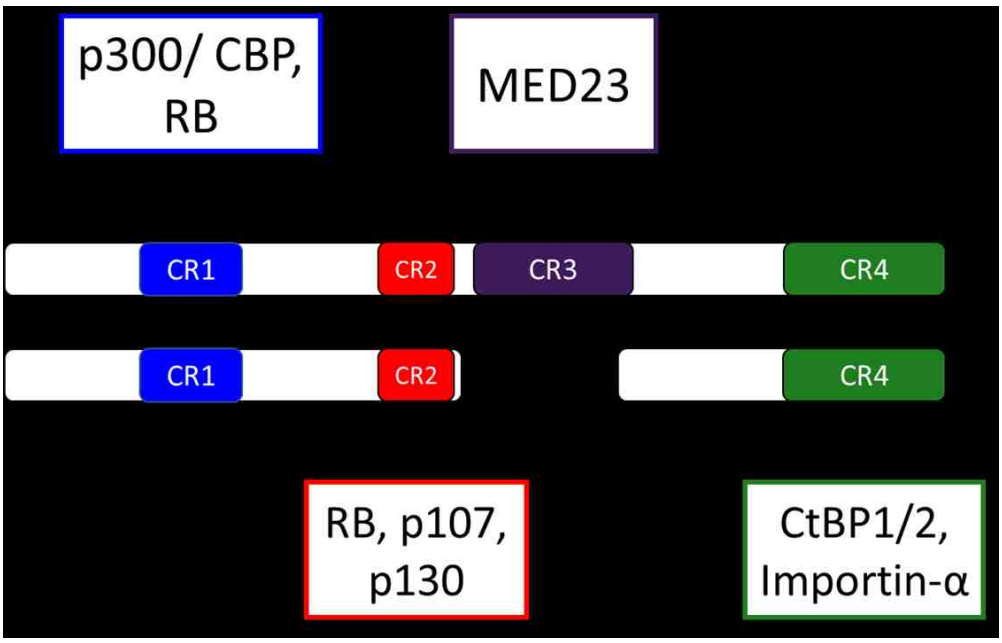

Figure 3: **E1A conserved regions and protein-protein interactions**
The E1A transcript is alternatively spiced into two major protein products: large and small E1A proteins (above and below, respectively). E1A proteins have four conserved regions (CR1 through CR4) that interact with a number of cellular proteins to both push the cell into S phase and active viral early gene transcription. The major interacting proteins are listed.

The E1B transcriptional unit encodes two polypeptides, E1B 19K and E1B 55K, which are translated from two different initiation codons in different reading frames (48). Both proteins serve important functions in blocking p53-dependent induction of apoptosis through different mechanisms. E1B 19K, a BCL2 homolog, stabilizes the proapoptotic cellular proteins BAK and BAX. During apoptosis, BAK and BAX form high molecular weight pore complexes imbedded in the mitochondrial membrane and allow the release of cytochrome C and SMAC/DIABLO (49). E1B 19K prevents the oligomerization of BAK and BAX, thus preventing apoptosis (50). On the other hand, E1B 55K stabilizes p53 and

the E1B 55K/E4 ORF6 complex recruits cellular E3 ubiquitin ligase components and selectively degrades p53, Mre11, DNA ligase IV, and other cellular components (45, 51–53). The E1B proteins also perform other functions such as suppressing the interferon (IFN) response and transporting viral mRNAs to the cytoplasm at late times during infection (54, 55).

The larger E1A protein stimulates expression of the other early viral genes between 10 and 100 fold though interaction with MED23 and other cellular transcription factors, which confers tight control of viral gene expression (46, 56, 57). The early region 2 (E2) gene products encode the viral DNA-dependent DNA polymerase (pol), preterminal protein (pTP, which is later proteolytically cleaved to TP), and the DNA binding protein (DBP), all necessary for viral DNA replication. The E4 transcriptional unit encodes several alternatively spliced mRNAs that code for 6 unique proteins which have a variety of functions including inhibition of the IFN and double stranded break repair responses (58).

The E3 transcriptional unit encodes species-specific repertoires of open reading frames (ORFs) encoding between five and nine proteins (59), and is dispensable for viral replication *in vitro* (60). The organization of E3 for the different HAdV species is shown in Figure 4. The species B,C,D, and E-specific E3 gp/19K protein interacts with the MHC class I molecules in the endoplasmic reticulum (ER) and prevents their translocation to the cell surface, interfering with antigen presentation (61). This function greatly reduces the pulmonary inflammatory response to HAdV infection in cotton rats (62). The membrane proteins RIDα and RIDβ are conserved among the HAdV species and work

together to downregulate cell surface expression of CD95 (Fas receptor) (63–65). The cytosolic 14.7K protein, which is also conserved among all HAdV members, functions to protect cells from TNF-mediated lysis (66, 67). Each HAdV species encodes two to four E3 CR1 ORFs (CDD: pfam02440) which encode nonstructural membrane glycoproteins of variable size. These proteins share some homology with the RL11 family of proteins encoded by human cytomegalovirus (68). The most extensively studied E3 CR1 protein, HAdV-C adenovirus death protein (ADP), is expressed at late time points post infection and facilitates efficient viral progeny release (69). In contrast, the E3 CR1 ORF located in the same region as ADP in the genomes of members of HAdV-D encodes a 49 kDa protein which is secreted and interacts with CD45 on lymphocytes and modulates their function (70). Martinez-Martin and colleagues recently used an extracellular protein microarray to screen for cellular protein-protein interactions with the ectodomain of HAdV E3 CR1 proteins from all species. Several candidate interactors were described (71), and future work is needed to validate these interactions during infection.

The ~150-200 nucleotide noncoding virus-associated RNA (VA RNA) transcripts VA RNAI and VA RNAII start to accumulate at early times post infection (72) and form highly structured RNAs (73). RNA polymerase III (Pol III) transcribes these RNAs under the control of a highly conserved internal Pol III promoter consisting of the promoter elements A and B (74). These transcripts function to suppress protein kinase R (PKR) activation by acting as competitive

substrates. In addition, they suppress RNAi by saturating the DICER complex (75).

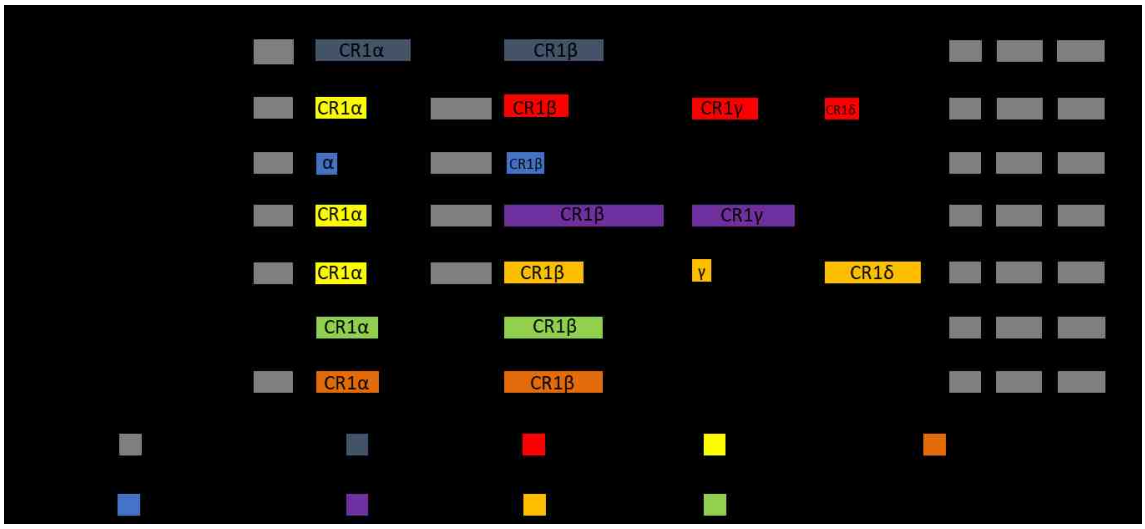

Figure 4: **Organization of E3 among the different HAdV species**
E3 Open reading frames (ORFs) are represented by boxes and aligned based on homology and location in the genome. Space between ORFs is not indicative of the untranslated region between ORFs. The ORFs for HAdV-E4 are based on the CL68578 sequence (AY487947). Adapted from Burgert and Blusch (59).

1.5.2 Late phase

The late phase of infection in hallmarked by DNA duplication and high activity levels of the major late promoter (MLP), which drives expression of the late genes. Viral DNA replication is facilitated by three viral proteins: pol, TP and DBP. Several cellular proteins also aid in DNA replication including NFI, NFIII, and OCT1. TP is covalently attached to the 5' end of AdV DNA. AdV pol initiates at the 5' end, using TP as a primer, and uses a strand displacement mechanism for duplication. The NFI and NFIII DNA binding motifs in the left hand inverted ITR also greatly enhance initiation for HAdV-C2 and HAdV-C5 (76). Interestingly,

the HAdV type 4 (HAdV-E4) prototype strain RI-67 only carries the NFIII recognition site, and both NFI and NFIII are dispensable for initiation of replication (77, 78). The freed single-stranded DNA molecule then circularizes to form a panhandle using the complementary sequences at the 5' and 3' ITR. This structure is recognized by pol, and synthesis is initiated again using strand displacement, with the result of two linear double-stranded DNA molecules (79).

Viral and cellular RNAs are translated simultaneously during the early phase of infection. In the late phase, however, viral transcripts are translated nearly to the exclusion of all cellular transcripts. This is accomplished by first shutting down host cell translation by dephosphorylation of eIF4E, an important eukaryotic initiation factor that binds to the 5' 7-methyl guanosine cap structure. Phosphorylation is normally accomplished by the cellular Mnk1 kinase which is bound to eIF4G. Mnk1 is displaced by the viral L4-100K protein, and host cell translation stops due to the dephosphorylated state of eIF4E (80, 81). An alternative form of translation is then used to synthesize late viral proteins: ribosome shunting. The 200 nucleotide non-coding tripartite leader (TPL) sequence spliced onto the 5' end of all late viral mRNAs eliminates the need of scanning by the 40s ribosome subunit for the initiator start codon, instead, the ribosome is shunted directly to the initiator start codon directly after the TPL sequence (82, 83).

Progeny virions are assembled in the nucleus. The multifunctional L4-100K protein facilitates folding and trimerization of the hexon subunits and subsequent transport into the nucleus (84). Assembly of pentameric penton

structures and association with trimeric fiber units is accomplished in the cytoplasm and subsequently imported into the nucleus (85, 86). Viral DNA is packaged into capsids, and minor structural proteins are proteolytically processed by the viral protease and incorporated into the virion (24, 25).

Viral progeny release is thought to occur through a lytic mechanism. For the six HAdV-C genotypes, the species-specific E3 protein ADP has been shown to be necessary for efficient release of mature viral particles (69, 87). Mutants lacking ADP produced similar titers of total infectious virus in submerged monolayer cultures *in vitro*. However, titers from cell culture supernatant were lower compared to those of WT-infected cells. Increased lysis of infected cells, dissemination in monolayers, and large plaque sizes are hallmarks of HAdV-C genotypes encoding ADP (69). The mechanism by which ADP functions is still under investigation. However, a yeast two-hybrid screen revealed interactions with MAD2 (88). Aberrant control of apoptosis due to mutations in the E1B 19K coding sequence or low levels of E1B 19K expression can also result in a large plaque phenotype (89, 90). Another mechanism of viral progeny release is thought to be cleavage of cytokeratin 18 by the late region 3 (L3) 23K protease, which has an overall effect of weakening the cytokeratin system and promoting cell lysis (91). Disruption of tight junctions by the PDZ protein-binding complex of E4 ORF1 or free fiber interactions with the tight junction protein CAR might also facilitate viral progeny release in HAdV-C (92, 93).

1.6 Diseases Associated with Human Adenovirus Infection

HAdVs are ubiquitous pathogens that are associated with a wide variety of diseases (3, 94). Causative agents of respiratory disease of variable severity include members of species HAdV-B, HAdV-C, and HAdV-E. Infections with HAdV-B, HAdV-D and HAdV-E strains have been associated with ocular disease, such as conjunctivitis. The more severe keratoconjunctivitis is specifically associated with infections by HAdV-D types 8, 19, and 37 (94, 95), and to a lesser extent by HAdV-E4 (96, 97). Infection of the gastrointestinal (GI) tract has been noted for members of HAdV-A, HAdV-D, HAdV-F, and HAdV-G (3, 94). Immunocompromised individuals, such as transplant recipients, patients receiving chemotherapy, or HIV-positive patients, are more susceptible to HAdV infections (98). Additionally, persistence in the GI tract has been described for most species (99, 100).

Adenovirus tropism is dependent on structural proteins, most importantly, the fiber protein (34, 36). As shown above, viruses from different species can have similar tropisms, even while using different receptors for attachment and entry. Retargeting AdV viral vectors by manipulating the hexon, penton, fiber, and pIX proteins can successfully alter tropism (101).

1.7 Animal Models of Acute Viral Pathogenesis

There are no suitable animal models of HAdV respiratory infection that recapitulate the full spectrum of virus-host interactions underlying human disease. Early attempts to develop an animal model began shortly after the initial

discovery of HAdV, although the animals tested, including mice, guinea pigs, hamsters, rabbits, and rhesus macaques, did not develop clinical symptoms (1). Currently, the most widely used small animal models are the mouse (*Mus musculus*), the Syrian hamster (*Mesocrietus auratus*), and the cotton rat (*Sigmodon hispidus*). HAdVs do not replicate in the lungs of intranasally-infected mice, although pneumonia, similar to that seen in humans, is observed (102). Despite these limitations, this model has been extensively used to study the role of early AdV genes in pathogenesis (103). A humanized mouse model has also been developed that recapitulates some features of acute and persistent infections (104).

The Syrian hamster model is almost exclusively used to study oncolytic viruses (105). A recent study observed positive immunohistochemical staining for virus structural proteins in bronchial epithelial cells of immunosuppressed hamsters inoculated intranasally with HAdV-C5 and HAdV-C6. While a higher burden of HAdV-C6 was observed in the lungs of infected animals, the authors did not demonstrate viral replication over time (106). This model has also been used to study the effects of antiviral drugs in respiratory infections (107, 108).

The cotton rat model is semipermissive to HAdV infection with modest viral replication in the lungs (109, 110). Similar to mice, cotton rats develop pneumonia upon infection with HAdV-C (110). This model has been used to study the role of early genes in adenovirus pathogenesis as well (111, 112). The importance of the proteins encoded in E3 was discovered using the cotton rat model. Ginsberg and colleagues observed significantly enhanced pulmonary

pathology in animals infected with a gp/19K knock out (KO) HAdV mutant, showing the importance of this protein in modulating the host response to infection (62). The majority of the studies to date examined pulmonary pathology that resulted from internasal infection with HAdV-C strains. Pacini and colleagues reported recovering the highest viral titers from adult animals infected with HAdV-C types (-C1,-C2,-C5, and HAdV-C6) while recovering very little or no virus from infection with HAdV-B3, HAdV-E4, and HAdV-B7 (109). Further refinement of this model is needed in order to investigate if this model can support infection with other genotypes.

1.8 Human Adenovirus Type 4

HAdV-E4 is unique in that it is the only human member of species *Human mastadenovirus* E (HAdV-E). HAdV-E also includes 12 simian AdVs (SAdV) types based on phylogenetic analysis: SAdV22, SAdV23, SAdV24, SAdV25, SAdV25.2, SAdV 26, SAdV30, SAdV36, SAdV37, SAdV38, SAdV39, and CHAdV-Y25 (113, 114).

It has been proposed that HAdV-E4 is the result of a zoonotic homologous recombination event between a yet unidentified SAdV and HAdV-B16. Bioinformatics analysis revealed HAdV-E4 consists of a “genome chassis” of SAdV26-like genome and loops 1 and 2 of the HAdV-B16 hexon (115). Unlike other HAdV species (12, 116, 117), HAdV-E does not undergo intraspecies homologous recombination as a source for genetic diversity as HAdV-E4 is the only human type in this species.

HAdV-E4 was originally isolated from a throat washing from a military recruit presenting with primary atypical pneumonia at Fort Leonard Wood, Missouri during the winter of 1952-1953 (2). Additional reports detail the leading role of HAdV-E4 as a causative agent of ARD in the military recruit training environment (118). In civilian populations, HAdV-E4 infections are continually associated with ARD (119, 120) as well as pharyngoconjunctival fever (121–123), conjunctivitis (124–127), and pneumonia (128).

HAdV-associated ARD constituted a significant burden among recruits at military training facilities in the United States in the 1950s and 1960s (129, 130). This prompted the development of the enteric coated bivalent live HAdV-E4 and HAdV-B7 vaccine for use only in military recruits (131, 132). The vaccine was tested extensively and shown to reduce ARD associated with HAdV infections (133, 134). Furthermore, a cost-benefit analysis demonstrated the value of vaccination (135). Vaccination protocols were implemented in all military recruits starting in 1971. By 1997, production problems resulted in the discontinuation of vaccination protocols (136). During the lapse in vaccination, continuous outbreaks of HAdV-associated ARD were reported in recruit training centers across the United States (137–141). A new manufacturer commenced production of the vaccine and restoration of vaccination protocols restarted in 2011 resulting in a dramatic reduction in the number of HAdV-associated ARD cases (142, 143).

HAdV-E4 has also shown some promise as a platform for other vaccines. Researchers have developed influenza vaccines based on the HAdV-E4 or

HAdV-B7 backbone with the rationale of vaccinating against both HAdV-E4 or HAdV-B7 and influenza through the enteric route (144, 145).

1.9 Human Adenovirus Type 4 Genetic Variability

RFLP (also referred in the literature as restriction enzyme analysis) has been used since the 1970s to distinguish HAdVs based on their genetic variability (146, 147). Importantly, this technique was able to discriminate genomic variants of a single genotype that were serologically indistinguishable before the widespread use of DNA sequencing (148–150). Two distinct evolutionary lineages of HAdV-E4 genomic variants have been described to the present: one comprising the p-like strains and another comprising the a-like genomic variants (149). Following the isolation of the prototype strain RI-67 (4p) in 1953 (2), other closely related strains (demonstrated by VN and RFLP analysis) were isolated from military recruits (147, 149). Of note, the vaccine strain, CL68578, was isolated in 1963 (131) and has been given the genomic variant designation “4p1”, although this is erroneous as benchtop and *in silico* RFLP analysis shows 4p and 4p1 strains have identical profiles (including the SmaI endonuclease profile, which was the only enzyme thought to produce a distinct profile) (151). The 4p4 genome variant, distinguishable by RFLP analysis using the EcoRI enzyme, was the only p-like strain isolated among unvaccinated recruits between 1997 and 2006 (139). A recent study sequenced a p-like strain from a civilian isolated in 1986 and was found to be of the 4p4 variant (152). The a-like genomic variants are profoundly distinguishable from p-like genomic

variants by RFLP analysis, only sharing ~45-60% percent comigrating restriction fragments (PCRF) (147, 149, 153). Multiple 4a genomic variants have been identified (128, 139, 149). The earliest reported a-like strain was a Chinese isolate from 1965, although information on the isolate is limited (149, 154). After 1965, a-like genomic variants were isolated from patients presenting with both respiratory and ocular disease worldwide (125, 126, 147). Molecular epidemiology studies of HAdV-E4-associated ARD in United States military recruits revealed frequent isolation of a-like genomic variants (139). Furthermore, a predominance of a-like genomic variants were isolated from patients presenting with influenza-like illness in the northeastern United States between 2011 and 2015 (128).

Limited comparative bioinformatics analysis is available for the two lineages of HAdV-E4 genomic variants. Dehghan and colleagues reported two a-like genomic variant WGS to have 95.1% sequence identity to RI-67 strain (115). Divergent regions between the two evolutionary lineages of HAdV-E4 variants map to the ITRs, VA RNAII, as well as the E1 and E3 regions (115, 155, 156).

Both p- and a-like genomic variants are remarkably similar to SAdVs classified within HAdV-E. This observation was originally made by comparison of comigrating fragments using RFLP analysis (147, 149), and later by comparison of whole genome sequences (114, 115, 157). a-like genomic variants were shown to have ~89-90% sequence identity to SAdVs (115) and the p-like strain RI-67 has 91.5% sequence identity to SAdV26.

1.10 Molecular Epidemiology of Human Adenovirus Type 4 Infections

The identification of HAdV-E4 as a causative agent of outbreaks of ARD in military recruits prompted researchers to investigate the epidemiology HAdV-E4 infections in this specific population. Outbreaks were seasonal, with high rates of infection occurring during the cold winter months (peaking in February) and low infection rates in the warm months (129, 158). In a study conducted at Fort Dix, it was found that 80% of military recruits were infected with HAdV-E4 during their basic training. Furthermore, 25% of the infected recruits would develop minor symptoms, and an additional 25% would require hospitalization (129). Many conditions are thought to contribute to the spread of HAdVs in these populations: overcrowding in military barracks, high levels of stress, and the ability of HAdVs to remain viable on surfaces and fomites for long periods of time (159, 160). Implementation of the HAdV-E4 vaccine (in combination with the HAdV-B7 vaccine) in 1971 greatly reduced the burden of HAdV-associated ARD in military training facilities (161).

As discussed previously, a discontinuation of HAdV-E4/B7 vaccination protocols occurred in the United States military between 1997 and 2011. During this lapse in vaccination, reemergence of vaccine-preventable ARD was observed (137–139, 141, 162). A dramatic decline in HAdV-E4-associated ARD cases was observed upon reimplementation of vaccination protocols in 2011 (142, 143). In addition, Broderick and colleagues also found that environmental samples collected at barracks and medical clinics at training facilities after 2011 were routinely negative, compared to 27% of environmental samples testing

positive for HAdV by polymerase chain reaction (PCR) before the 2011 reimplementation of the vaccine (143).

HAdV-E4 outbreaks in civilian populations have also been reported worldwide, although surveillance programs specifically targeting HAdV infections are limited (163, 164). Molecular epidemiology data from recent studies suggest a predominance of a-like strains over p-like strains are currently circulating in association with disease. This was recently highlighted by Kajon and colleagues in a survey of cases of HAdV-E4 respiratory infections in the Northeast United states (128). In this study, only one of the examined strains belonged to the p-like lineage (genetically different from the vaccine strain), while all others were a-like. In a molecular epidemiology study examining 1500 HAdV-E4 isolates from military recruits during the lapse in vaccination (Figure 5), 90% of the isolated strains were found to be a-like (139). The factors that contribute to a-like strains being isolated more frequently than p-like strains in association with disease is unknown.

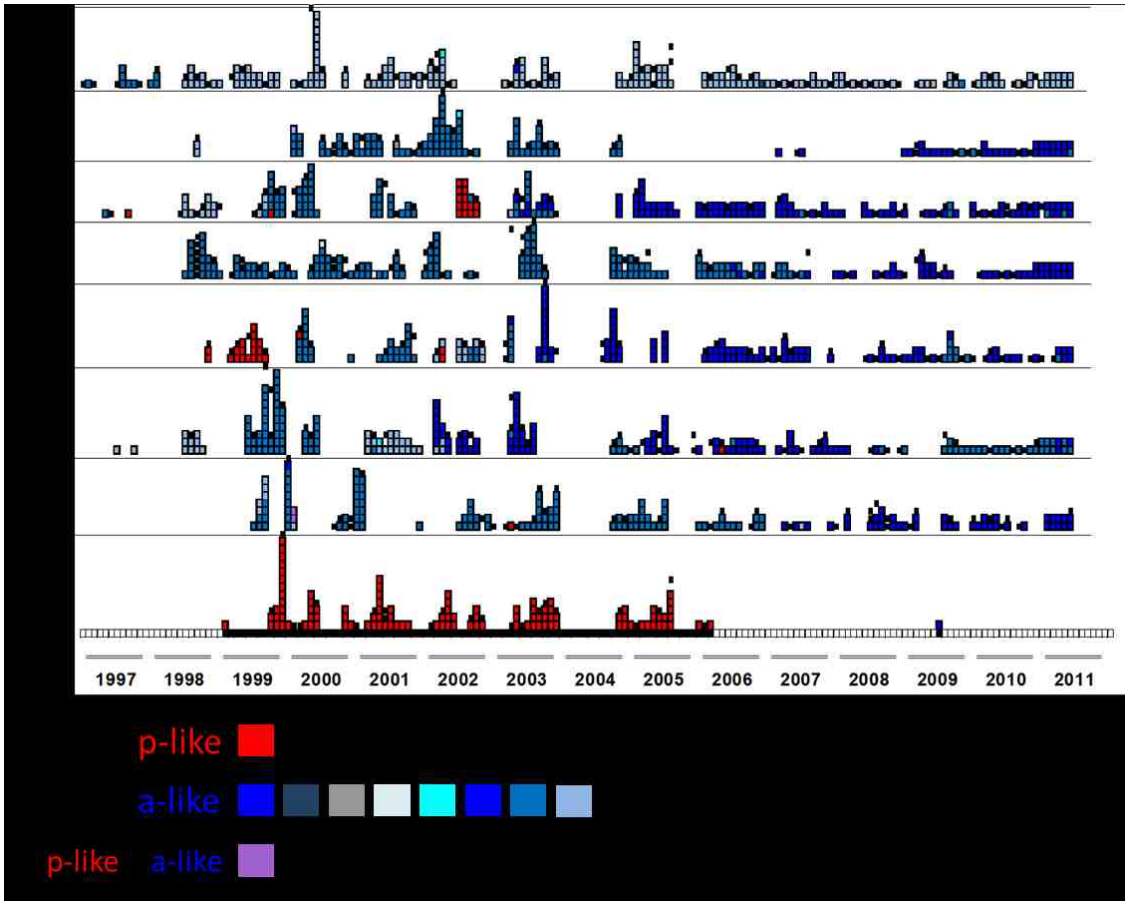

Figure 5: **Molecular epidemiology of HAdV-E4 respiratory infection among military recruits presenting with ARD**
Each row represents a single military recruit training facility (CA, Marine Corps Recruit Depot, San Diego, California; TX, Lackland Air Force Base, San Antonio, Texas; MO, Fort Leonard Wood, Missouri; IL, Naval Recruit Training Command, Great Lakes, Illinois; GA, Fort Benning, Georgia; SC, Fort Jackson, South Carolina; SC, Marine Corps Recruit Depot, Parris Island, South Carolina; NJ, Coast Guard Training Center, Cape May, New Jersey). Each box represents a single isolate genotyped by RFLP analysis.

1.11 Gaps in the Knowledge

HAdV-E4 intratypic genetic variability has been described since the 1980s (146, 147, 149). RFLP analysis with up to 16 endonucleases was used to distinguish p-like and a-like genomic variants. The description of genetic variability using this approach was low resolution as only ~2% of the 36 kb

genome was analyzed (149), although still valuable for analyzing large numbers of samples in epidemiology studies (21). The advent of next generation sequencing (NGS) and the decline in its cost in recent years have provided an affordable platform for examining differences among WGS, nucleotide by nucleotide. Dehghan and colleagues compared WGS from two a-like strains to the prototype and vaccine p-like strains (115). In this study the authors only discussed differences in the hexon and ITR sequences. A more detailed description of other regions of the genome is needed as it is likely that there are other important sequence differences in other regions of the genome. Larger collections representing the identified spectrum of genetic variability also need to be examined.

The observation of the relative predominance of a-like strains over p-like strains among circulating HAdV-E4 strains suggests that a-like strains may have a fitness advantage, such as transmissibility, or an enhanced ability to replicate in the host. Furthermore, it is also possible that a-like strains are more pathogenic as most studies only characterize virus isolates from cases of disease and not from asymptomatic individuals. The factors that contribute to the detection of a-like strains more frequently in association with disease remains is a gap in the knowledge.

Descriptions of replication kinetics and biological features of HAdV-E4 were published within 15 years of the discovery of AdV by Maurice Green, Harold Ginsberg, and others (165–168). Basic biological descriptions of p-like and a-like strains, however, have not been reported with one important exception:

Crawford-Miksza and colleagues described sequence differences in the hypervariable regions (HVR) 1-7 HVRs of the hexon sequences between the RI-67 strain and an a-like strain designated ZG 95-873 that were associated with a fourfold difference in the neutralization titers (169). The results from this study provide the rationale to examine other regions of the genome to identify genetic differences that may confer differences in phenotypes relevant to pathogenesis.

The implications of HAdV-E4 intratypic genetic variability in pathogenesis are not known. The hypothesis that HAdV intratypic genetic variability contributes to discriminable *in vitro* and *in vivo* phenotypes has only been explored to a limited extent in the AdV literature. As an example, Radke and colleagues reported the HAdV-B14p1 genomic variant exhibited low levels of E1B 19K expression which resulted in larger plaque sizes and enhanced immunopathogenesis in the Syrian hamster model compared to the HAdV-B14 prototype virus (90), despite that these two viruses are ~99.7% identical (170). Dehghan and colleagues reported ~95% sequence identity between the HAdV-E4 a-like strains and the prototype strain with important differences mapping to the ITRs (115); however it is not clear if these or other genetic differences contribute to variability in phenotypes that are relevant to pathogenesis. This remains a significant gap in the current knowledge.

1.12 Hypothesis and Specific Aims

I hypothesize that HAdV-E4 comprises two distinct evolutionary lineages that differ in their *in vitro* growth and *in vivo* pathogenetic phenotypes.

In this dissertation, this hypothesis was tested through the execution of the following specific aims:

Specific Aim 1 – To characterize the HAdV-E4 genetic variability by examination of WGS of a large collection of strains isolated worldwide between 1953 and 2015.

Specific Aim 2 – To evaluate the contribution of HAdV-E4 intratypic genetic variability to *in vitro* and *in vivo* phenotypes relevant to pathogenesis.

Subaim 1 – To compare the growth and cell killing phenotypes of HAdV-E4 PG I and PG II genomic variants in cell culture

Subaim 2 – To compare the pulmonary pathogenic phenotypes of HAdV-E4 PG I and PG II genomic variants in a cotton rat model of HAdV respiratory infection

Chapter 2 – Materials and Methods

2.1 Phylogenetic Analysis of HAdV-E4 WGS

WGS for 15 new HAdV-E4 strains were determined by next generation sequencing techniques in collaboration with Gabriel Gonzalez and Hidemi Watanabe at Hokkaido University and Daryl Lamson at the Wadsworth Center, New York State Department of Health, using the Ion Torrent (described by Kaján and colleagues (20)) and MiSeq (as previously described by Kajon and colleagues (128)) platforms, respectively. An additional 32 WGS (for 30 unique strains) were retrieved from the NCBI GenBank database. Two WGS for strains 1 (RI-67) and 2 (CL68578) are included in this analysis. Accession numbers for all WGS are listed in Table 4. The accession numbers for WGS of SAdV strains are as follows: SAdV23 (AY530877), SAdV24 (AY530878), SAdV25 (AF394196 and FJ025918), SAdV26 (FJ025923), SAdV30 (FJ025920), SAdV36 (FJ025917), SAdV37 (FJ025921 and FJ025919), SAdV38 (FJ025922), SAdV39 (FJ025924), and ChAdV-Y25 (JN254802; note: this strain was isolated in 1969 by Hillis and Goodman (171) before the AdV field standardized the naming scheme for AdV isolates from non-human primates (NHP)). Accession numbers for HAdV-B WGS used in phylogenetic analysis are as follows: HAdV-B3 (DQ086466), HAdV-B7 (KF268134), HAdV-B 1 (AF532578), HAdV-B14 (FJ822614), HAdV-B16 (JN860680), HAdV-B34 (AY737797), HAdV-B35 (AY271307), HAdV-B55 (FJ643676), HAdV-B66 (JN860676), HAdV-B68 (JN860678), and HAdV-B79 (LC177352).

Alignments of WGS were performed using MAFFT V7.388 in the Geneious v11.1.4 suite (Biomatters, https://www.geneious.com). ClustalW V2.1 was used for alignments of protein sequences or short nucleotide sequences in Geneious. Average percent sequence identity was calculated by first aligning sequences using the MAFFT algorithm in Geneious, then analyzing the distance using MEGA X v10.0.5 (172). Average percent identity is reported with the standard deviation calculated by Microsoft Excel. Percentage of genomic guanine-cytosine content (%G+C) was calculated by Geneious and reported with the standard deviation calculated by Excel. SAdV26 was deposited in GenBank as an unannotated genome in 2009 (114). Prediction of SAdV26 ORFs was accomplished by comparison with WGS from the SAdV25 (AF394196) and the CL68578 (AY594254) strains.

Phylogenetic trees were constructed using MrBayes v3.2.7 (173) using the general time-reversible substitution model with heterogeneity among sites, modeled under a gamma distribution and allowing for a proportion of invariable sites (GTR+Γ+I) as a substitution model, chosen as the model with the highest corrected Akaike information criterion (AICc) calculated with jModelTest 2 for the multiple sequence alignments. Trees were inferred with chain lengths of 10^6 states to assure convergence.

Simplot, a sequence similarity plotting tool (174), was used to identify conserved and divergent regions along the genomes of the examined HAdV-E4 strains. WGS were first aligned with MAFFT then imported into Simplot. A similarity plot was generated in Simplot v3.5.1 using the following parameters:

200 nucleotide sliding window, 20 nucleotide step size, GapStrip On, and Kimura distance model and Ts/Tv=2.0.

To test whether the HAdV-E4 genomic sequence data set provided enough data to analyze the temporal signal, the clock-likeness was checked by performing a linear regression between the parameters “root-to-tip divergence” and “sampling data” with TempEst (175). Time to the most recent common ancestor (tMRCA) was estimated by independent Bayesian Markov Chain Monte Carlo coalescent analyses by BEAST v2.4.6 (176) with chain lengths of 5×10^7 to assure an effect sample size of > 300 in all parameters of the models. Analyses were performed separately for WGS in the two groups of strains identified as p-like (PG I) and a-like (PG II). The tMRCA was also estimated for both groups by analyzing a combination of CDS alignments excluding those suspected to have resulted from recombination events. The strict and relaxed clock models were considered for the data sets. The coalescent constant, exponential, and Bayesian skyline models were considered for the populations (177, 178). The marginal likelihood of the combination of models and data was estimated in BEAST and with the Path-Sampler. Additionally, the distribution of the mutation rate for the two PGs was analyzed in TreeStat v1.2 in BEAST software suite.

2.2 Cell Culture

The A549 cell line (human type II alveolar epithelial cells, ATCC CL-185) was cultured in A549 Growth Medium (Minimum Essential Medium (MEM, Gibco)

supplemented with 8% (v/v) heat-inactivated New Born Calf Serum (HI-NBCS, Rocky Mountain Biologicals), 1.5 g/ml Na_2CO_3 (Amresco), 2 mM L-glutamine (Corning), 10 U/ml penicillin (Corning), 10.0 µg/ml streptomycin (Corning), and 25.0 mM HEPES (Corning)). The Calu-3 cell line (human airway epithelial cells, ATCC HTB-55) was cultured in Calu-3 Growth medium (RPMI-1640 medium (Corning) supplemented with 10% Fetal Bovine Serum (Atlanta Biologicals), 2.0 mM L-glutamine, 10.0 U/ml penicillin, 10.0 µg/ml streptomycin, and 25 mM HEPES). The Cotton Rat Lung Cell (CRLC) line (ATCC PTA-3930, currently discontinued) was cultured in CRLC Growth medium (Minimum Essential Medium (MEM, Gibco) supplemented with 10% (v/v) heat-inactivated Fetal Bovine Serum (Atlanta Biologicals), 1.5 g/ml Na_2CO_3 (Amresco), 2.0 mM L-glutamine (Corning), 1mM sodium pyruvate (Corning), 10.0 U/ml penicillin (Corning), 10.0 µg/ml streptomycin (Corning), and 25.0 mM HEPES (Corning)). For virus infections, cells were cultured in Infection Medium (identical to growth medium except the serum was reduced to 2%).

2.3 Viruses

A list of virus strains selected for the *in vitro* and *in vivo* studies (see Chapter 4) are found in Table 5 (Note: NHRC 25562 is 99.9% identical to Strain 31 in Table 4). Virus stocks were produced in A549 cells maintained in A549 Infection Medium (identical to A549 Growth Medium, except for the supplementation of 2% (v/v) NBCS). The infections were harvested by 3 rounds of freeze/thaw cycles. For elimination of the membrane fraction, cell lysates were

extracted with dd-H_2O-saturated chloroform at a final concentration of 5%. The upper phase was removed and vented overnight to remove the last traces of chloroform. Adenovirus stocks were then aliquoted and titered by plaque assay.

The 4p CL68578 vaccine strain was derived from the pVQ WT #11183 genomic clone (ABL, Inc. through an MTA with the NIH). Briefly, the genomic clone was released from the bacterial plasmid by PacI digestion and 1.0 µg of linearized HAdV-E4 DNA was transfected into A549 cells using the Effectene Transfection Reagent (Qiagen) following the manufacturer's recommendations. The transfected cells were then treated as infected cells. Infectious virus was passaged minimally in A549 cells to make the stock virus using the procedure described above.

2.4 Animals

Cotton rats (*Sigmodon hispidus*) used in this study were obtained from an inbred colony at Sigmovir Biosystems Inc. (SBI). Animal studies were performed after approval from SBI's Institutional Animal Care and Use Committee. Animals were housed in large polycarbonate cages and fed a diet of standard rodent chow and water. Four-week-old female cotton rats were inoculated with $5x10^6$ plaque forming units (PFU) of either the HAdV-E4 CL68578 or NHRC 42606 strain in each naris under isoflurane anesthesia. Mock-infected animals were inoculated in the same manner with chloroform-extracted supernatants of A549 cells maintained in A549 Infection Medium. Cotton rats were sacrificed at 1, 2, 3, and 6 days post infection (dpi) by CO_2 asphyxiation. Animals were dissected, and

the following lung lobes were used for downstream analysis: left lobe, molecular viral load; left lingular lobe, mRNA reverse transcription for cytokine gene expression; and right lung, histopathology. All lung lobes (except for the right lobe, see Histological Analysis below) were snap frozen in liquid nitrogen and stored at -80°C until processing.

2.5 Plaque Assay

A549 cells were grown to confluence in 6 well plates, and 0.1 ml of serially diluted virus (diluted 1:10 in 1x PBS) were used to inoculate a single well. The diluted virus was incubated at 37°C at 5% CO_2 for 1.0 hour with periodic rocking. The monolayer was then overlaid with a solution consisting of equal parts of 1.4% (w/v) Low Melt Agarose (G-BioSciences) and 2x MEM (Gibco) supplemented with 4% (v/v) HI-NBCS, 4.0 mM $_L$-glutamine, 20.0 U/ml penicillin, 20.0 µg/ml streptomycin, and 25mM $MgCl_2$. At 7 dpi, infected A549 monolayers were fixed with formaldehyde (final 1% formaldehyde (Sigma), 0.15M NaCl) and stained with crystal violet (EMD-Millipore Sigma).

2.6 Plaque Development Assay

A549 cells were seeded in 15mm x 60mm dishes to be confluent on the day of infection. Stocks were diluted in 1x PBS so that approximately equal number of PFUs of each strain were used to inoculate each dish in biological triplicate. Growth medium was aspirated, and the cells were inoculated with diluted virus and synchronized on ice for 10 minutes. Inoculated cells were then

incubated for two hours at 37°C 5% CO_2. Following absorption, 5.0 ml of overlay medium (described above) were added and allowed to solidify at room temperature (RT), then incubated at 37°C 5% CO_2. At 3 dpi, an additional overlay (prepared as previously described, except with the addition of neutral red (JT Baker Chemicals) at a final concentration of 0.0015%) was added, allowed to solidify at RT, and then incubated at 37°C, 5% CO_2. Starting a 4 dpi, plaques were counted daily using a lighted background and marked with a pen. The assay was terminated when no more plaques developed. The data are presented as % final titer (total number of plaques for a given day divided by the total number of plaques at the end of the assay) on each day.

2.7 Plaque Size Assays

A549 cells in 6 well plates were infected with approximately 20-40 PFU of each virus strain. After absorption for 1 hour at 37°C and 5% CO_2 with occasional rocking, the infected monolayers were overlayed as described above. At 7 dpi, plaque morphology was photographed using an CKX41 microscope (Olympus) with the Infinity 2 digital camera (Teledyne Lumenera). The images were captured using the Infinity Capture software V6.5.4 (Teledyne Lumenera). The plaque assays were then fixed and stained as indicated above.

2.8 Growth Curves

A549 cells seeded in 10mm x 35mm cell culture dishes and grown to 80% confluence were inoculated with HAdV-E4 strains at a multiplicity of infection

(MOI) of 1.0 PFU/cell, incubated on ice for 10 minutes, then absorbed for one hour at 37°C and 5% CO_2 with periodic rocking. Unbound virus was removed by aspiration and the infected cell monolayers were washed twice with 1x PBS. Cells were then replenished with A549 Infection Medium and incubated at 37°C with 5% CO_2. At various times post infection, infected cell monolayers were frozen at -80°C and subjected to a total of three rounds of freeze/thaw cycles. Cell debris was pelleted at 300 xg for 10 minutes and infectious virus titers were determined by plaque assay as described above.

2.9 Dissemination Assays

A549 cells were seeded on 48 well dishes to be 100% confluent at the time of infection. Growth medium was aspirated off, and the cells were inoculated with 100 µl of virus stock diluted in 1x PBS at MOIs of 10.0, 1.0, 0.1, 0.01, and 0.001 PFU/cell, then set on ice for 10 minutes. The inoculated cells were then incubated at 37°C and 5% CO_2 for 1.25 hours. The inoculum was then removed by aspiration, and the cells were washed twice with 1x PBS, then replenished with A549 Infection Medium and incubated at 37°C and 5% CO_2. At 7 dpi, the cells were fixed with 1% formaldehyde diluted in 0.15M NaCl, then stained with crystal violet.

2.10 Cell Viability

Cell viability was assessed by lactate dehydrogenase (LDH) release from infected cells into the cell culture medium using the CytoTox 96 Non-radioactive

Cytotoxicity Assay Kit (Promega). Briefly, A549 cells were seeded in 48 well plates to be confluent at time of infection. Cells were inoculated with virus diluted in 1x PBS at a MOI of 1.0 PFU/cell in biological triplicate and incubated on ice for 10 minutes. Inoculated cells were then incubated at 37°C for 1 hour at 5% CO_2. The inoculum was then removed, and the cells were washed twice with 1x PBS, then replenished with A549 Infection Medium. At 1, 2, and 3 dpi, the supernatant was removed and spun at 300 xg for 10 minutes. LDH activity was then assessed according to the manufacturer's directions (with the suggested controls) in technical quadruplicate. The data are reported as mean absorbance (490nm) ± the standard error of the mean (SEM).

As an alternate approach, intracellular ATP levels were measured as a surrogate for cell viability using the CellTiter-Glo 2.0 kit (Promega) according to the manufacturer's specifications. Briefly, A549 cells were seeded in 96 well dishes to be 75% confluent on the day of infection. Cells were inoculated at a MOI of 10.0 PFU/cell with virus diluted in 1x PBS or mock-infected with 1x PBS in biological quadruplicate and incubated on ice for 10.0 minutes. The inoculated cells were then incubated at 37°C for 2 hours at 5% CO_2. The inoculum was then removed, and the cells were washed twice with 1x PBS, then replenished with 50.0 µl of A549 Infection Medium. At various times post infection, ATP levels were measured by adding an equal volume of CellTiter-Glo 2.0 reagent to each well, mixing on an orbital plate shaker at 2000 rpm for 2.0 minutes, then incubating at RT for 10.0 minutes. Relative luminescent units were then

measured using a Luminoskan Ascent Type 392 (ThermoFisher Scientific). The data are reported as mean relative luminescence units ± SEM.

2.11 Polarization of Calu-3 Cells and Measurement of Transepithelial Electrical Resistance (TER)

Calu-3 cells were seeded onto transwell inserts (0.4µm pore size, Corning) at a density of $5.0x10^5$ cells/well, and Calu-3 Growth Medium was added to both the apical and basal compartments. Two days post seeding, the cells were washed with 1x PBS++ (Dulbecco's Phosphate-Buffered Saline with Magnesium and Calcium, Gibco). All liquid was then removed from the apical chamber, and the cells were grown at an air/liquid interphase for 10 days with medium changes every 48 hours.

Polarization of Calu-3 cells was evaluated by measuring the TER using a Millicell ERS meter (Millipore). Before measurement, the medium was removed from the basal compartment, and 1x PBS++ was added to the basal and apical compartment, then allowed to equilibrate at 37°C 5% CO_2 for 1.0 hour. TER was then measured using chopstick electrodes. Cells were considered polarized when TER values were between 500-600 Ωcm^{-2}.

2.12 Infection of Polarized Calu-3 Cells

For infection of Calu-3 cells, medium was removed from the basal compartment, and Calu-3 Infection Medium was added. Virus diluted in 1x PBS++ was then added to the apical compartment at a multiplicity of infection of

10.0 PFU/cell. After absorption at 37°C, 5% CO_2 for 1.0 hour, the inoculum was removed, and the cells were washed with 1x PBS++. All liquid in the apical and basal compartments was removed, and fresh Calu-3 Infection Medium was added to the basal compartment. The cells were then incubated at 37°C, 5% CO_2. At 1-3 dpi, the infected cells were processed by washing the apical compartment twice with a total of 400 µl of 1x PBS ++. Infectious virus titers in the apical wash were then determined by plaque assay.

2.13 Assessment of Pulmonary Viral Load in infected Cotton Rats

Frozen left lobe sections were weighed then transferred into a prechilled 2.0 ml SafeLock tube (Eppendorf) containing a prechilled 5mm stainless steel bead (Qiagen, previously sterilized with 70% ethanol) and 1.0 ml of serum-free A549 growth medium. The samples were then homogenized using the TissueLyser II apparatus (Qiagen) at 30 hz for 30 seconds for a total of three cycles, chilling on ice between each step. The samples were then spun at 16,000 xg for 10.0 minutes, and the supernatant was aliquoted into three separate tubes of equal volume.

DNA was extracted from 200.0 µl of the supernatants from lung homogenates using the MagNA Pure Total Nucleic Acid Isolation protocol on the MagNA Pure LC 2.0 instrument (Roche Diagnostics). 5.0 µl of the Simplexa Extraction and Amplification Control (DiaSorin Molecular) were added to each sample prior to extraction. Samples were eluted in a volume of 50.0 µl.

The real-time PCR assay was developed on the LIAISON® MDX instrument (DiaSorin Molecular) using the Universal Disc (96 well, DiaSorin Molecular) and DiaSorin Molecular Adenovirus analyte-specific reagents. The Adenovirus 3' hexon primer pair and the Adenovirus 5' hexon primer with a FAM-labeled integrated probe were used to amplify and detect a conserved region of the HAdV hexon gene. Internal Control (SEAC) Primer Pair with a Quasar® 760-labeled integrated probe was used to amplify and detect the SEAC DNA fragment. The 5' and 3' hexon primer pairs are a proprietary bi-functional fluorescent primer-probe set targeting the 3' and 5' regions of the HAdV hexon gene. Each reaction contained 4.0 µl of 2.5x Universal Master Mix, 0.2 µl Adenovirus 3' Hexon primer pair, 0.2 µl Adenovirus 5' Hexon primer pair, 0.2 µl internal control primer, 0.4 µl water, and 5.0 µl extracted template for a total reaction volume of 10µl. PCR amplification with real-time detection was performed using the following cycling conditions: denaturation, 97°C for 120 seconds (1 cycle); denaturation at 97°C for 10 seconds, followed by anneal/extension at 60°C for 30 seconds (40 cycles). Fluorescence was measured at the end of each anneal/extension cycle with quantitative values calculated by the LIAISON® MDS software. Standard curves were generated from highly pure HAdV-E4 DNA extracted from either CL68578 (p-like vaccine strain) or NHRC 42606 (a-like strain)-infected A549 cells using a slightly modified version of the protocol developed by Shinagawa and colleagues (179). The calibrator values ranged from $1.2x10^6$ to $1.2x10^2$ cp/ml (CL68578) and from $2.8x10^6$ to $2.8x10^2$ cp/ml (NHRC 42606). Each standard was extracted in

singlicate with each extract amplified in quadruplicate in a single run. Quantitative analysis was performed by the LIAISON® MDX Software. Standard curves were used for all subsequent viral load determinations.

2.14 RNA Isolation and Reverse Transcription

Total RNA was extracted from the left lingular lobes using the RNAqueous kit (ThermoFisher Scientific). Frozen lung sections were transferred from their storage tube into a prechilled 2.0 ml SafeLock tube along with a prechilled, previously sterilized 5 mm stainless stead ball. Lysis/Binding solution from the RNAqueous kit (1.0 ml) was then added to each sample. The samples were then homogenized using the TissueLyser II at 30hz for 30 seconds for a total of three cycles, chilling on ice between each step. The samples were then spun at 16,000 xg for 2.0 minutes at 4°C. The supernatant was then collected, and total RNA isolated using the RNAqueous kit according to the manufacturer's recommendations. Residual DNA was then removed from 20.0 µg of total RNA using the TurboDNA-free kit (ThermoFisher Scientific). To ensure that contaminating DNA was removed, PCR was performed with primers specific for the rig/S15 gene (see Table 3) using the goTaq Flexi DNA polymerase (Promega) using the following cycling conditions: 1 cycle of 95°C, 5 minutes; 50 cycles of 95°C for 30 seconds, followed by 57°C for 30 seconds, then 72°C for 30 seconds; 1 cycle of 72°C for 5 minutes. No PCR product was detected. Reverse transcription was then performed on 1.0 µg of DNAse-treated RNA using the

RetroScript Reverse Transcription kit (ThermoFisher Scientific) following the manufacturer's recommendations.

2.15 Analysis of Cytokine Gene Expression in the Lungs of HAdV-E4-Infected Cotton Rats

cDNA (described above) was subjected to real-time quantitative PCR (RT-qPCR) analysis using primers described previously (180–182) and shown in Table 3. RT-qPCR reactions were carried out using 3.0 µl of cDNA template and the QuantiFast SYBR Green PCR kit (Qiagen) using the MyiQ single color Real-time PCR instrument (Bio-Rad) using cycling conditions previously reported (180–182). Relative quantification of PCR products was performed by normalizing to β-actin using the $\Delta\Delta C_T$ method. The data are presented as mean fold induction ± SEM.

Table 3: Primers Used in the Analysis of Cytokine Gene Expression

Gene	Primer Sequence	
Rig S/15	Forward	5'-TTC CGC AAG TTC ACC TAC C-3'
	Reverse	5'-CGG GCC GGC CAT GCT TTA CG-3'
β-Actin	Forward	5'-GGC CAA CCG TGA AAA GAT GAC TC-3'
	Reverse	5'-GTC CGC CTA GAA GCA TTT GCG-3'
IFN-β	Forward	5'-GCA GCA TTT CAG AAT GTC TAG AGC-3'
	Reverse	5'-ATC TTA ATA AGT CTT CCC ATG G-3'
IL-6	Forward	5'-GGC ACA CTT AGG CAC AGC ATA CTC G-3'
	Reverse	5'-CAC AAC TCC ATC TGC CCT CCA GGA-3'
MCP-1	Forward	5'-GAT GCA GTT AAT GCC CCA CTC ACC-3'
	Reverse	5'-CAG TGG GAA ATG GAA GAG CAG AGG-3'
IP-10	Forward	5'-AAC CAG AGA GAA GCC GAT CA-3'
	Reverse	5'-GGC CGA TAG TAA GCC ATG AA-3'
Rantes	Forward	5'-AGC AGC AAA TGC TCC AAC TT-3'
	Reverse	5'-CCA GGC TCT GAA GAG GAC AC-3'
GRO-α	Forward	5'-GCA GGG GTT CAC TTC AAG AAC-3'
	Reverse	5'-GGT GTT TCA GAA GCC AGC ATC-3'

2.16 Histologic Analysis

Dissected lungs (right lobe) were inflated with 10% neutral buffered formalin, then immersed in formalin for fixation. The lungs were then paraffin-embedded, sectioned, then stained with hematoxylin and eosin (H&E) at Histoserv, Inc.. The stained lung sections were then scored blindly at SBI on a scale of 0 to 4 (absent, minimal, mild, moderate, and marked) for the following indices of pulmonary inflammation: peribronchiolar inflammatory cell infiltration (inflammatory cell infiltration around the bronchioles), perivascular inflammatory cell infiltration (inflammatory cell infiltration around the small blood vessels), interstitial pneumonia (inflammatory cell infiltration and thickening of alveolar walls), and alveolitis (cells within the alveolar spaces) (183).

2.17 Statistical Analysis

All statistics (unless otherwise noted) were calculated using GraphPad Prism v8.1.0 for Microsoft Windows (GraphPad, https://www.graphpad.com). Figure legends indicate the specific statistical test used as well as the number of replicates. p values < 0.05 were considered statistically significant. The sample size for animal experiments was determined by power analysis using G*power software v3.1.9.2 (184) specifically to observe differences in pulmonary pathology scores. With an effect size of 1.5 pathology score units, a standard deviation of the virus-infected groups of 1.0, and achieving <80% power with a 0.05 significance level, 6 animals were needed per group.

Chapter 3 – Aim 1: To Characterize the HAdV-E4 Genetic Variability by Examination of WGS of a Large Collection of Strains Isolated Worldwide Between 1953 and 2015

3.1 HAdV-E4 Strains Cluster into Two Distinct Evolutionary Lineages

WGS of HAdV-E4 strains isolated in the United States and Japan were combined with publicly available WGS to compile a total of 47 genomic sequences from 45 unique HAdV-E4 strains from respiratory and ocular specimens isolated between 1953 and 2015 that represent a diversity of genomic variants and geographic locations (Table 4). Confirmation of genotype identity (p-like or a-like) was carried out by *in silico* RFLP analysis (Table 4). Phylogenetic analysis of WGS representing 45 different strains confirmed the previous observation from Li and Wadell (149) that HAdV-E4 strains cluster into two district evolutionary lineages (Figure 6), referred hereafter as phylogroups (PGs). Phylogroup I (PG I) comprises p-like strains that are closely related to the prototype strain RI-67, and Phylogroup II (PG II) comprises the a-like genomic variants. Figure 6 also includes the SAdV members of HAdV-E, which bear strong sequence homology to HAdV-E4, as well as members from HAdV-B. Further analysis of WGS revealed differences in the percentage of genomic guanine-cytosine content (%G+C) between PG I and PG II (see Table 4), which further supports their distinctions as separate evolutionary lineages; PG I genomes had a mean %G+C of 57.7% ± 0.013 and PG II genomes had a mean %G+C of 56.3% ± 0.015. Furthermore, the average intra-PG I sequence identity

to RI-67 was 99.84% ± 0.12, while the average intra-PG II sequence identity to V0014 (strain 13, the earliest available PG II strain) was 99.88% ± 0.09.

Table 4: Origin and Genomic Characteristics of HAdV-E4 Strains Included in the Analysis

				Isolation					Genomic data		Restriction Fragment Length Polymorphisms (RFLP) * (# of sites)			
No.	Strain ID	Phylogroup	Genome type	Year	Place	Specimen	Accession number	WGS source	Genome Length (bp)	G+C (%)	BamHI	SmaI	SspI	XhoI
1	RI67			1953	MO,USA	respiratory	AY594253	GenBank	35990	57.7	7	20	4	9
	prototype strain						KX384949	GenBank	35990	57.7	7	20	4	9
2	CL 68578			1963	NC,USA	respiratory	AY487947	GenBank	35994	57.7	7	20	4	9
	vaccine strain						AY594254	GenBank	35994	57.7	7	19	4	9
3	RU2533			1966	USA	respiratory	MF002043	NYSDOH	35975	57.7	7	20	4	9
4	RDU2954			1966	NJ,USA	respiratory	KX384948	GenBank	35991	57.7	7	20	4	9
5	RU4445			1968	EGP	respiratory	KX384947	GenBank	35991	57.7	7	20	4	9
6	RU7872	I	p-like	1971	MN,USA	respiratory	KX384950	GenBank	35983	57.7	7	20	4	9
7	V1003			1981	NY,USA	respiratory	KX384957	GenBank	35929	57.7	7	20	4	9
8	V2029E			1986	GA,USA	respiratory	KX384946	GenBank	35904	57.7	7	20	4	9
9	NHRC90255			2000	NJ,USA	respiratory	AP014852	Hokkaido	35914	57.7	7	20	4	9
10	NHRC90870			2004	NJ,USA	respiratory	AP014853	Hokkaido	35914	57.7	7	20	4	9
11	NHRC90339			2011	NJ,USA	respiratory	EF371058	GenBank	35914	57.7	7	20	4	9
12	NYS 15-4054			2015	NY,USA	respiratory	KY996447	GenBank	35968	57.7	7	20	4	9
13	V0014			1978	FRA	respiratory	KX384956	GenBank	35960	56.4	8	15	5	10
14	J1007			1981	JPN	respiratory	KY996452	NYSDOH	35962	56.3	8	15	5	10
15	NA			1984	JPN	ocular	AB679754	Hokkaido	35960	56.3	8	15	5	10
16	V1933			1985	NM,USA	respiratory	KX384955	GenBank	35961	56.3	8	15	5	8
17	NA			1991	JPN	ocular	AB679755	Hokkaido	35961	56.3	8	15	5	10
18	ZG 95-873			1995	CA,USA	respiratory	KX384951	GenBank	35967	56.3	8	14	5	10
19	078Jax			1997	SC,USA	respiratory	KX384953	GenBank	35963	56.3	8	15	5	10
20	186Jax			1998	SC,USA	respiratory	KX384952	GenBank	35963	56.3	8	15	5	10
21	10Jax			2001	SC,USA	respiratory	KX384954	GenBank	35962	56.3	8	15	5	10
22	NA			2001	JPN	ocular	AB679756	Hokkaido	35963	56.3	7	14	5	10
23	NHRC11023			2001	IL,USA	respiratory	AP014849	Hokkaido	35973	56.3	8	14	5	9
24	NHRC50654			2001	TX,USA	respiratory	AP014850	Hokkaido	35964	56.3	8	14	5	9
25	T158			2002	SC,USA	respiratory	KX384945	GenBank	35965	56.3	8	15	5	10
26	NHRC3			2002	TX,USA	respiratory	AY599837	GenBank	35965	56.3	8	14	5	10
27	NHRC42606	II	a-like	2003	SC,USA	respiratory	AY599835	GenBank	35965	56.3	8	15	5	10
28	NHRC70935			2004	SC,USA	respiratory	AP014844	Hokkaido	35967	56.3	8	14	5	10
29	NHRC22650			2006	CA,USA	respiratory	AP014841	Hokkaido	36155	56.3	8	15	5	10
30	GZ01			2008	CHN	respiratory	KF006344	GenBank	35960	56.3	8	14	5	10
31	NHRC23703			2008	CA,USA	respiratory	AP014842	Hokkaido	35959	56.3	8	15	5	10
32	NHRC92165			2009	NJ,USA	respiratory	AP014845	Hokkaido	35964	56.3	8	15	5	10
33	WPAFB7			2009	CA,USA	respiratory	AP014847	Hokkaido	35961	56.3	8	13	6	10
34	TB071911			2011	CT,USA	respiratory	KY996453	GenBank	35952	56.3	8	15	5	10
35	NHRC36401			2011	MO,USA	respiratory	AP014851	Hokkaido	35960	56.3	8	13	6	10
36	NYS 12-12752			2012	NY,USA	respiratory	KY996450	GenBank	35955	56.3	8	15	5	10
37	NYS 12-27440			2012	NY,USA	respiratory	KY996451	GenBank	35948	56.3	8	14	6	10
38	NYS 13-5497			2013	NY,USA	respiratory	KY996449	GenBank	35960	56.3	8	13	6	10
39	NYS 14-4876			2014	NY,USA	respiratory	KY996448	GenBank	35934	56.3	8	15	5	10
40	NYS 14-38662			2014	NY,USA	respiratory	KY996443	GenBank	35960	56.3	8	14	6	10
41	NYS 14-38813			2014	NY,USA	respiratory	KY996444	GenBank	35948	56.3	8	14	6	10
42	NYS 14-33430			2014	NY,USA	respiratory	KY996445	GenBank	35948	56.3	8	14	6	10
43	NYS 14-9111			2014	NY,USA	respiratory	KY996442	GenBank	35948	56.3	8	14	6	10
44	NYS 15-3477			2015	NY,USA	respiratory	KY996446	GenBank	35949	56.3	8	14	5	9
45	NYS 15-1428			2015	NY,USA	respiratory	MF002042	GenBank	35960	56.3	8	14	6	10

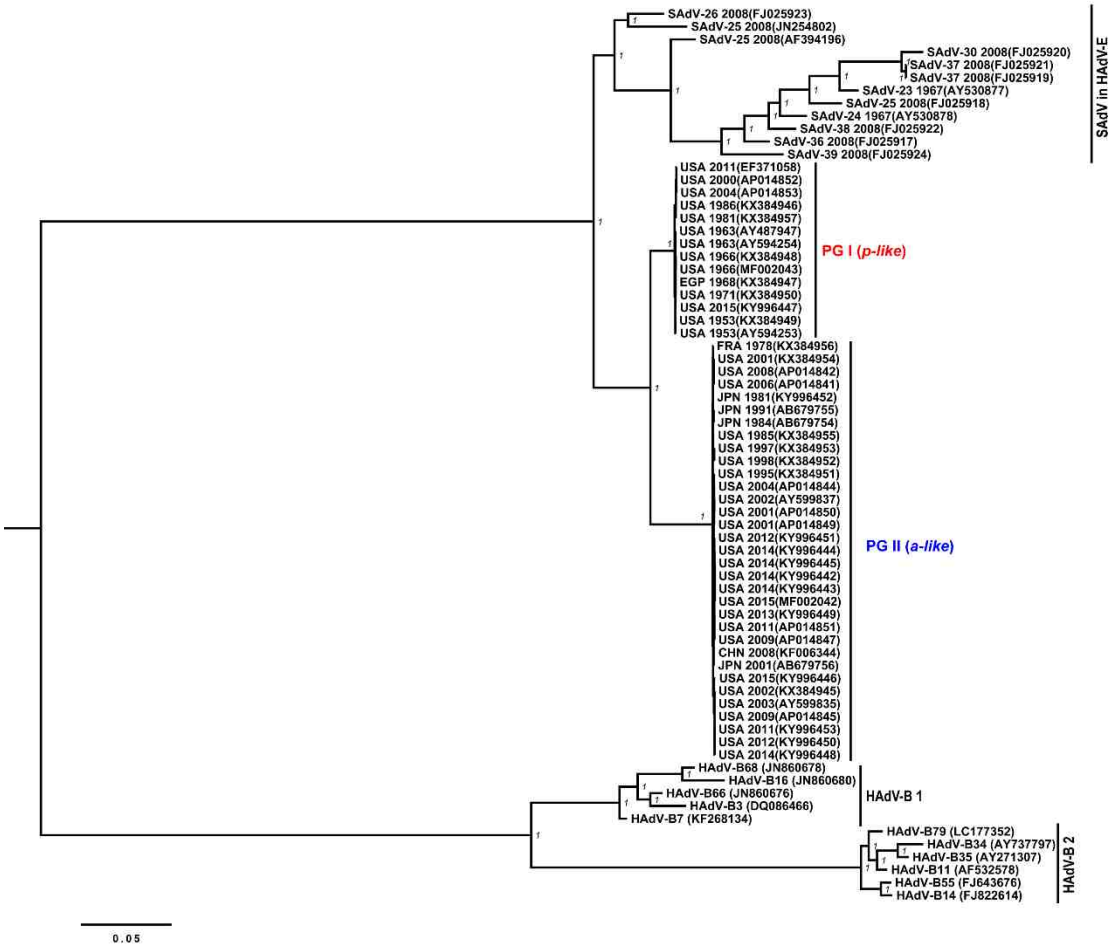

Figure 6: **HAdV-E4 comprises two distinguishable phylogroups**
Phylogenetic tree of whole genome sequences of HAdVs of species B, E, and SAdVs of species HAdV-E. Bayesian posterior probability support is shown next to the branches.

3.2 Estimation of the Time to the Most Recent Common Ancestor for HAdV-E4 Strains

Available records show 12 years between the first documented isolation of a p-like HAdV-E4 strain (RI-67, USA, 1953(2)) and the first documented isolation of an a-like strain (strain BC 129, China,1965 (149, 153)). As these dates are not necessarily reflective of real timelines of circulation, the tMRCA was estimated. A Bayesian approach using the BEAST software package was used to calibrate the

tree with isolation year of each strain. An exponential molecular clock was used to demonstrate that both PGs diverged from the common ancestor approximately 602 years before the present (ybp), or in 1413 in the absolute time scale with 2015 as the most recent calibration date (Figure 7). This analysis also showed that PG II had a slightly higher mutation rate than PG I (3.69×10^{-5} compared to 3.24×10^{-5} mutations/site/year for PG II and PG I, respectively). The results suggest that PG I strains are descendants from a strain circulating approximately 91 ybp (1924 in the absolute time scale) in the 95% highest posterior density range (95% HPD) [67, 144ybp] while PG II strains descended from an ancestral strain circulating approximately 54 ybp (1961 in the absolute time scale) in the 95% HPD [40, 84 ybp] (Figure 7).

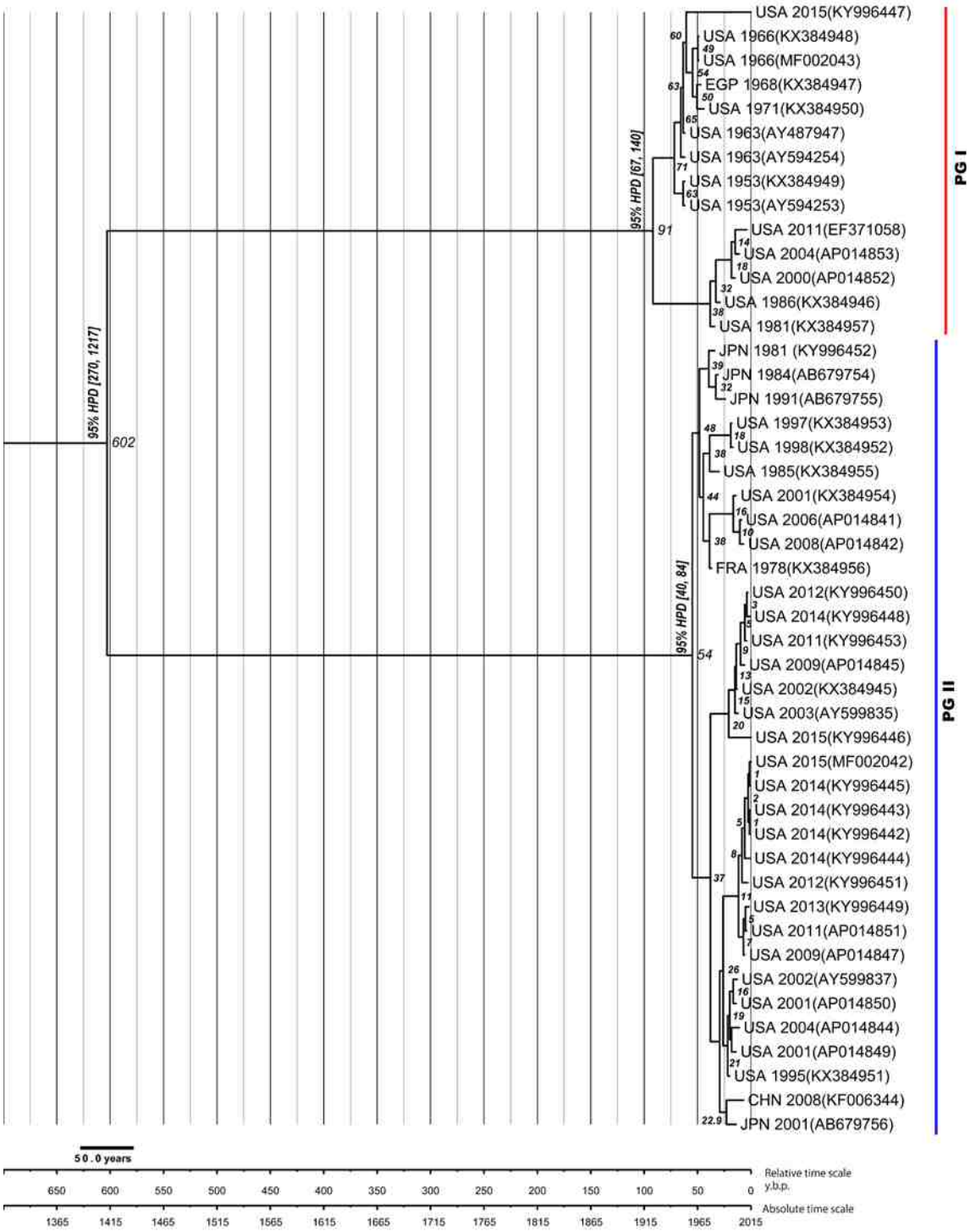

Figure 7: **Bayesian estimation of the time to the most recent common ancestor for HAdV-E4 strains in PG I and PG II**
The phylogenetic tree is annotated in the branches with years before the present. The 95% highest posterior density (HDP) ranges for tMRCAs of all sequences are shown for both phylogroups between brackets.

3.3 Detailed Analysis of Sequence Diversity Between PG I and PG II

On average, PG I genomes were found to be ~94.5 % identical to genomes in PG II. Interestingly, this level of genetic relatedness is comparable to that between any two different HAdV genotypes of the same species: 94% ± 5 for HAdV-B; 96% ± 1 for HAdV-C; and 94% ± 1 for HAdV-D, many of which are also serologically distinguishable. An analysis was conducted using Simplot to identify conserved and divergent regions along the genomes of PG I and PG II strains. A representative plot including three genomic variants from each PG is shown in Figure 8. Nucleotide similarity versus nucleotide position is plotted for the HAdV-E4 WGS compared with the query strain, RI-67. WGS closely related to the RI-67 WGS will plot higher on the Y axis, while those more distantly related will plot further down on the Y axis. This analysis clearly shows differences in genetic content between PG I and PG II strains. The most striking differences between PG I and PG II sequences map to the ITRs and E3, although additional mutations with potential to result in phenotypic differences relevant to pathogenesis are found in multiple genomic loci, including E1, VA RNA, L3, and L4 as described and discussed in detail below.

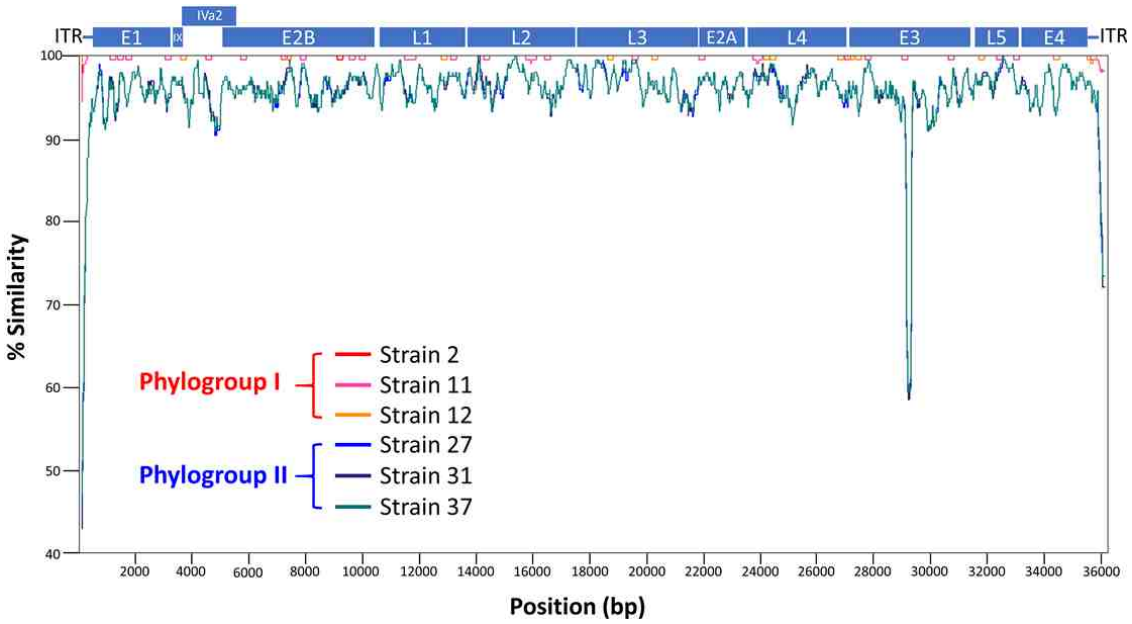

Figure 8: **Analysis of genomic sequences of representative strains of PG I and PG II for regions of divergence and similarity**
A similarity plot was generated using the Simplot software comparing HAdV-E4 strains representing the major genomic variants with the RI-67 as the query strain. MAFFT was used to align WGS prior to Simplot analysis with the following parameters: window size, 200 nucleotides; step size, 20 nucleotides; GapStrip, on; distance model, Kimura.

3.3.1 Inverted Terminal Repeat (ITR)

The analysis of 12 WGS in PG I and 33 WGS in PG II confirmed previous reports of differences in the ITR sequences between the two lineages of HAdV-E4 genomic variants including differences in length (115, 155). PG I genomes had an average ITR length of 113.8 bp ± 3.4 and an average intragroup percent identity of 98.6% ± 1.8, whereas the average length for PG II genomes was 206.5 ± 2.7 and the intragroup percent identity was 99.6% ± 0.3. As shown in Figure 9, the ITR sequences of PG I genomes have a higher sequence identity with SAdV26, while the PG II sequence is closer to that of HAdV-B16. It has

been suggested that the ancestor PG II strain obtained this unique ITR through intraspecies recombination events (115, 155).

	Strain 27	HAdV-B16	Strain 2	SAdV26
Strain 27		89.74%	61.34%	63.03%
HAdV-B16	89.74%		58.47%	64.41%
Strain 2	61.34%	58.47%		78.81%
SAdV26	63.03%	64.41%	78.81%	

Figure 9: **Percent identity matrix for the ITR region among PG I and PG II strains with other AdVs**
The ITR region for Strains 1 and 27 (representing PG I and PG II, respectively) as well as HAdV-B16 and SAdV26 was aligned using ClustalW in the Geneious software package, and the percent identity was calculated.

This analysis also confirms the differences between nuclear factor recognition sites between PG I and PG II ITR sequences originally identified by Dehghan and colleagues (115, 185). Examination of WGS from 45 HAdV-E4 strains did not reveal any intragroup differences in the NFI or NFIII sites among PG II genomes. Interestingly, a subset of the PG I strains (strains 9-11) shared the NFIII binding motif (5'-TATGTAAATAA-3') with PG II strains; this motif was different from that of the prototype strain (5'-TATGCAAATAA-3').

Differences in the terminal 8 bp of the ITR sequences have been noted for PG II strains (155). In the present analysis, only one strain examined had the 5'-CTATCTAT-3' sequence (strain 1, RI-67 reported by Paurkayastha and colleagues (157)), while most others carried the 5'-CATCATCA-3' sequence (Figure 10). Interestingly, Hang and colleagues reported RI-67 to carry the 5'-CATCATCA-3' ITR sequence (KX384994, (152)). This discrepancy has been noted in the literature (186) and may be due to variation in the stocks of the RI-67

virus (ATCC VR-4 (5'-CTATCTAT-3') submitted by Maurice Hilleman compared to ATCC VR-1572 (5'-CATCATCA-3') submitted by Wallace Rowe), as RI-67 has been passaged continuously in culture since its isolation more than 60 years ago. Figure 10 also shows a minority of strains had noncanonical sequences (5'-ATAATATA-3', 5'-AATAATAT-3', 5'-GCATCATC-3', and 5'-CAATAATA-3'). These differences may be genuine or might be the result of different ITR sequencing methodologies; the authors who published these sequences do not specifically discuss the ITR regions (128, 152).

Terminal ITR Sequence (8 bp)	Strains
5'-CATCATCA-3'	1, 2, 4-7, 9-11, 13, 15-33, 35, 38, 40, 45
5'-CTATCTAT-3'	1
5'-CAATAATA-3'	12, 36, 37, 39, 41-43
5'-GCATCATC-3'	14
5'-ATAATATA-3'	34
5'-AATAATAT-3'	3, 8, 44

Figure 10: **Terminal 8 bp sequence in HAdV-E4 ITR**
The HAdV-E4 ITR was analyzed from WGS data from 45 HAdV-E4 strains. Note that strain 1 (RI-67) is listed twice as the two WGS available report differences in this region.

Lastly, the NHRC 22650 strain (#29 in Table 4) was observed to have a 194 bp insertion by duplication of the neighboring genomic loci adjacent to the right hand ITR. The impact of this unique feature on viral replication is unknown.

3.3.2 Early Region 1

Early region 1A (E1A)

While the genomes of PG I encode 28.0 kDa (257 aa) and 24.6 kDa (226 aa) polypeptides, the PG II genomes encode slightly shorter polypeptides of 27.0 kDa (246 aa) and 23.5 kDa (215 aa), respectively. The predicted polypeptide sequences encoded by all examined genomes in PG I are identical, while PG II sequences are slightly different and on average 87.8% similar to those of the prototype strain RI-67 in PG I. The most striking difference between the E1A polypeptides encoded by the two PGs is an 11 amino acid deletion (aa 82-94) between the conserved regions CR1 and CR2 found in all examined PG II genomes (Figure 11). The deletion includes a leucine at position 91 and a threonine at position 93 which Avvakumov et al. described as highly conserved amino acids in the E1A proteins encoded by members of species HAdV-B, HAdV-D, and HAdV-E, although no function has been assigned to these residues (187). Interestingly, the 11 amino acid deletion was not present in any of the examined genomes of simian members of species HAdV-E. Conservation of the E1A polypeptide sequences among HAdVs varies between species (44), and in general most functional studies have focused on the function of E1A for HAdV-C. Examples of sequence variation resulting in differences in function have been noted (188, 189), and additional work in identifying functional differences among species-specific E1A proteins is needed.

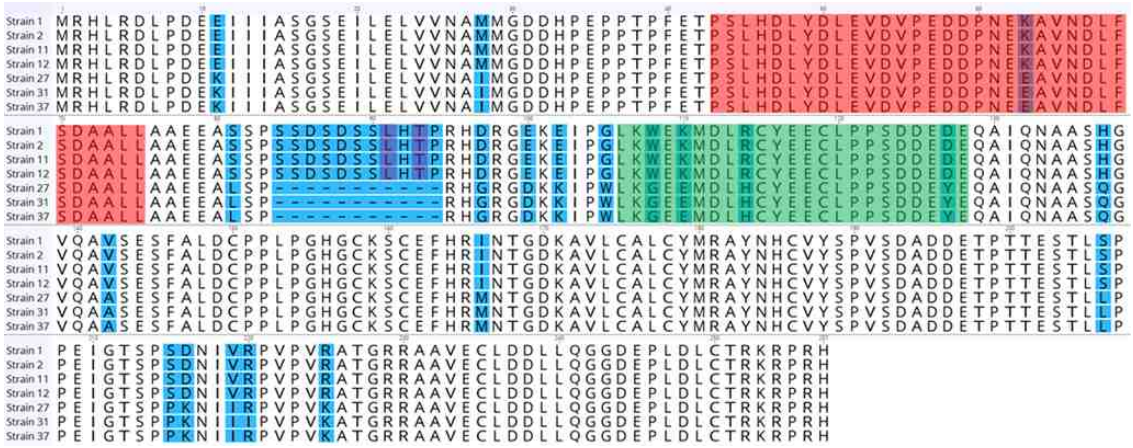

Figure 11: **Sequence divergence of the HAdV-E4 large E1A polypeptide** Large E1A polypeptide sequences from HAdV-E4 strains representing the spectrum of genetic diversity (strains 1, 2, 11, 12, 27, 31, and 37) were aligned using ClustalW. Amino acids highlighted in red and green represent CR1 and CR2 sequences, respectively. Amino acids highlighted in purple represent evolutionary conserved amino acids not present in PG II sequences.

Early region 1B (E1B)

The predicted polypeptide sequence for E1B 19K is conserved among members of PG I as well as among members of PG II with an 89.6% inter-PG sequence identity. There are eight non-synonymous mutations that result in amino acid changes. Additionally, there is a 33 nucleotide (11 amino acid) in-frame insertion among PG II members located in the shared coding region for E1B 19K and E1B 55K. This insertion is also present in the coding sequence for E1B 19K in the genomes of SAdV23, SAdV24, SAdV25, SAdV26, and ChAdV-Y25, although only 5 of the 11 amino acids are conserved within PG II sequences (Figure 12).

The predicted sequences for E1B 55K encoded by all examined PG I strains were identical and the sequences for E1B 55K encoded by PG II strains had an average sequence identity to the prototype PG I strain RI-67 of 93.6%. In

addition, all PG I strains are characterized by an 11 amino acid insertion at their N-terminus arising from the 33 nucleotide insertion event described above for E1B 19K (Figure 12). This region of the protein is characterized by low sequence homology to other E1B sequences from other HAdV species (187), and further work will be needed to identify the functional impact of this deletion as well as other mutations distinguishing the E1B proteins encoded between PG I and PG II strains.

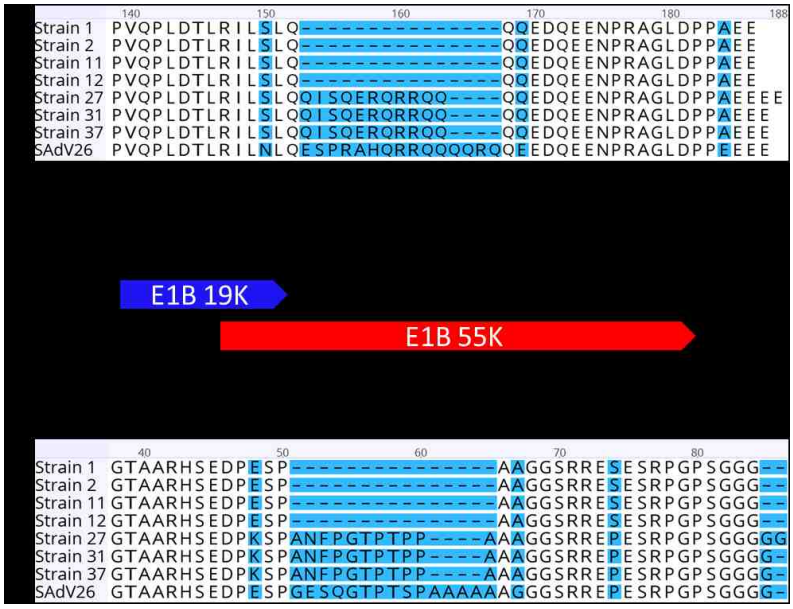

Figure 12: **HAdV-E4 sequence divergence in the shared E1B coding region** Cartoon schematic of the E1B coding region with flanking nucleotide positions (middle). The translated sequence for E1B 19K (above) and E1B 55K (below) demonstrating the 11 amino acid insertion in PG II strains. Strains 1, 2, 11, 12, 27, 31, 37, and SAdV26 are shown as representative strains.

3.3.3 Virus-associated RNAs

Consistent with the original observations reported by Kidd and colleagues (156), all PG II genomes examined in this study exhibit a 65 bp deletion in VA RNAII starting at position 10593 (relative to prototype strain RI-67) that partially

ablates the promoter element A, and that results in the complete loss of promoter element B. VA RNAII is predicted to not be expressed in PG II strains (156), as VA RNAs are not expressed in viruses that carry mutations in these promoter elements (190, 191). The genomes of a subset of PG I strains (#8, 9, 10, and 11) have an additional 20 bp deletion starting at nucleotide position 10639 that involves the last two nucleotides in the sequence of the promoter element B (Figure 13).

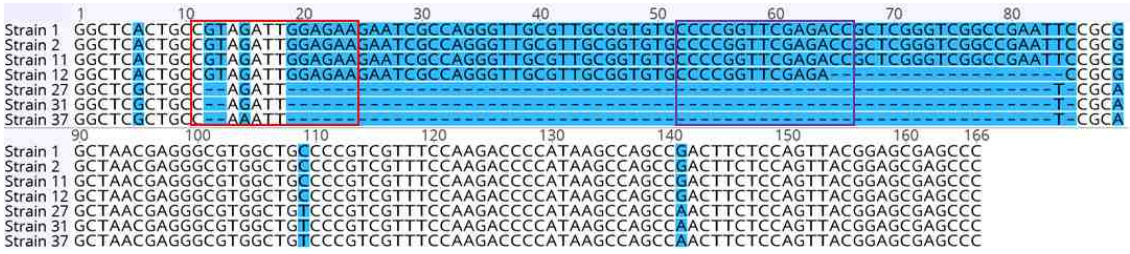

Figure 13: **HAdV-E4 VA RNAII sequence**
The VA RNA II sequences for strains 1, 2, 11, 12, 27, 31, and 37 were aligned using ClustalW. Elements A and B are shown in red and purple boxes, respectively.

3.3.4 Hexon Hypervariable Region 1-7

PG I and PG II strains had an average of 99.7% and 97.1% sequence identity with the RI-67 strain, respectively. The analysis focused on hypervariable regions 1-7 of the hexon gene (HVR 1-7) which encode the serotype-specific residues displayed in loops 1 and 2 of the hexon capsid protein that project from the surface of the virion (192). No difference in HVR 2 was observed among PG I and PG II strains (data not shown). Several nonsynonymous point mutations in HVR 1 and 3-7 that distinguish the genomes of PG I and II were identified. Interestingly, a subset of PG II strains (strains 7-11), typed as the 4p4 genome

variants, exhibited a 4 amino acid deletion in HVR 3. A summary of the genetic differences between PG I and PG II sequences are found in Figure 14.

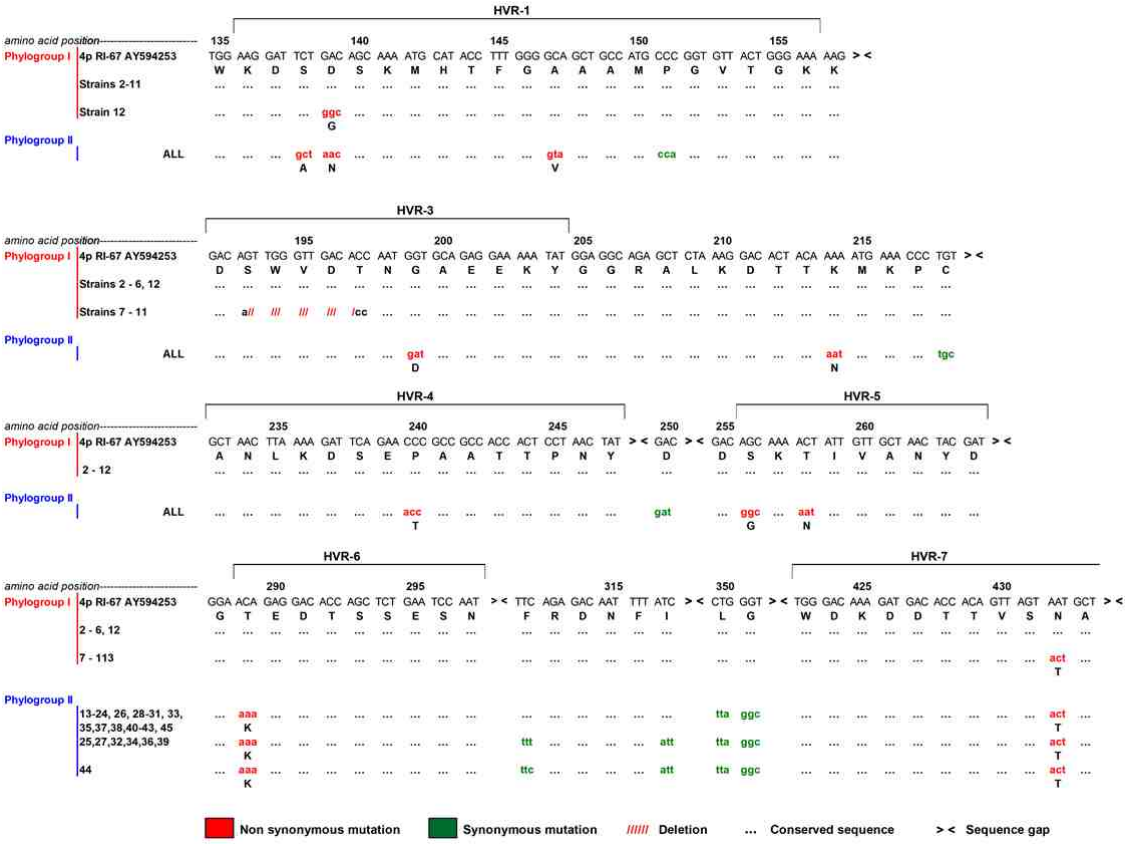

Figure 14: **Amino acid differences identified in the HVR 1 and 2-7 of the hexon polypeptide among examined strains of PG I and PG II**

3.3.5 Late Region 4 100K

The predicted L4-100K amino acid sequence encoded by PG I strains was on average 99.8% identical to that of RI-67 whereas the PG II sequence was on average 96.3% identical. PG I strain #12 described by Kajon and colleagues exhibited a single glutamine insertion (nucleotides CAG) at amino acid position 20 (128). Several differences were identified between PG I and PG II sequences

in the glycine-arginine rich (GAR) C-terminal region of L4-100K. GAR regions are sites of arginine methylation with the common consensus sequence arginine-glycine-glycine (RGG) (193, 194). In HAdV-C5, the GAR region contains three RGG repeats as well as other arginines that are post-translationally methylated. Mutations of these arginines in HAdV-C5 L4-100K interfere with the protein's interactions with late viral transcripts, potentially disrupting the role of L4-100K in hexon trimerization and preventing shuttling of L4-100K to the nucleus, ultimately resulting in decreased viral replication (195, 196). The GAR region for PG I strain RI-67 and its conservation among HAdV species was described by Iacovides and colleagues (195). Comparisons of PG I and PG II sequences identified a 5 amino acid deletion (glycine-glycine-glycine-arginine-serine) in all PG II strains between amino acid positions 755 and 761 (relative to RI-67) that disrupts the third RGG repeat in the GAR region (Figure 15). In addition, a single glycine insertion at position 743 (relative to RI-67) is encoded in the genomes of all examined strains of PG II creating an additional RGG tripeptide. The genomes of examined strains #18, 23, 24, 26, 28, 33, 35, 37, 38, and 40 - 43 also exhibit a glycine to glutamic acid replacement at position 717 that disrupts the consensus for an RGG tripeptide (Figure 15). The methylation state of the L4-100K polypeptide for HAdV-E4 has not been examined experimentally and further work will be needed to elucidate whether the sequence differences detected at the C-terminus of L4-100K between PG I and PG II strains affect viral replication.

Figure 15: **L4-100K GAR region for HAdV-E4 strains**
The C-terminus of the L4-100K polypeptide was aligned using ClustalW. RGG tripeptides are boxed in red. An additional RGG tripeptide found only in PG II sequences are boxed in purple.

3.3.6 Early Region 3

In the same location as HAdV-C E3-11.6K encoding ADP (69), the E3 region of members of species HAdV-E encodes two or three CR1 genes (11, 68) of unknown function. As shown schematically in Figure 16A, while the genomes of SAdV of species HAdV-E encode three CR1 genes designated CR1β, CR1γ and CR1δ (115, 157, 186), CR1γ is absent in the genomes of both HAdV-E4 PGs. As originally reported by Jacobs and colleagues, a vestigial E3 CR1γ sequence lacking an initiating ATG and splice acceptor site is present in the genomes of PG I strains due to a 326 bp deletion starting at position 29,449 relative to the SAdV26 genome (186). A unique 318 bp deletion in this region (starting at 29,603 in the SAdV26 genome) of PG II genomes results in a similar vestigial sequence (Figure 16A). Additionally, while unlikely to be expressed, a short evolutionarily unrelated 328 bp ORF that has been annotated as E3-6.3K (197, 198) is present in this region for PG I strains. As a result of a 29 bp deletion which introduces an early stop codon, the vestigial sequence is shorter in the genomes of PG II strains, and the E3-6.3K ORF is significantly truncated (Figure 16A-B). Marked amino acid sequence differences resulting from non-

synonymous point mutations as well as from INDELs in the N-terminal ectodomains of E3 CR1β and E3 CR1δ (Figure 16C-D) distinguish the genomes of PG I and PG II and highlight the divergence of these two genes in HAdV-E4 from those encoded by the closest SAdV, SAdV26. These genes have very low sequence similarity to any other homologous genes in the NCBI database, thus making sequence-based prediction of biological activity and function challenging.

3.4 Summary of Findings for Aim 1

The analysis of WGS from 45 HAdV-E4 strains isolated worldwide between 1953 and 2015 demonstrated that HAdV-E4 strains cluster into two distinct evolutionary lineages: PG I comprises strains closely related to the prototype strain isolated in 1953, and PG II comprises the a-like genomic variants. These findings confirmed previous observations from the 1980s analyzing PCRF from HAdV-E4 genomes (149) as well as data from more recent studies analyzing small sample sets of WGS (115, 199). Bayesian analysis estimated the time to the most recent common ancestor for the PG I and PG II lineages at 602 ybp, indicating that these strains have been evolving independently for a longer period of time than has previously been suggested (155). Comparative analysis of PG I and PG II WGS revealed differences in coding and noncoding regions that may affect viral replication and/or pathogenesis.

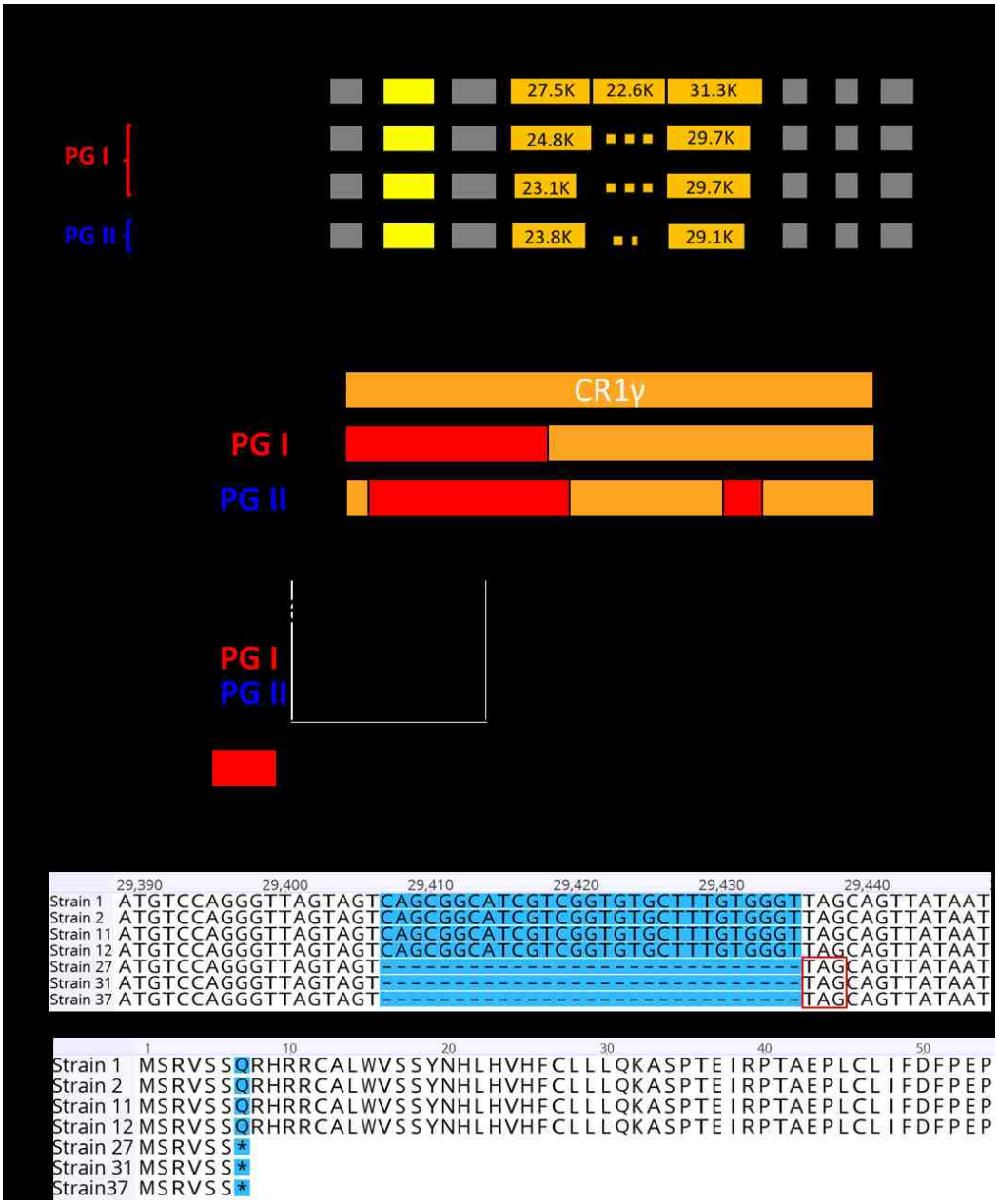

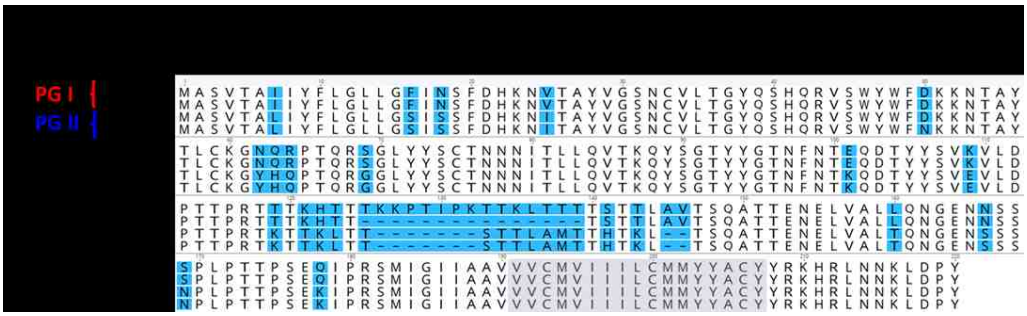

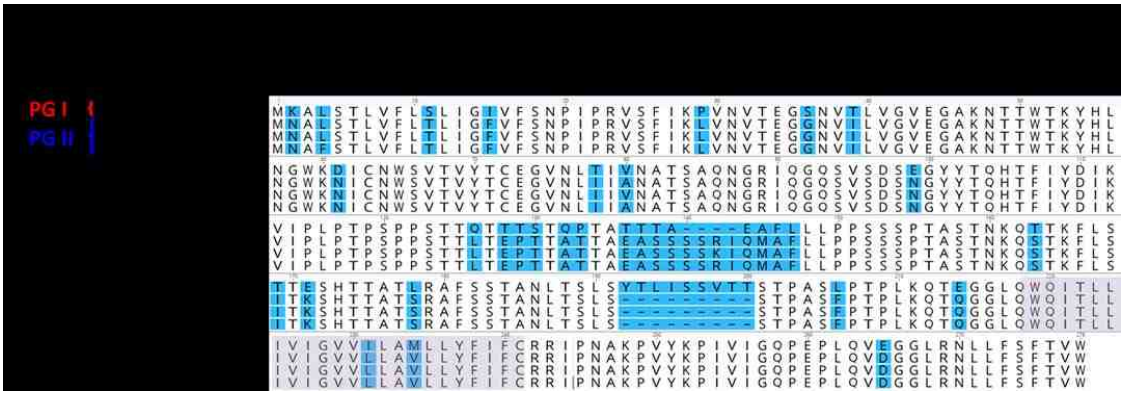

Figure 16: **Genetic diversity in the E3 region among HAdV-E4 strains**
(A) Schematic comparing the genetic content of the E3 region for SAdV26 and PG I and PG II strains. Differences in the CR1γ region among members of HAdV-E are noted: SAdV26 encodes a 22.6K ORF while PG I and PG II strains do not. See text for details. (B) Top panel, alignment of the 5' end of the 6.3K ORF of PG I and PG II strains. Premature stop codon (TAG) is boxed in red. Bottom panel, alignment of the predicted E3-6.3K polypeptide sequences of PG I and PG II strains. Alignment of E3 CR1β (C) and E3 CR1δ (D) polypeptides for PG I and PG II strains. Transmembrane regions are highlighted in purple.

3.5 Limitations of This Study

This bioinformatics study provides insight into the phylogenies and genetic variability of a comprehensive collection of HAdV-E4 strains, but it does have limitations. While the collection of strains used in this study is comprehensive, it would benefit from the addition of historical WGS from HAdV-E4 strains that are no longer available (for example, PG II strain BC 129 isolated in 1965, as well as PG II strains isolated in Rome in 1975 and New York in 1978 (125, 147, 149, 153)). These historical strains would provide valuable historical points for calibrating molecular clocks for Bayesian analysis of tMRCA.

There may be more genetic differences between PG I and PG II strains that may contribute to differences in *in vitro* and *in vivo* phenotypes that have yet to be described. The genetic variability described in this study included differences due to INDELs or mutations with a known impact on certain phenotypes and is a valuable starting point for future studies examining the impact of HAdV-E4 genetic variability on *in vitro* and *in vivo* phenotypes.

Chapter 4 – Aim 2: To Evaluate the Contribution of HAdV-E4 Intratypic Genetic Variability to *in vitro* and *in vivo* Phenotypes Relevant to Pathogenesis.

4.1 Subaim 1: To Compare the Growth and Cell Killing Phenotypes of HAdV-E4 PG I and PG II Genomic Variants in Cell Culture

4.1.1 Virus Strains Used in this Study

To examine the differences in the biological properties among HAdV-E4 strains, a panel of HAdV-E4 strains that represent the spectrum of described genomic variants in PG I and PG II were selected (Table 5). These strains included the prototype strain, RI-67 as well as the closely related vaccine CL68578 strain (99.94% whole genome sequence identity to RI-67), and two other prototype-like strains that have been previously described (128, 139): the recently isolated vaccine-like strain NY-15-4054 (99.94% sequence identity to RI-67) and strain NHRC 90339, a 4p4 variant (99.63% sequence identity to RI-67). PG II strains that represent the 4a, 4a1, and 4a2 genomic variants (NHRC 25562, NY-12-27440, and NHRC 42606, respectively) were also included.

Table 5: HAdV-E4 Strains Included in the Experiments Conducted for Aim 2

RI-67	4p	1953	Phylogroup I	AY594253
CL68578	4p	1963	Phylogroup I	AY594254
NY-15-4054	4p	2015	Phylogroup I	KY996447
NHRC 90339	4p4	2001	Phylogroup I	EF371058
NHRC 25562	4a	2011	Phylogroup II	AP014843
NY-12-27440	4a1	2012	Phylogroup II	KY996451
NHRC 42606	4a2	2002	Phylogroup II	AY599835

4.1.2 HAdV-E4 PG I Strains Exhibit a Large Plaque Phenotype and an Enhanced Cell-to-cell Spread Phenotype Compared to PG II Strains

The ability of HAdV-E4 strains to form plaques in A549 cells was examined first. Progeny virions released from infected cells under a semi-solid agarose overlay disseminate laterally to neighboring cells. Viruses with the ability to effectively lyse the infected cell or replicate faster will form larger plaques, while viruses deficient in these abilities will form smaller plaques (69, 87). A549 cells in 6 well plates were infected with PG I and PG II strains following the traditional plaque assay protocol and fixed and stained with crystal violet at 7 dpi. PG I strains were observed to form larger plaques than PG II strains (Figure 17). Variability in plaque size was also observed among PG I strains; the CL68578 strain formed the largest plaques, while the NY 15-4054, RI-67, and NHRC 90339 strains have incrementally decreasing plaque size. All PG II strains formed uniformly small plaques (compared to the CL68578 strain). Variation in plaque size in a single strain of virus was also observed. For example, in Figure 17, the

RI-67, CL68578, and NY-15-4054 strains forms both small and large plaques. This has been noted in the literature, and may be due to variation in virus infection or viral gene expression during infection (89, 200, 201). The analysis of brightfield images of plaques at day 7 dpi showed no differences in plaque morphology.

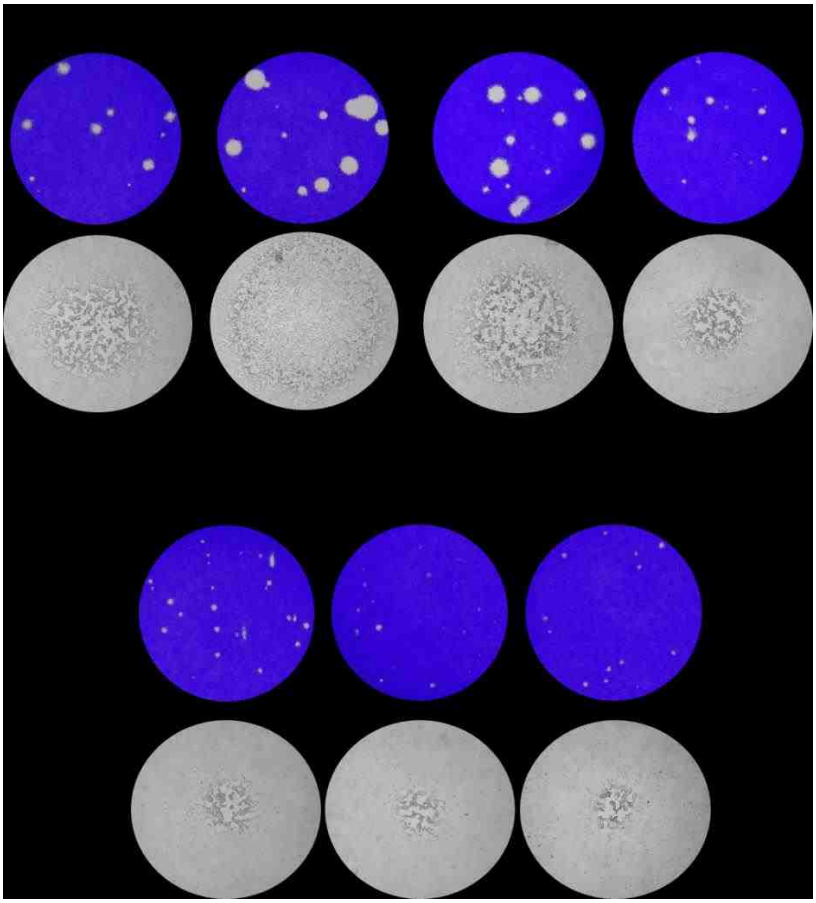

Figure 17: **PG I strains have larger plaques compared to PG II strains** Plaque assays from PG I (RI-67, CL68578, NY-15-4054, and NHRC 90339) or PG II (NHRC 25562, NY-12-27440, and NHRC 42606) strains were fixed and stained with crystal violet at seven days post infection. Brightfield images of plaque morphology are shown below plaque assays. This assay was representative of three independent experiments.

The rate at which plaques from PG I and PG II strains develop over time was next examined as described for HAdV-C laboratory mutants (69, 87). The data are presented as a percentage of the final titer, where the number of total plaques counted on a given day is divided by the total number of plaques observed on at the termination of the assay (day 25). It was observed that the plaques for all PG I strains were visible one day earlier (day 4) than plaques from PG II strains (day 5). In addition, a subset of PG I strains exhibited a faster rate of plaque development than all others, namely the CL68578 and the NY-15-4054 strains, while plaques for all other strains developed at similar rates. At 10 dpi, about 90% and 70% of plaques were visible for the CL68578 and NY-15-4054 strain, respectively. In contrast, on day 10 only 30-40% of plaques of all other strains were visible (Figure 18). The faster rate of plaque development for the CL68578 strain correlates with its larger plaque size shown in Figure 17.

Cytopathic effect (CPE) was examined at different multiplicities of infection in submerged infected monolayers to evaluate the cell-to-cell spread phenotype as described for HAdV-C5 mutants lacking or overexpressing the ADP gene (202, 203). A549 cell monolayers were infected at MOIs ranging from 0.001 to 10.0 PFU/cell, then fixed at 7 dpi. PG II strains spread at a restricted rate compared to PG I strains (Figure 19). PG II-infected cells stained with crystal violet were still attached to the plastic at the MOI of 1.0 PFU/cell while no cells were visible among monolayers infected with PG I strains. PG I strains had similar spread phenotypes with the CL68578 strain showing the most extensive

CPE at lower MOIs (particularly evident at 0.01 PFU/cell) compared to other strains. These data are consistent with the plaque size phenotypes.

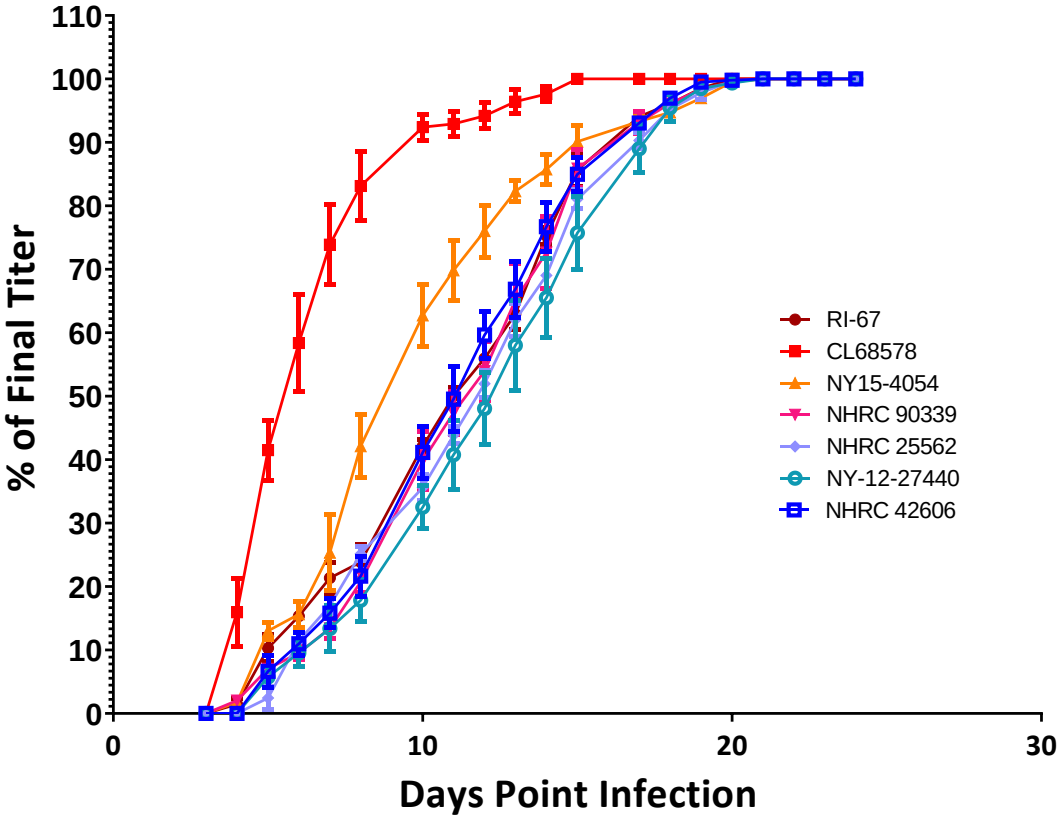

Figure 18 **The rate of plaque development is faster for certain PG I strains compared to other examined strains**
Plaques were counted every one to two days in plaque assays performed in 60mm dishes in biological triplicate. The total number of plaques observed on a given day is plotted as a percentage of the total number of plaques observed on the final day. This assay was representative of two independent experiments.

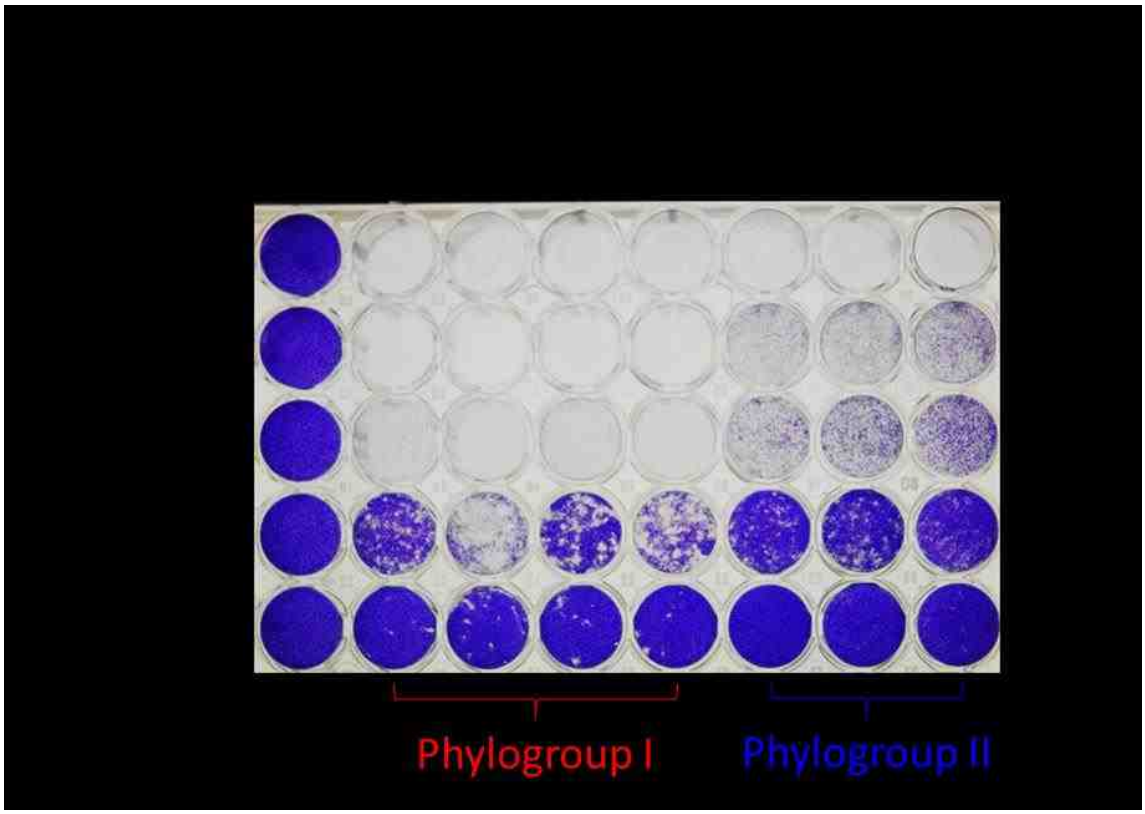

Figure 19: **PG I strains exhibited an enhanced spread phenotype in submerged A549 cells**
A549 cells were infected at MOIs ranging from 0.001 to 10.0 PFU/cell (shown in rows on the left side of the plate) with PG I or PG II strains (labeled in columns at the top of the plate). At 7 days post infection, cell monolayers were fixed and stained with crystal violet. This assay was representative of two independent experiments.

4.1.3 HAdV-E4 PG I Strains Exhibit Faster Replication Kinetics Than PG II Strains

The large plaque phenotype in Figure 17 could either be an indication of increased viral replication kinetics or enhanced cell lysis as a result of infection. To compare the growth kinetics of PG I and PG II strains, monolayers of A549 cells were infected at a MOI of 1.0 PFU/cell and infectious virus was harvested at 12, 24, 48, and 72 hours post infection (hpi). Infectious virus yield was then determined by plaque assay in A549 cells. Higher infectious virus yields were

detected in PG I-infected monolayers at 24 hpi (Figure 20) while infectious virus titers were similar at 48 and 72 hpi. This indicates that PG I strains have faster replication kinetics among all examined strains at early times post infection.

Next, the kinetics of viral progeny release of select PG I and PG II strains were assessed in a polarized lung epithelial cell model. Polarized Calu-3 cells were infected apically at a MOI of 10.0 PFU/cell, and the infectious virus yield from apical washes was determined by plaque assay in A549 cells. Higher infectious virus titers were detected in the apical compartment of the PG I strain CL68578-infected polarized Calu-3 wells at 48 and 72 hpi (Figure 21). This result could be attributed to faster virus replication kinetics and/or lytic release from the infected cell.

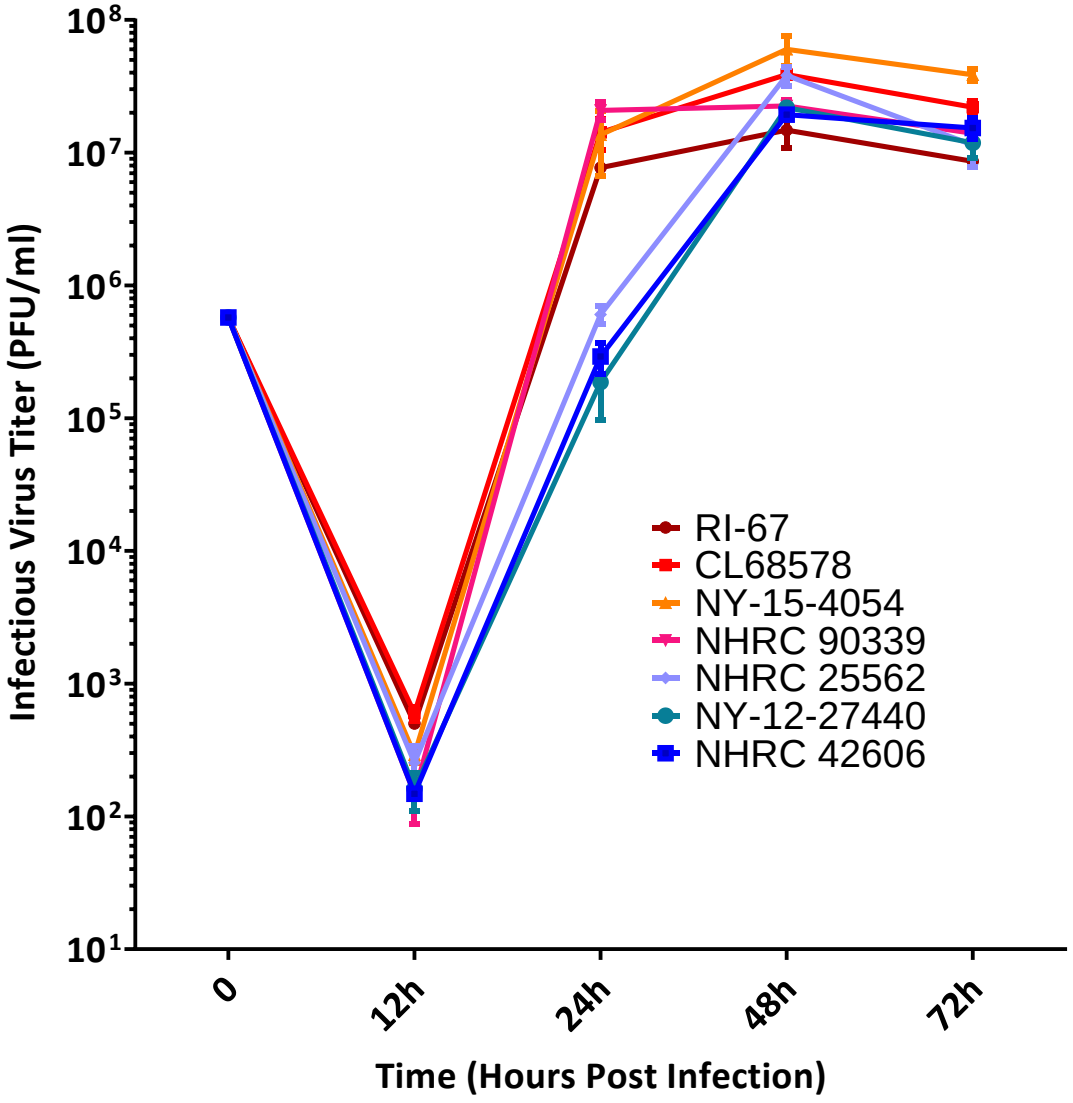

Figure 20: **PG I strains exhibit faster replication kinetics *in vitro***
Submerged A549 cell monolayers were infected with PG I or PG II strains at a MOI of 1.0 PFU/cell in biological triplicate. Infectious virus yield was determined for the indicated time points by plaque assay in A549 cells. This assay was representative of two independent experiments.

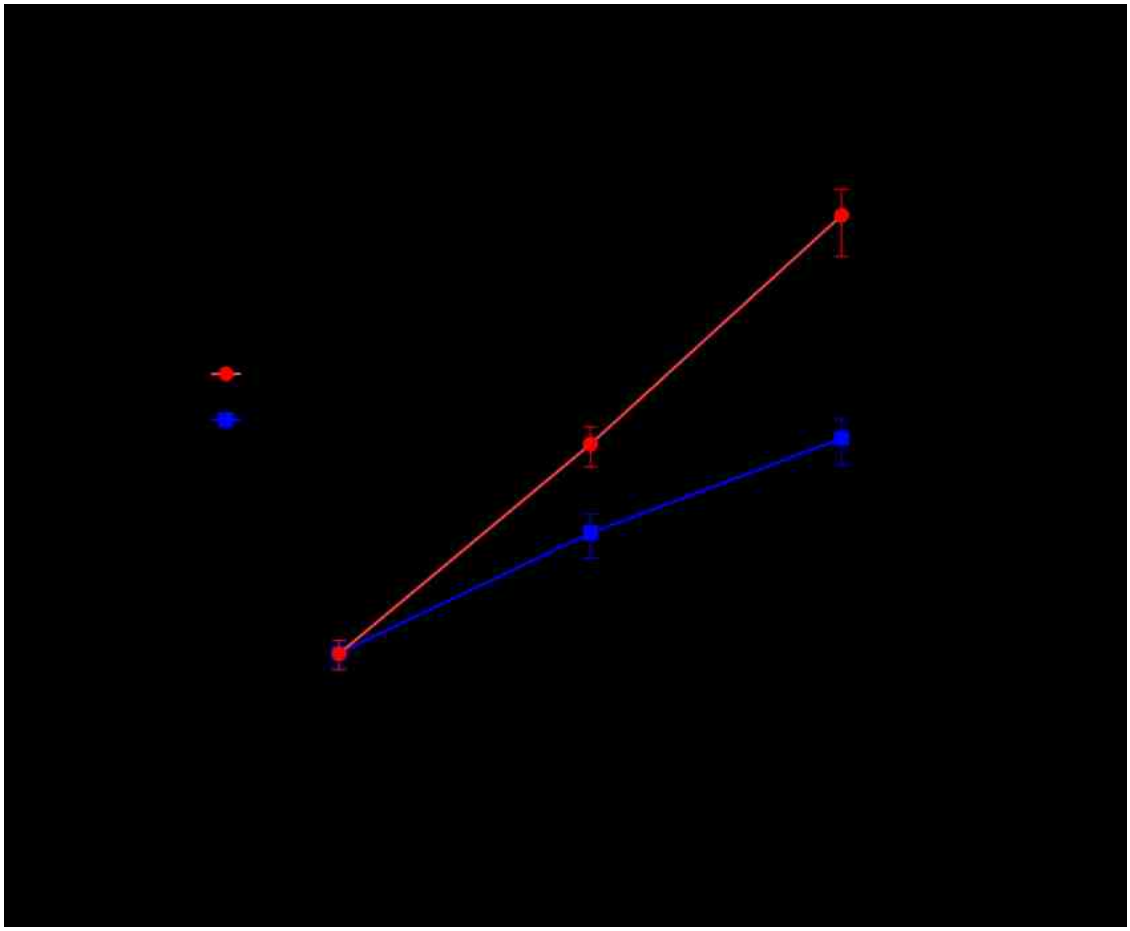

Figure 21: **Increased infectious virus yield was detected in the apical compartment from PG I-infected polarized Calu-3 cells**
Polarized Calu-3 cells were infected apically at a MOI of 10 PFU/cell in biological triplicate. At the indicated time points, apically released virus was determined by plaque assay in A549 cells. This assay was representative of two independent experiments.

4.1.4 Increased Cell Death Is Observed in Cells Infected with PG I Strains

Increased cell lysis is observed for HAdV-C genotypes, which encode ADP, compared to ADP-null HAdV-C mutants (69). In these studies, cell lysis correlated with plaque size. LDH activity from cell culture supernatants of PG I- or PG II-infected A549 cells was determined as a surrogate of cell viability. Viable cells with intact membranes will not release LDH into the supernatant, whereas

LDH activity can be detected from supernatants of cells undergoing apoptosis or necrosis (204). A significant increase in membrane permeability (as evidenced by the higher A490 reading) was observed in CL68578-infected cells compared to the NHRC 42606-infected cells (Figure 22).

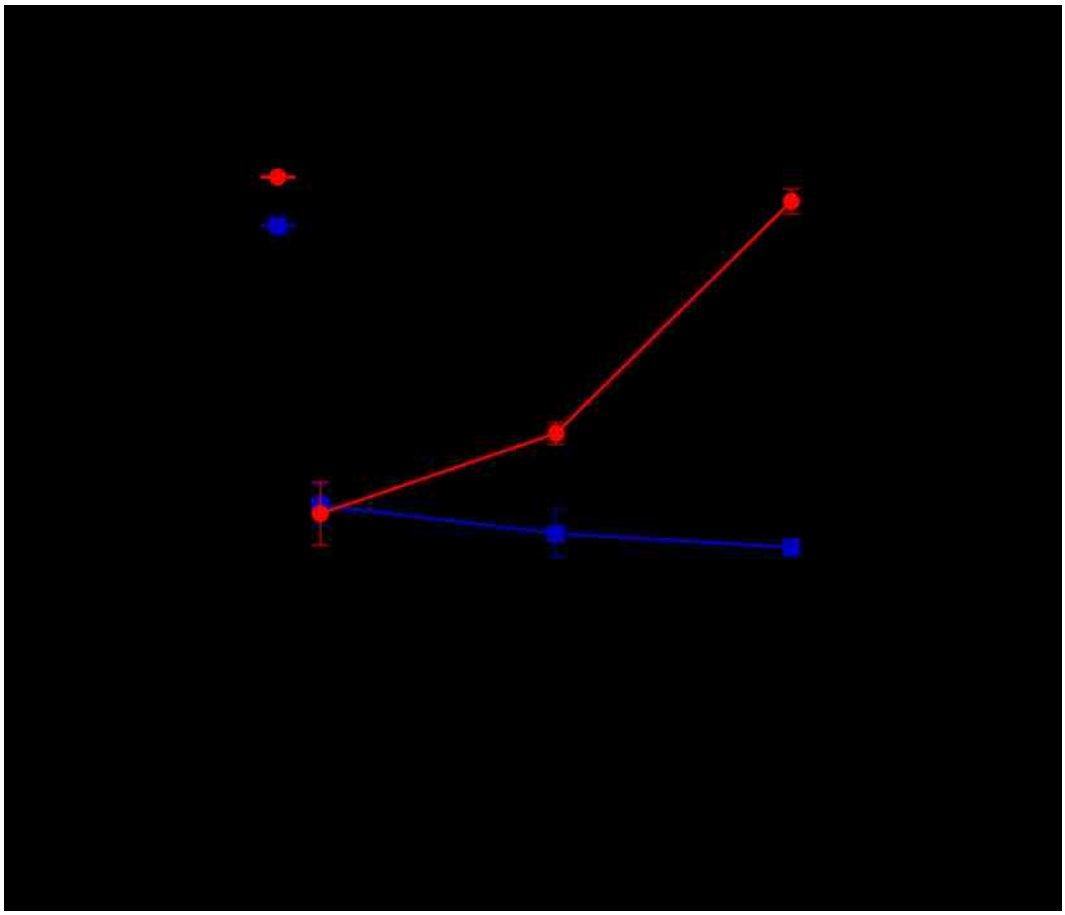

Figure 22: **Higher levels of lactate dehydrogenase activity are detected in the cell culture medium of CL68578-infected A549 cells than in NHRC 42606-infected A549 cells**
A549 cell monolayers were infected at a MOI of 1.0 PFU/cell in biological triplicate and cell lysis was assessed by determining lactate dehydrogenase activity in the cell culture medium in technical quadruplicate. Statistical significance was assessed by Student's *t* test, *p < 0.05, ****p < 0.0001.

Intracellular ATP levels following HAdV-E4 infection of A549 cells were measured as another surrogate for cell viability. The concentration of ATP is

proportional to the amount of viable cells (205). A549 cells were infected at a MOI of 10 PFU/cell, and intracellular ATP was measured at 96 hpi. Significantly more viable cells were observed at late time points post infection for PG II-infected cells than for PG I-infected cells. While the ATP levels from PG II-infected cells were relatively similar at 96 hpi, variability was observed among PG I-infected cells. Lower levels were observed in RI-67- and CL68578-infected cells compared to NY-15-4054- and NHRC 90339-infected cells (Figure 23). These data examining cell viability reveal increased cell killing by PG I strains compared to PG II strains.

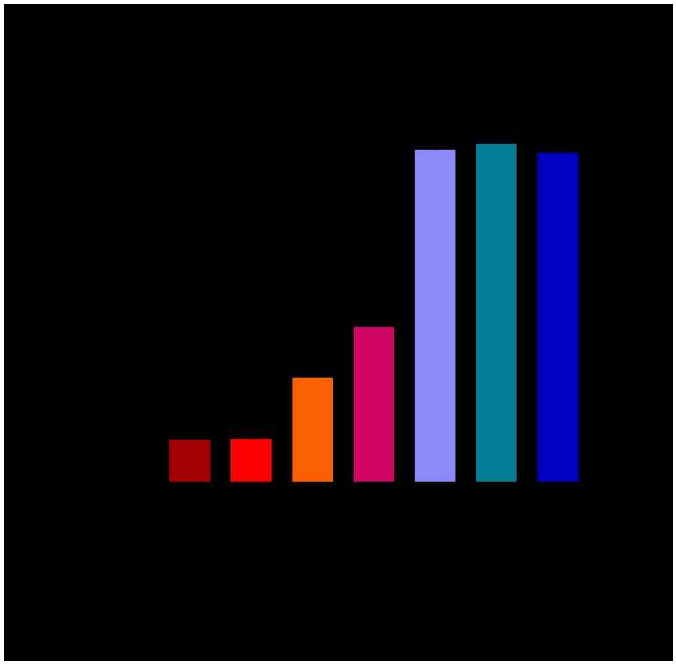

Figure 23: **A549 cells infected with PG II strains remain viable for longer periods of time**
A549 cells were infected at a MOI of 10.0 PFU/cell in biological triplicate. At 96 hours post infection, intracellular ATP concentration as a surrogate for cell viability. Statistical significance was assessed by one way ANOVA analysis, $F(7, 24) = 140.9$, $p < 0.0001$. Tukey's posthoc comparisons to mock-treated cells revealed a significant difference, **** $p < 0.0001$.

4.1.5 Summary of Results for Subaim 1

In summary, PG I and PG II strains have distinct *in vitro* growth and cell killing phenotypes. PG I strains had: 1. faster replication kinetics in A549 cells at early time points post infection, 2. increased viral progeny release in polarized Calu-3 cells, 3. larger plaque sizes, 4. an enhanced cell killing phenotype, and 5. an enhanced cell-to-cell spread phenotype compared to PG II strains.

4.1.6 Limitations of this Study

This study provides new data demonstrating that PG I and PG II strains have distinct *in vitro* phenotypes, however there are more questions that require attention. Firstly, the mechanisms underlying the observed phenotypes are not known and require further examination. For example, it is not known if PG I viruses have faster replication kinetics due to enhanced infectivity (more infectious virus particles enter cells) or due to differences in regulation of virus or cellular genes during infection. It is also not clear why PG II-infected cells remain viable for longer periods of time. Preliminary experiments examining apoptosis markers in PG I and PG II-infected cells were inconclusive (data not shown). Lastly, evaluation of these phenotypes in a broader range of cells lines, including primary lung epithelial cell lines, is needed. An exploratory experiment demonstrated an enhanced CPE phenotype in PG I-infected immortalized human bronchial epithelial cells (HBEC-2 cell line (206)) compared to PG II-infected cells (data not shown).

4.2 Subaim 2: To Compare the Pulmonary Pathogenic Phenotypes of HAdV-E4 PG I and PG II Genomic Variants in a Cotton Rat Model of HAdV Respiratory Infection

4.2.1 Description of the Animal Study Design

The cotton rat (*Sigmodon hispidus*) has been used to study pulmonary pathogenesis in association with adenovirus infection (110) as well as the contribution of E1 and E3-encoded proteins in pulmonary pathogenesis (62, 112). These studies exclusively used HAdV-C2 or HAdV-C5. A few other studies have examined viral pathogenesis of HAdV-E4 (207, 208), but none have examined the contribution of HAdV-E4 intratypic genetic variability to pulmonary pathogenesis.

Before using the cotton rat model, the ability of a cotton rat lung epithelial cell line (CRLC, ATCC PTA-3930) to support viral replication was examined. CRLC monolayers were infected at a MOI of 5.0 PFU/cell and total infectious virus yield was determined by plaque assays in A549 cells at various time points post infection. Replication for both the CL68578 PG I and NHRC 42606 PG II strains was observed (Figure 24). The yield of infectious virus was between 0.5 and 1.0 logs higher for the PG I strain at 12 and 24 hpi, recapitulating our observations in A549 cells (Figure 20).

In the *in vivo* study, 4-week-old female cotton rats (n=6 per group per day) were infected with $1.0x10^7$ PFU intranasally with either the CL68578 (PG I) strain or NHRC 42606 (PG II) strain. Animals were sacrificed at 1, 2, 3, and 6 dpi.

Lungs were harvested and processed for: 1. viral load by qPCR (left lobe), 2. histopathology (right lung), and 3. cytokine gene expression (left lingular).

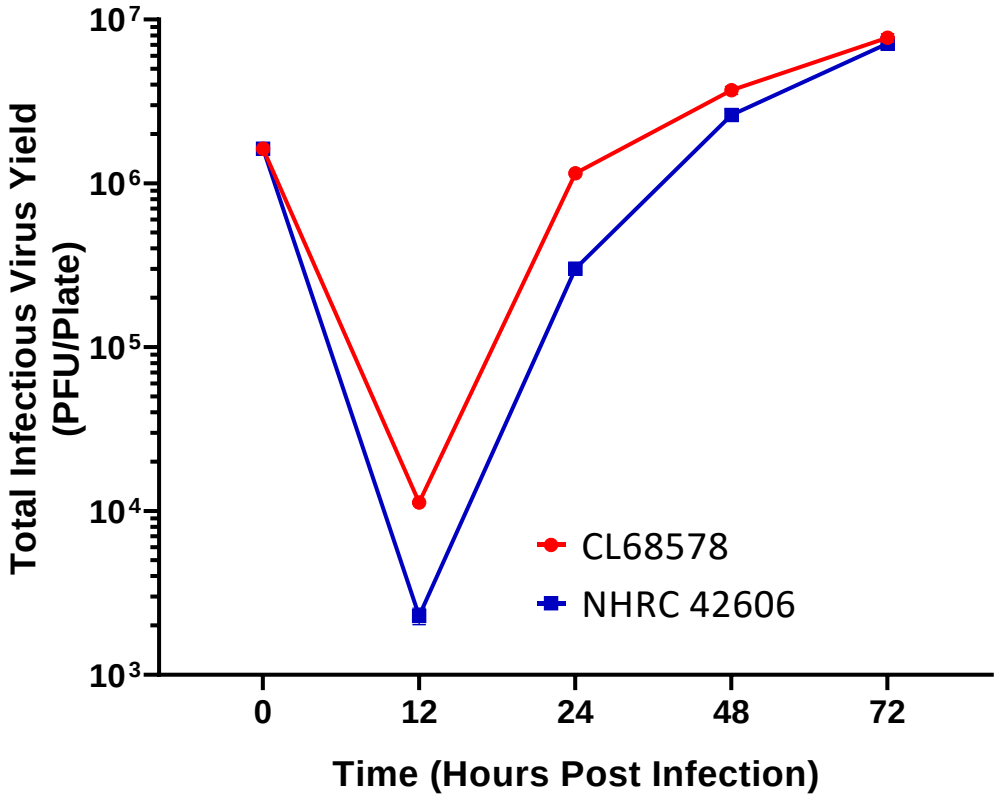

Figure 24: **Cotton rat lung cells support HAdV-E4 virus replication *in vitro*** Submerged CRLC monolayers were infected with PG I or PG II strains at a MOI of 5.0 PFU/cell in biological triplicate. Infectious virus yield was determined for the indicated time points by plaque assay in A549 cells.

4.2.2 Fatal Outcomes

Two cotton rats infected with the PG II strain succumbed to infection at 3 dpi. These animals were not available from tissue collection, and no postmortem examination was performed per standard operating procedure (SOP) at SBI.

4.2.3 Higher Viral Loads were Detected in the Lungs of Cotton Rats Infected with the PG I Strain

Viral load in the supernatants of lung homogenates was determined by qPCR analysis using a proprietary platform developed by DiaSorin Molecular LLC. Similar numbers of genome copies in the lungs of animals infected with either strain were observed at one day post infection (Figure 25). For the CL68578-infected animals, an increase in viral load was observed at 2 dpi with a gradual decline thereafter, indicating limited viral replication followed by clearance (Figure 25). In contrast, a continual decrease in viral genome copies in the lungs of animals infected with the PG II strain was observed at 2-6 dpi, suggesting rapid clearance following infection (Figure 25).

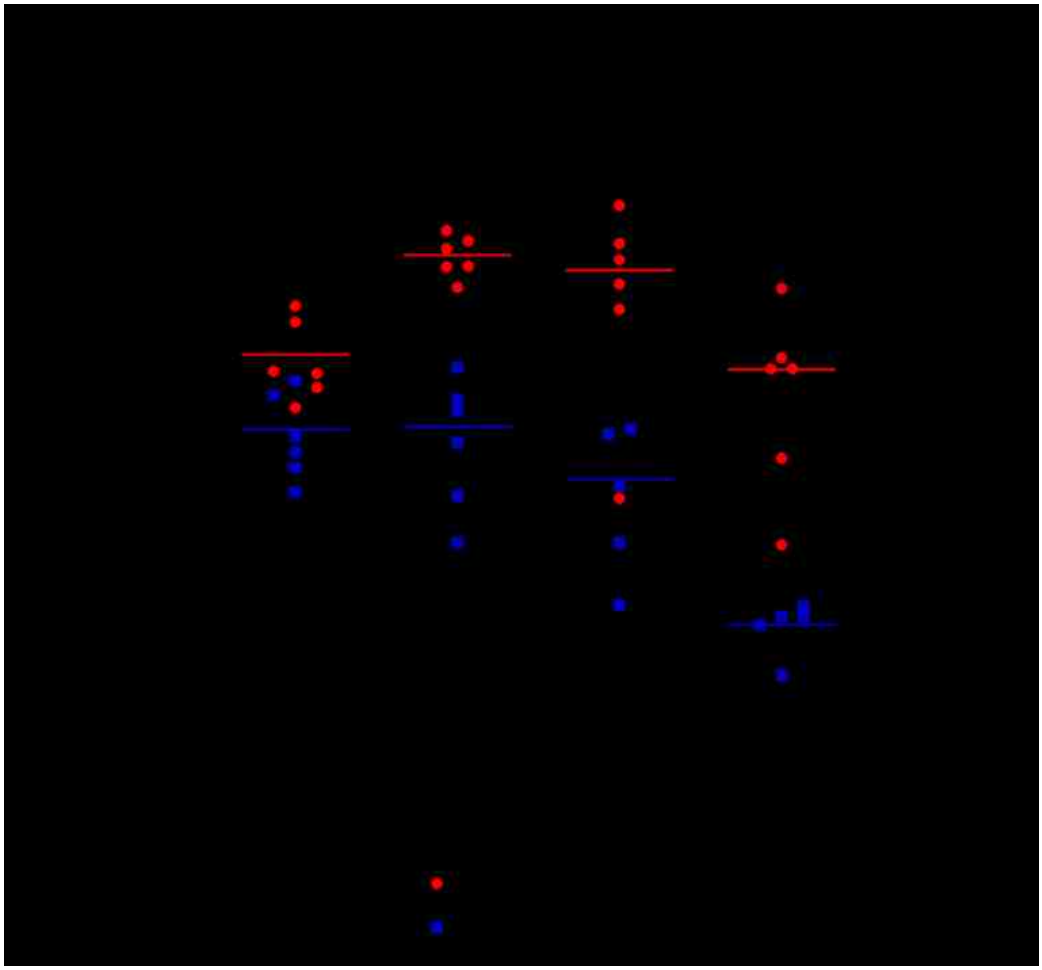

Figure 25: **Cotton rats infected with the PG I strain had higher pulmonary viral loads at 2, 3, and 6 days post infection**
The viral load was determined using a *proprietary qPCR platform developed by DiaSorin Molecular* from the supernatants of left lung homogenates from PG I and PG II-infected cotton rats at the indicated times post infection. Genome copy numbers were normalized to the mass of homogenized tissue. n = 6 for each group.

4.2.4 Cotton Rats Infected with the PG II strain Exhibited Enhanced Pulmonary Pathology than Animals Infected with the PG I Strain

To evaluate the extent of pulmonary pathology resulting from infection in cotton rats, the right lungs of mock-infected and HAdV-E4-infected cotton rats were fixed, sectioned, and stained with H&E. The following histological features were blindly scored by our collaborator Dr. Jorge Blanco at SBI: peribronchiolitis, perivasculitis, alveolitis, and interstitial pneumonia. Representative H&E-stained lung sections from animals sacrificed at 1 and 3 dpi are shown in Figure 26A-F. Animals infected with the NHRC 42606 strain exhibited significantly higher average combined pathology scores at 1, 2, and 3 dpi (Figure 26G). Specifically, NHRC 42606-infected cotton rats had higher average alveolitis and interstitial pneumonia scores, as well as a nonstatistically significant trend of higher perivasculitis scores (Figure 26G). In addition, the PG II strain-infected animals had higher average peribronchiolitis scores at 6 dpi. (Figure 26G). Qualitative examination of the sections at higher magnification revealed the majority of the infiltrating cells were polymorphonuclear cells and macrophages (data not shown), which is consistent with descriptions of pulmonary pathology of cotton rats infected with HAdV-C5 by Prince and colleagues (110).

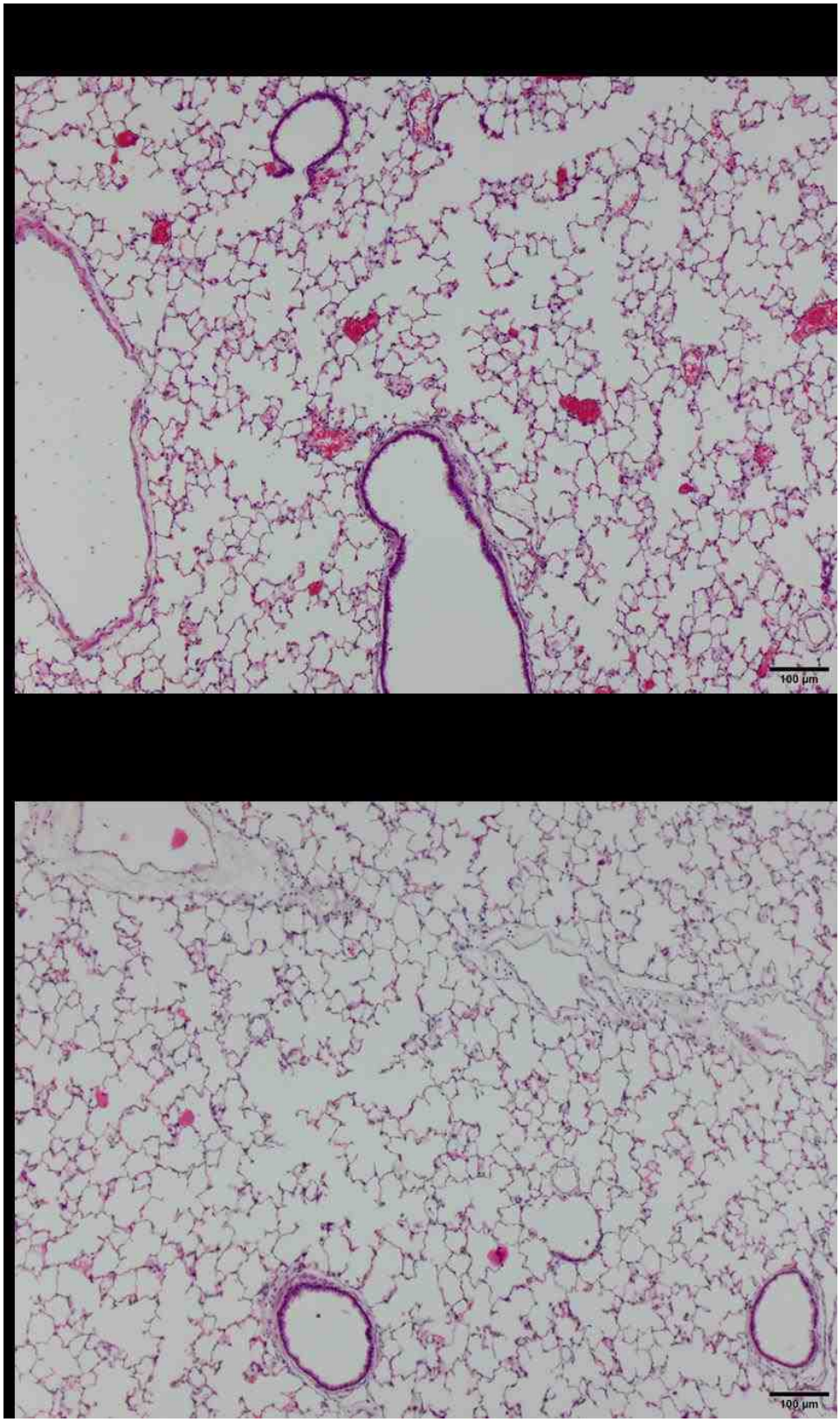

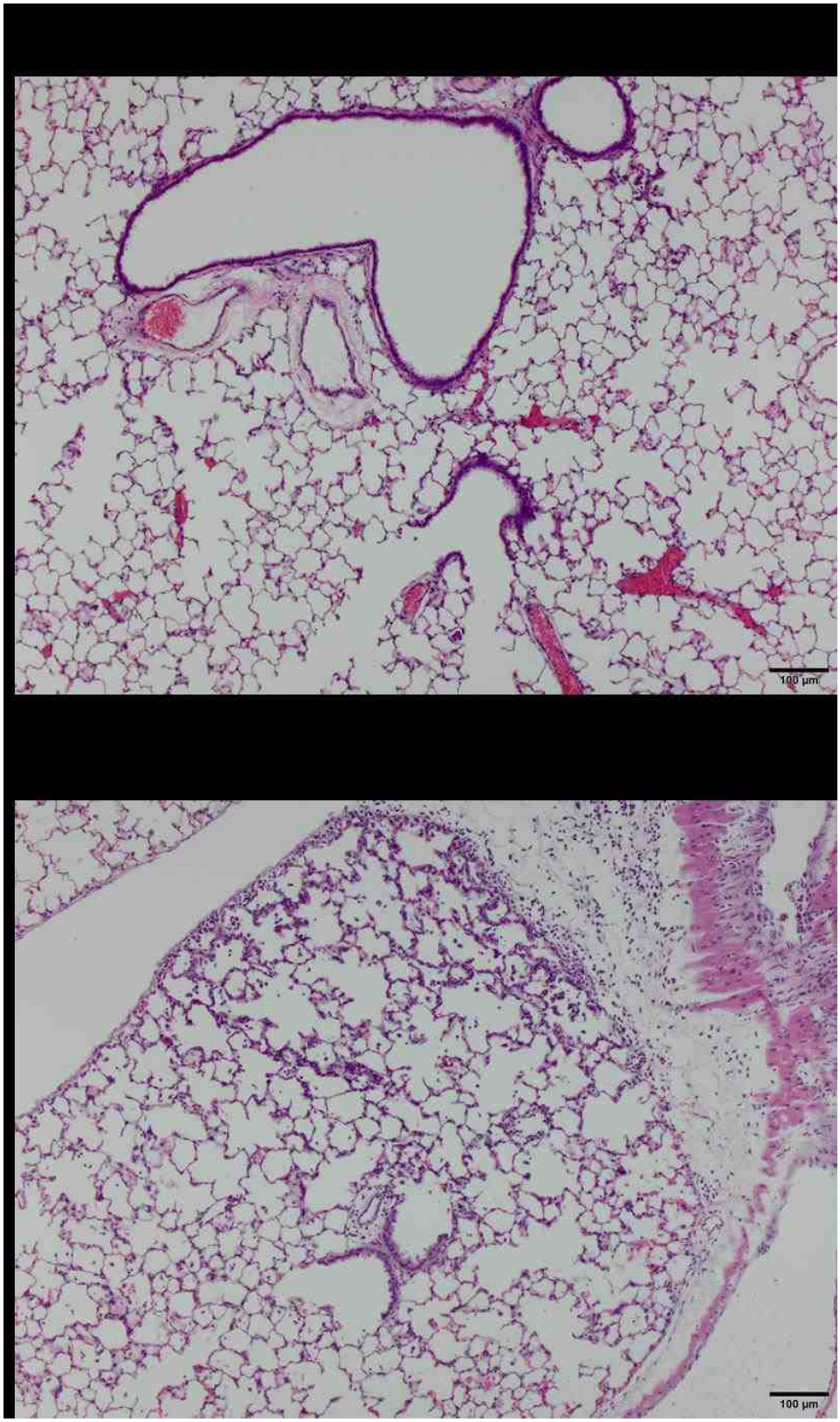

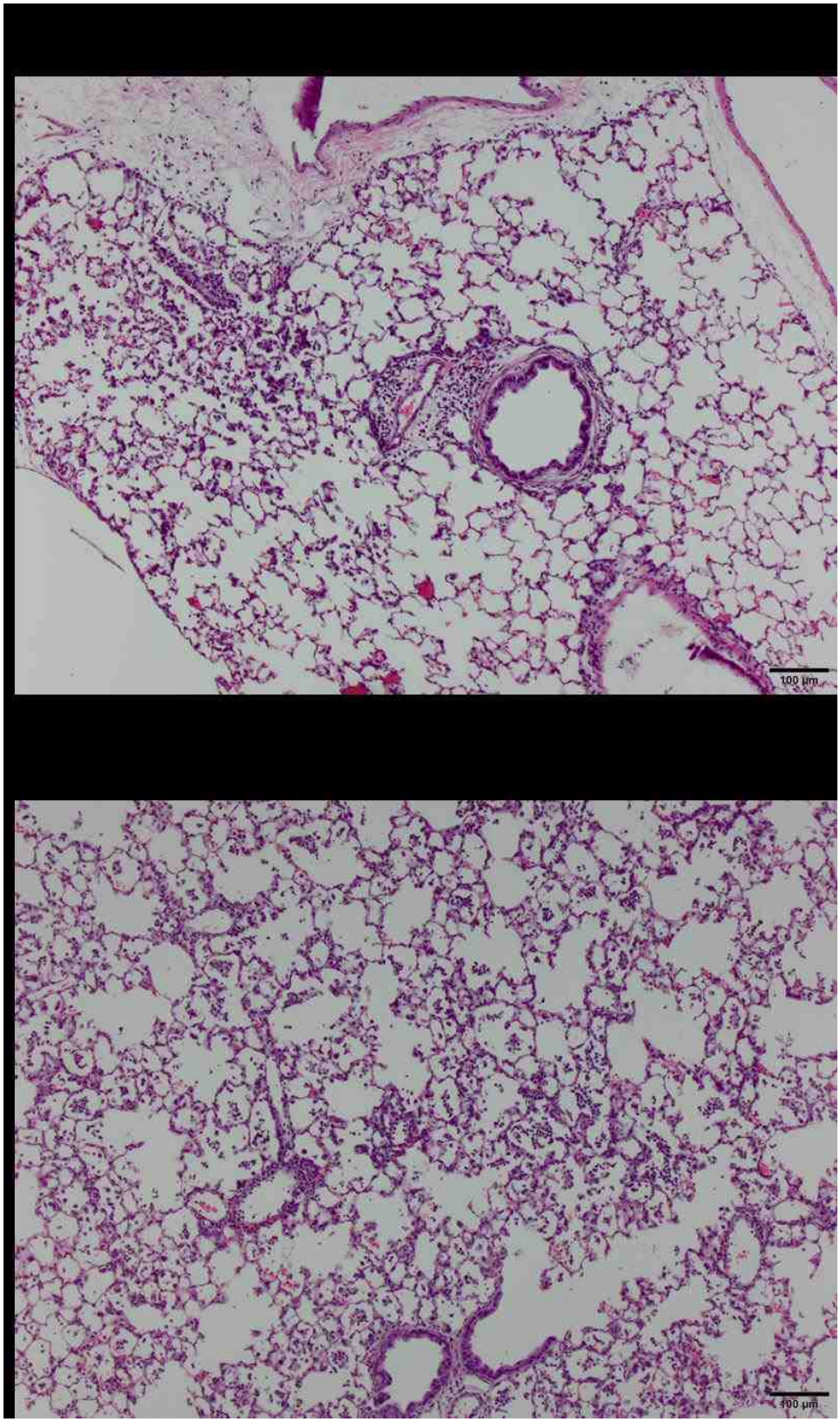

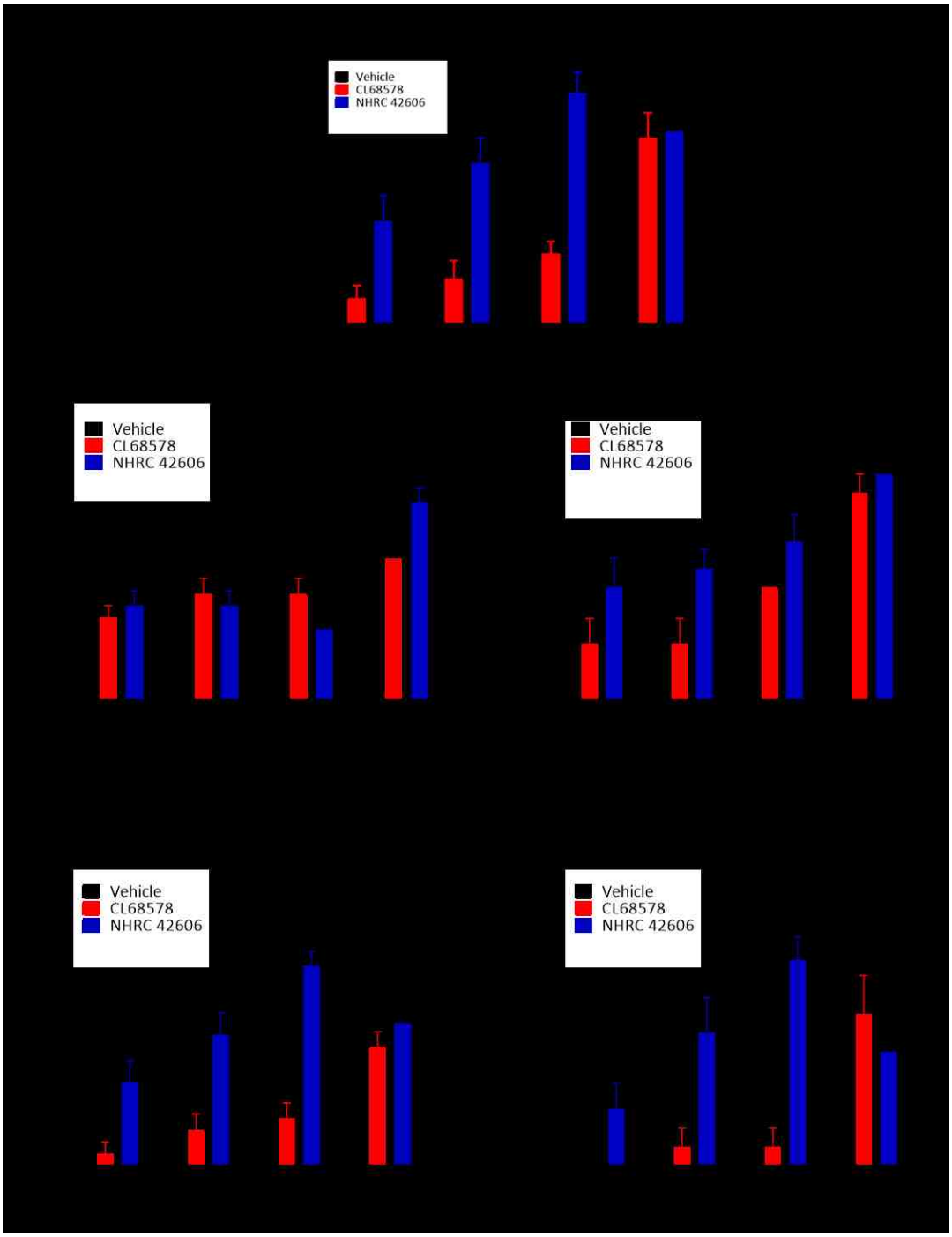

Figure 26: **Cotton rats infected with the PG II strain exhibited higher pulmonary pathology scores**
(A-F) The right lungs of mock or HAdV-E4-infected cotton rats were harvested and stained with hematoxylin and eosin for microscopic comparison of lung pathology: A, mock 1 dpi; B, mock 3 dpi; C, CL68578 1 dpi; D, NHRC 42606 1 dpi; E, CL68578 3 dpi; F, NHRC 42606 3 dpi. Scale = 100 μm. (G) Average pathology scores of hematoxylin and eosin-stained lung sections. n = 5-6, *p < 0.05, **p < 0.01, Mann-Whittney U test between CL68578 and NHRC 42606.

4.2.5 Higher Levels of Proinflammatory Cytokine Gene Expression Were Observed in Cotton Rats Infected With the PG II Strain at One Day Post Infection

The levels of proinflammatory cytokine gene expression in the lungs of infected animals were evaluated as reported for other models of respiratory viral infection (180, 181). At one day post infection, higher levels of proinflammatory chemokine gene expression was observed in the lungs of animals infected with the PG II virus including MCP-1, IP-10, and Rantes. (Figure 27). In addition, statistically higher levels of IL-6 and IFNβ transcripts were observed in animals infected with the NHRC 42606 strain (Figure 27). There was a nonsignificant difference in the transcript levels for TNFα and GRO. These results are consistent with the observation of increased cellular infiltrates in NHRC 42606-infected animals and the known function of GRO, MCP-1, IP-10, and Rantes as chemokines (209). Cytokine transcript levels were evaluated at all other time points, but levels were not found to be statistically different between groups.

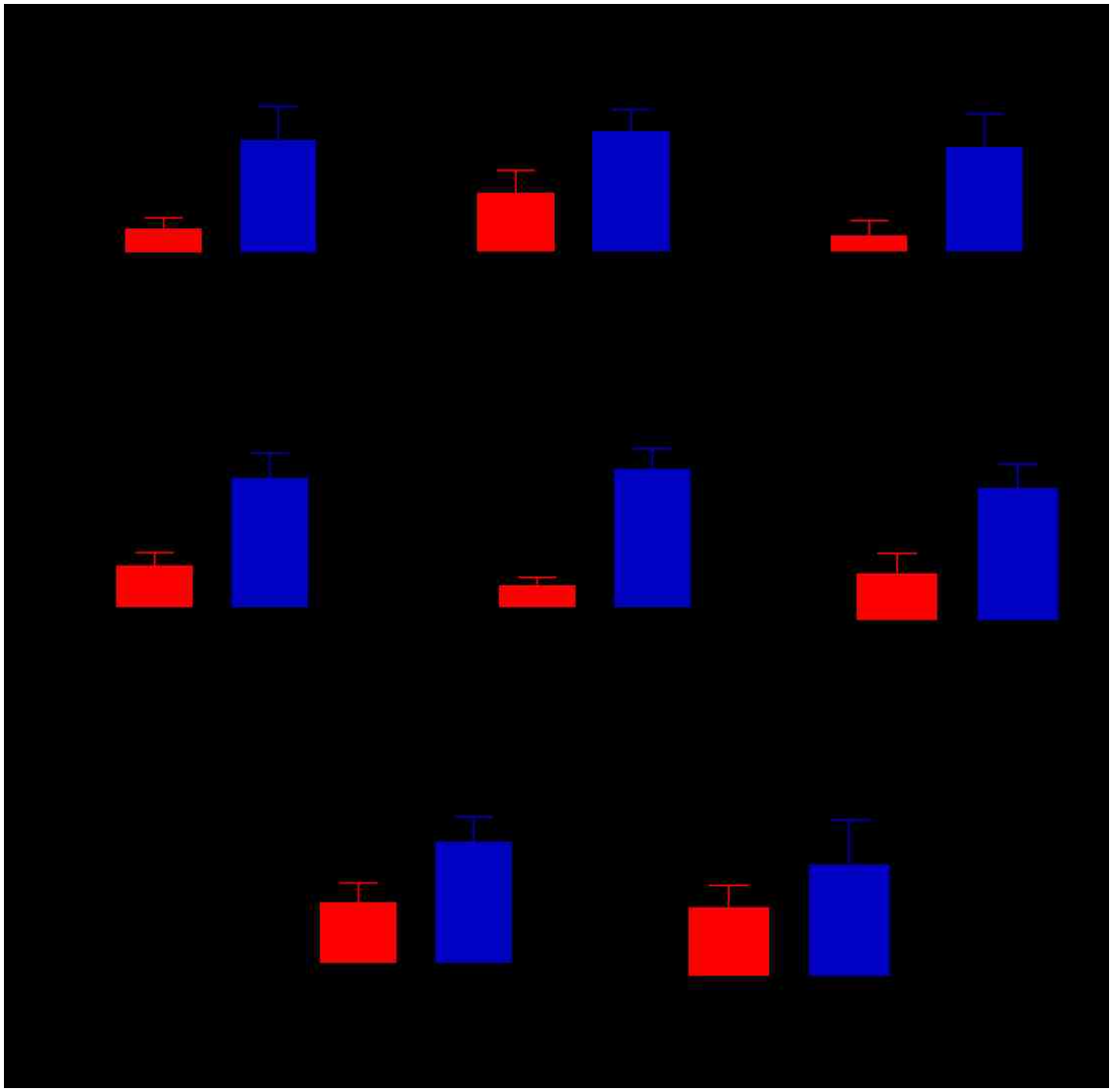

Figure 27**: Higher levels of proinflammatory cytokine gene expression were observed in cotton rats infected with the PG II strain at one day post infection**
The levels of proinflammatory cytokine gene expression from the lungs of HAdV-E4- or mock-infected cotton rats were determined by RT-qPCR.
n = 5-6, $p < 0.05$ Student's *t* test. n=6 for each group.

4.2.6 Summary of Results for Subaim 2

HAdV-E4 strains representative of PG I and PG II exhibited different replication kinetics and associated pulmonary pathology in a cotton rat model of

HAdV respiratory infection. Viral load in the lungs of cotton rats infected with the PG I strain CL68578 increased at 2 dpi and declined thereafter. In contrast, pulmonary viral load in animals infected with the PG II strain NHRC 42606 decreased steadily through day 6, suggesting rapid clearance. Interestingly, animals infected with the NHRC 42606 strain exhibited more severe pulmonary pathology and higher levels of proinflammatory cytokine gene expression compared with animals infected with the CL68578 strain. Additionally, fatalities were only documented in animals infected with the PG II strain.

4.2.7 Limitations of this Study

This cotton rat model of HAdV-E4 respiratory infection provides novel insights into the contribution of HAdV-E4 genetic variability on viral pathogenesis, however, additional experiments are needed. First, it will be important to evaluate differences in replication and pathology in both male and female animals. Next, while this study exclusively examined pulmonary pathogenesis, there are other organs and portions of the respiratory tract that should also be examined for pathogenesis and infection such as the liver, lymph nodes, nasal cavity, and trachea. Also, the cause of death of animals infected with the PG II strain is not known. From the data of the animals that were sacrificed, it is assumed that they succumbed to infection, possibly from pulmonary complications resulting from inflammation. Postmortem examination of these animals would have been informative. Furthermore, monitoring the animals for signs of illness, such as weight loss, would also have been informative. Lastly, the cellular source of

proinflammatory cytokine gene expression during infection is not known. In mice, alveolar macrophages, not epithelial cells, were found to secrete cytokines (210). Studies using *in situ* hybridization of sectioned lung tissue could provide insight into which cell type(s) produce cytokines at early time points post infection. Future work will also include immunohistochemical staining for HAdV structural proteins to identify which pulmonary cell types are infected.

Chapter 5 – Summary of Findings and Discussion

5.1 HAdV-E4 Strains Isolated Between 1953 and 2015 Comprise Two Distinct PGs That Have Been Evolving Independently for ~602 Years

In this study the HAdV-E4 intratypic genetic variability was examined by bioinformatics analysis of WGS of a collection of strains isolated worldwide between 1953 and 2015. This analysis confirmed the previous observation by Li and Wadell in 1988 that HAdV-E4 strains cluster into two distinct evolutionary linages (149). This observation was based on RFLP analysis and assessment of the PCRF. While PCRF analysis is a low resolution technique (21), it was, at the time, the only available tool to compare HAdV-E4 genomes. Dehghan and colleagues also reported distinct phylogenetic clustering of HAdV-E4 strains (115). The lack of available WGS for a larger sample of HAdV-E4 strains was a major limitation of their study which included only four strains.

In the present study, WGS of 45 unique HAdV-E4 strains were compared, making this analysis of HAdV-E4 genetic variability the most extensive conducted to date. Data from this study also demonstrate the existence of two distinct clades of HAdV-E4 strains. Both phylogroups (PGs) have very similar intra-PG sequence identity.

The origins of HAdV-E4 are still debated between researchers in the AdV research community. It has been suggested that because both PG I and PG II strains have a genome chassis composed 97% of a SAdV26-like genome with a hexon containing loops 1 and 2 from HAdV-B16, they originated from an

interspecies recombination event (115). What has not been elucidated yet is the estimated timeline of circulation of PG I and PG II strains in human populations and divergence from a common ancestor. The conclusion that PG II strains originated from a PG I strain (due to the isolation of PG I strains predating those of PG II) may be premature (155, 185), as close inspection of PG I and SAdV WGS separately from PG II and SAdV sequences reveals distinct differences. As an example, the E1A amino acid sequence identity for PG I strains is closer to SAdV26 than PG II strains due to the 11 amino acid deletion observed in PG II sequences. Conversely, sequence identity of the E1B 19K protein is closer for PG II and SAdV strains as a result of the 11 amino acid deletion in the PG I strains. Other evidence, including the differences in the vestigial E3 CR1γ region, suggest at the very least that PG I and PG II strains have been evolving independently for some time. In agreement with this, Bayesian analysis of the tMRCA estimates that these PGs diverged 602 ybp and have been evolving independently since then. The isolation of BC 129, the oldest recorded PG II strain, dates 13 years before the oldest PG II strain in our collection (V0014, see Table 4). This suggests that PG I and PG II strains may have been circulating for similar periods of time, and the estimated tMRCA would be more accurate if the whole genomic sequence for BC 129 was available. Additionally, describing PG I and PG II strains as “old” and “new” strains, respectively (155), or as “emerging” (199) is misleading because they likely have been cocirculating in human populations for a long period of time but went undetected until the 1950s and 1960s. Furthermore, it is likely there are many unreported infections and

outbreaks due to a lack of robust surveillance programs monitoring HAdV outbreaks and the generally self-limiting nature of HAdV-E4 infections.

I hypothesize that the higher mutation rate observed in PG II strains is due to a higher number of infections by PG II that increased the overall frequency of mutations despite a similar mutation rate in each replication cycle. The documented higher frequency of isolation of PG II strains from cases of HAdV-E4-associated disease suggests that these viruses may have a higher level of viral fitness or may be more virulent.

5.2 Strains of PG I and PG II Differ in Their *in vitro* and *in vivo* Phenotypes Relevant that are to Pathogenesis

Analysis of 45 HAdV-E4 WGS showed that PG I and PG II strains share approximately 94.5% sequence identity. This study identified differences in coding and noncoding regions among PG I and PG II genomes. The discussion of the implications of these genetic differences for the observed *in vitro* and *in vivo* phenotypes is detailed below.

PG I strains, particularly the CL68578 vaccine strain, form larger plaques, have enhanced virus spread and cell killing phenotypes, and have faster replication kinetics compared to PG II strains. Interestingly, variability in these phenotypes was observed among PG I strains. The CL68578 strain formed the largest plaques and had the fastest plaque development rate compared to any other strain tested. Intermediate phenotypes were also observed for other PG I strains in cell viability assays. The PG I strains CL68578 and RI-67 strains were

isolated within a period of nine years (see Table 4) and are 99.95% identical. The genomes have only 20 nucleotide differences, 12 of which map to the ITRs (although the ITR regions for CL68578 and the RI-67 ATCC VR-1572 stock are identical). The other differences are located in E2B, late region 1 (L1), L3, and L4. The only nonsynonymous mutations distinguishing both strains map to the L4-100K CDS (T357I) and an in frame three nucleotide insertion (alanine) in the vaccine strain in the L4-33K CDS. This alanine insertion is also present in all the PG II strains. At present, it is unclear which of these differences contributes to the plaque phenotype. It is also unclear if these *in vitro* differences will translate to differences in pathogenicity in the cotton rat model. As reported by Kajon and colleagues, only 10 point mutations distinguish the PG I strain NY-15-4054 from the CL68578 vaccine strain (128). Slightly different cell killing and plaque size phenotypes were observed between these two strains. The NHRC 90339 strain, a 4p4 variant (139), is 99.66% identical to the vaccine strain, showing the highest level of divergence of any of the PG I strains. Additionally, this strain also had the smallest plaques of any PG I strain. The growth phenotype among all PG I strains, however, was similar.

Interestingly, no phenotypic differences were observed between the PG II strains in plaque size, cell killing, virus spread, or replication kinetics (Figures 15-18 and 21). PG II strains have an average intra-group sequence identity of 99.88% compared to the earliest isolated PG II strain in our collection, strain 13. The only noticeable difference among the PG II genomes was a 194 bp insertion adjacent to the right hand ITR in strain 29. This strain was not included in the

panel of viruses for the *in vitro* or *in vivo* studies, so the implications of this insertion for replication remains to be evaluated. It is interesting that while *in vitro* phenotypic variability in PG I strains with an overall similar inter-PG I percent sequence identity was observed, no phenotypic differences were observed among PG II strains. It is possible that our assays were not sensitive enough to detect subtle phenotypic differences between PG II strains.

The genetic determinants of the large plaque phenotype observed among PG I strains are unknown. Large plaque phenotypes can be a result of several factors, including virus replication and enhanced cell killing (69). The results from the studies described in this dissertation suggest that the large plaque phenotype of PG I strains may be a result of both mechanisms. Growth curve experiments show a lag in virus replication among PG II strains at 24 hpi, although infectious titers were comparable at 48 and 72 hpi. Additionally, more infectious virus was detected in the apical compartment of infected Calu-3 cells. Enhanced replication kinetics can be attributed to the genetic makeup at several regions of the HAdV genome, including the ITRs and E1A.

Mutations in the ITR sequences have been shown to affect viral replication. Wunderlich and colleagues reported that a change in the terminal 8 bp of the ITR sequences (5'-CATCATCA-3' to 5'-CTATCTAT-3') can dramatically improve viral replication efficiency of E1-depleted HAdV-B35 vector using E1 complementing cell lines (211). Additionally, they report that the majority of human and nonhuman AdVs carry the "original" 5'-CATCATCA-3' terminal sequence with some reported sequences carrying "alternate" ITRs (211). The

present study reports differences in HAdV-E4 ITR sequences. Specifically, the RI-67 strain contains a variant 5'-CTATCTAT-3' sequence while CL68578 and most others carry the 5'-CATCATCA-3'. In addition, a minority of HAdV-E4 strains examined in this study have various other sequences (Figure 10). Wunderlich and colleagues demonstrated that their recombinant HAdV-B35 vector with the 5'-CTATCTAT-3' terminus replicated faster than a vector encoding the terminal 5'-CATCATCA-3' sequence (211). In the present studies, the RI-67 strain replicates similarly in culture to CL68578, although the vaccine strain exhibits larger plaque sizes. The strains with other alternate terminal sequences were not used in *in vitro* studies, so it remains to be seen if these noncanonical sequences contribute to differences in the replication phenotype. It is important to note that some of these variant sequences carry trinucleotide terminal direct repeats (for example 5'-**AATAAT**AT-3' or 5'-**ATAATA**TA-3') which are important in the "jumping-back" mechanism of replication proposed by King and van der Vliet (212, 213). Some alternative sequences do not have a terminal direct repeat, which may indicate limitations in the sequencing technology used. Wunderlich and colleagues could not recapitulate this phenotype when manipulating the ITR sequence of a recombinant HAdV-C5 vector, which may indicate that the enhanced growth kinetics phenotype documented for the 5'-CTATCTAT-3' sequence may be limited to HAdV-B35.

Dehghan and colleagues identified differences in the nuclear factor recognition sites among a small sample size of PG I and PG II genomes. They found that the NFI recognition site in PG II ITRs is remarkably similar to those in

HAdV-B genomes and suggested that this “adapted” NFI binding site may enhance replication (115). This hypothesis was again stated in another study describing recent HAdV-E4 viruses circulating in China (199). Conserved NFI and NFIII transcription factor binding sites in HAdV ITRs have been shown to enhance replication *in vitro*. However, these binding sites in PG I ITRs are not required for replication and only the terminal 18bp of the ITR is necessary for initiation of replication (77, 78). Instead, an unidentified nuclear factor from a HeLa cell extract enhanced *in vitro* replication, suggesting a different mechanism (77). It is possible that the PG II ITR, with an “adapted” NFI site, might enhance initiation and subsequent replication better than the PG I ITR, however, there are no reports that have compared PG I and PG II ITR initiation *in vitro*. The work presented in this dissertation suggests that PG I strains replicate more efficiently *in vitro* and *in vivo*, although this phenotype cannot specifically be attributed to the ITR, as numerous sequence differences throughout PG I and PG II genomes were identified, many of which were in regions that have been shown to affect viral replication.

Using HAdV-C as a model, it has been demonstrated that mutations in conserved regions in E1A leads to inefficient stimulation of other early viral genes and stunts replication at low MOIs (214). The bioinformatics analysis of the E1A gene conducted in this study identified an 11 amino acid deletion in all PG II genomes between CR1 and CR2. This region is highly variable among the species of HAdV and no specific function has been attributed to the residues in this region. There are several residues, however, that are conserved among the

different species in this region, including a leucine at position 91 and a threonine at position 93, that have not been associated with any particular function. Several publications have shown that variation in E1A between HAdV-E4 and other HAdV species results in differential interaction with cellular factors (189, 215, 216). These studies only used PG I E1A proteins, and follow up studies with E1A from PG II strains would be necessary to elucidate if there are differences between species in E1A binding to cellular proteins.

Enhanced cell killing can also result in a large plaque phenotype. Two important genes that influence plaque size as a result of cell killing are the HAdV-C-specific ADP proteins and E1B 19K. ADP has been shown to promote viral progeny release in WT viruses (69, 87) and its overexpression greatly enhances this characteristic (202, 203). The mechanism of action of ADP remains to be elucidated. HAdV-E4 strains do not encode the ADP gene, and mutant PG I strains (derived from the CL68578 strain) which do not encode the HAdV-E4-specific E3 CR1 proteins (located in the same region as ADP in HAdV-C) do not exhibit a reduction in plaque size or slower replication kinetics (data not shown).

Using random UV mutagenesis of the ADP-null mutant (strain dl327), Subramanian and colleagues isolated large plaque mutants. They determined that 62% of these viruses had mutations in the E1B 19K gene. Dysregulation of the apoptosis pathway led to increased cell lysis (89). Radke and colleagues also discovered decreased E1B 19K expression in a HAdV-B14p1 strain compared to the HAdV-B14p strain also led to larger plaque size, although the specific mechanism was not elucidated (90). While sequence divergence among AdV

types has been noted for the E1B polypeptides (187, 217, 218), the effect of variation in E1B promoter activity (219) and the functional differences of E1B 19K and E1B 55K proteins among the different HAdV species have only been examined to a limited extent (187, 220–222). For HAdV-E4, differences in the E1B coding regions map to regions that are not well conserved among the HAdV species (217), and future work will be needed to elucidate the contribution of mutations, if any, to the function of the E1B-encoded proteins during infection.

Higher levels of pulmonary pathology were observed in cotton rats infected with the PG II strain NHRC 42606 compared to the PG I vaccine strain. There are several explanations for this result. One hypothesis is that animals infected with the PG II strain may not express high levels of HAdV-E4-encoded immunomodulatory proteins as a result of decreased viral replication. In the cotton rat studies, an increase in viral load at 2 dpi in animals infected with the PG I strain was observed, followed by a steady decline thereafter. In contrast, there was no increase at any time point in viral load in lungs of animals infected with the PG II strain. Immunomodulatory functions are encoded in several regions of the genome, including E1, E3, E4, and VA RNA (55). It has been shown that prevention of AdV genome replication suppressed E3 gene expression (223). Therefore, increased viral replication would result in increased levels of the early and late gene products, and thereby have a greater effect in modulating the host response to infection.

Another explanation may be that the genetic variability in the genes that modulate the host response to infection affects pathogenicity. The specific impact

of the genetic variability in E1, E3, L4, and VA RNA on their function is not known. The CR1 region of the E1A as well as E1B 55K are known to potently block expression of interferon-stimulated genes (ISGs) (224–226). These functions have never been tested for HAdV-E4 strains, and further work will be needed to characterize differences, if any, between PG I and PG II strains in modulation of ISG expression. E4 ORF3 acts to block promyelocytic leukemia protein (PML) body formation and antagonizes the IFN response (58, 227, 228). In the present study, however, no significant difference in this coding region was observed.

The noncoding VA RNAs antagonize PKR activation and saturate the DICER complex (55, 229). While mutation of the HAdV-C5 VA RNAs results in a 60 fold decrease in viral titers, only a 20 fold decrease was seen when VA RNAI alone was deleted, and no measurable difference was observed when only VA RNAII was deleted (72, 190). This appears to be the result of limited levels of Pol III during the late phase of infection with the consequence of preferential transcription of VA RNAI (190). Studies examining the effects of HAdV-E4 VA RNAs have not been reported and would be important for the elucidation of the role of each VA RNA in replication. This work also identified differences in VA RNAII for 4p4 PG I genomic variants, including partial deletion of one of the protomer elements. Further experiments are needed to elucidate the impact of this mutation on transcription of VA RNAII. It is possible that reduced IFN antagonism by VA RNAs of PG II strains could elicit a stronger immune response and will need to be evaluated in an animal model.

The major neutralizing epitopes for HAdVs are located in the major structural proteins: hexon, penton base, and fiber (230–233). Hexon evolution is driven by illegitimate recombination and mutations caused by polymerase slippage in the HVR 1-7 regions (192). This work identified several synonymous and nonsynonymous mutations in HVR 1 and 3-7 that distinguish PG I and PG II strains. The impact of this genetic drift observed among HAdV-E4 strains is unknown, and likely doesn't impact the observed *in vitro* and *in vivo* phenotypes. Recently, Tian and colleagues published the identification of a neutralizing epitope for the HAdV-E4 hexon in HVR 7 (234). This epitope was conserved among all 45 HAdV-E4 strains examined in the present study (data not shown). In VN assays, PG II strains are neutralized with antisera raised against the PG I strain RI-67 (123, 125, 126), although Crawford-Miksza and colleagues reported a fourfold reduction in neutralization in a PG II strain (169). The present work identifying additional differences in the hexon HVR regions provides the rationale for additional VN tests encompassing a more comprehensive panel of HAdV-E4 strains.

The multifunctional L4-100K protein aids in hexon trimerization (84), efficient translation of late mRNAs (235, 236), and prevents granzyme B-mediated cell death (237). Each of these functions is important in virus replication. PG I and PG II genomes exhibit differences in the GAR region of the L4-100K protein, which may affect the methylation state of the protein. Disruption of these methylation sites negatively impacts viral replication for HAdV-C5 (196, 238). The methylation state for HAdV-E4 strains has not been determined and

future work is needed to identify if genomic differences in the L4-100K coding region affects virus replication.

The proteins encoded in E3 also modulate the host response to infection in a variety of ways as previously discussed. The most dramatic differences in E3 for HAdV-E4 map to the species-specific E3 CR1 genes, E3 CR1β and E3 CR1δ. Martinez-Martin and colleagues demonstrated physical interaction between the ectodomain of E3 CR1β and the host LILRB1 protein, which could have implications on the activation of NK cells (71). The implication of intratypic genetic differences in E3 CR1β are currently not known. While the function of E3 CR1δ has not been reported, preliminary work in our laboratory using a E3 CR1δ KO mutant in a genomic clone of the CL68578 strain has showed that it may be involved in modulating the inflammatory response in our cotton rat model (data not shown). Further work is needed to characterize the differences, if any, in pulmonary inflammation between the PG I and PG II-encoded E3 CR1δ. Previously, marked increase in peribronchiolitis, perivasculitis, and alveolitis scores were observed in cotton rats infected with a HAdV-C E3 gp/19K mutant compared to the WT control (62). PG I and PG II strains show conservation in the gp/19K polypeptide, including conserved cysteines thought to be important for the function of the HAdV-C5-encoded protein (239). Further biochemical characterization will be needed to determine if there is a difference among HAdV-E4 strains in the ability to sequester MHC I molecules in the ER.

Few studies have correlated HAdV intratypic genetic differences to *in vitro* or *in vivo* phenotypes. Using the Syrian hamster model, Radke and colleagues

found that a HAdV-B14p1 strain, which produced larger plaques *in vitro,* elicited a markedly higher inflammatory response in the lungs compared to the HAdV-B14p strain. The authors attributed this result to reduced E1B 19K expression by the HAdV-B14p1 strain. They showed that fixed HAdV-B14p1-infected A549 cells stimulate a strong NF-κB-dependent cytokine response from macrophages in culture and observed higher amounts of infiltrating immune cells in the alveolar, peribronchiolar, and perivascular spaces in their animal model (90). The work presented in this dissertation using the cotton rat model of HAdV-E4 respiratory infection produced the opposite result: the PG II strain (small plaques) elicited a stronger inflammatory response in the lungs than the PG I strain (large plaques). Additionally, higher levels of cytokine gene expression in the lungs of animals infected with the PG II virus was observed. It is likely that the mechanisms underlying the phenotypes observed in our studies and those reported by Radke and colleagues for HAdV-B are different.

Another example of correlating *in vitro* and *in vivo* phenotypes is HAdV-C ADP laboratory mutants. There is ample evidence in the literature demonstrating differences in plaque size and cell killing phenotypes among WT and ADP-mutants (69, 87). Ginsberg and colleagues did not observe a difference in pneumonia of cotton rats infected with an ADP mutant (62). This suggests that increased cell lysis due to the activity of ADP did not trigger a stronger inflammatory response compared to the ADP-null mutant, although cellular lysis due to ADP was not specifically addressed by Ginsberg and colleagues using this model (62). In agreement with this, Tollefson and colleagues hypothesized

that an apoptosis-like mechanism is responsible for ADP-dependent cell death in HAdV-infected cells (69). HAdV-E4 strains do not seem to encode an ADP-like CR1 protein. Furthermore, the mechanism of cell death is currently not known for HAdV-E4 strains, and further work will be needed to determine if cell death from PG II virus-infected cells is proinflammatory compared to PG I virus-infected cells.

5.3 Future Directions

This work builds the foundation for future investigation into the molecular basis of HAdV-E4 pathogenesis. This work has identified distinct phenotypic differences between PG I and PG II strains in cell culture regarding plaque size and development, growth kinetics, viral progeny release, and cell killing as well as differences in pathogenesis in a cotton rat model of HAdV respiratory infection. The gene product(s) that contribute to these *in vitro* and *in vivo* phenotypes are unknown. The most straightforward way to address this question is assessment of these phenotypes using isogenic mutant viruses.

I propose the use of the PG I CL68578 genome clone, pVQ WT #11183 which our laboratory has obtained under material transfer agreement with Advanced Bioscience Laboratories Inc.. The protocols for constructing mutant viruses in our laboratory have already been established and a cartoon schematic of this process is shown in Figure 28. Briefly, a shuttle plasmid containing the target region of interest (ROI) from a HAdV-E4 genomic variant is obtained either by conventional cloning techniques using purified PG II DNA, or it is

commercially synthesized. Recombination of the ROI from the shuttle into the PG I genomic clone is then performed using commercially available homologous recombination-competent E. coli cells. This new mutant genomic clone is then linearized to remove the pBR322 low copy plasmid sequence and transfected into A549 cells. Infectious supernatants from freeze-thawed cell culture material are then serially passaged in A549 cells until high titers of virus are obtained.

I propose the construction of several mutant PG I viruses that encode PG II ROIs to elucidate the molecular basis of HAdV-E4 pathogenesis. The candidate ROIs include genes in the following regions: E1A, E1B, L4, and E3. In addition, I propose the construction of mutant PG I viruses that carry the PG II sequences for the ITR and VA RNAII. E1A is a potent transactivator of viral early gene transcription (41, 42). Growth experiments showed higher levels of PG I infectious virus at early time points, which may indicate deficiencies in early gene expression in PG II viruses. Mutations in the ITR regions also affect virus replication kinetics (211, 240), and substitution of the PG II ITR into the PG I backbone may be sufficient for decreased replication kinetics *in vitro*. E1B 19K and E1B 55K are potent inhibitors of apoptosis, and decreased E1B 19K gene expression has been shown to increase apoptosis (90, 241). Viruses with mutations in E1B 19K have been shown to exhibit larger plaque sizes (89, 90). PG I viruses have larger plaque sizes, which may suggest decreased E1B 19K expression. L4-100K is an important regulator of late gene expression (235), and disruption of arginine methylation negatively affects replication (196). Differences in the L4-100K coding region affecting post-translational methylation could

explain faster replication kinetics among PG I. E1A, E1B, E3, and VA RNA modulate the host response to infection (59, 224, 225, 242, 243), and differences in these regions may contribute to the increased pulmonary inflammation observed in cotton rats infected with the PG II strain.

It is possible that differences in multiple coding regions contribute to the *in vitro* and *in vivo* phenotypes observed in these studies. Differences in phenotypes from isogenic laboratory mutant viruses are attributed to the gene or region that is manipulated. The viruses tested in this study are naturally occurring variants with multiple differences across the entire genome, and multiple loci may be contributing to the observed phenotypes. For example, differences in E1A, E1B, E3, and VA RNA are present among PG I and PG II strains, and the reduction in the pulmonary inflammatory response observed among PG I strains may be a result of a synergistic contribution of one or more of these coding regions. Another example is the mechanisms that underly the large plaque phenotype observed in AdVs. It is possible that PG I strains induce apoptosis to a greater extent than PG II strains via differences in E1A and simultaneously have limited expression of E1B which prevents apoptosis. Therefore, the reduction of plaque size may only be readily observed when mutating both the E1A and E1B regions. As previously mentioned, multiple coding and noncoding regions of the genome affect virus replication, and manipulation of multiple loci in the PG II genome may be needed to observe the PG II phenotype.

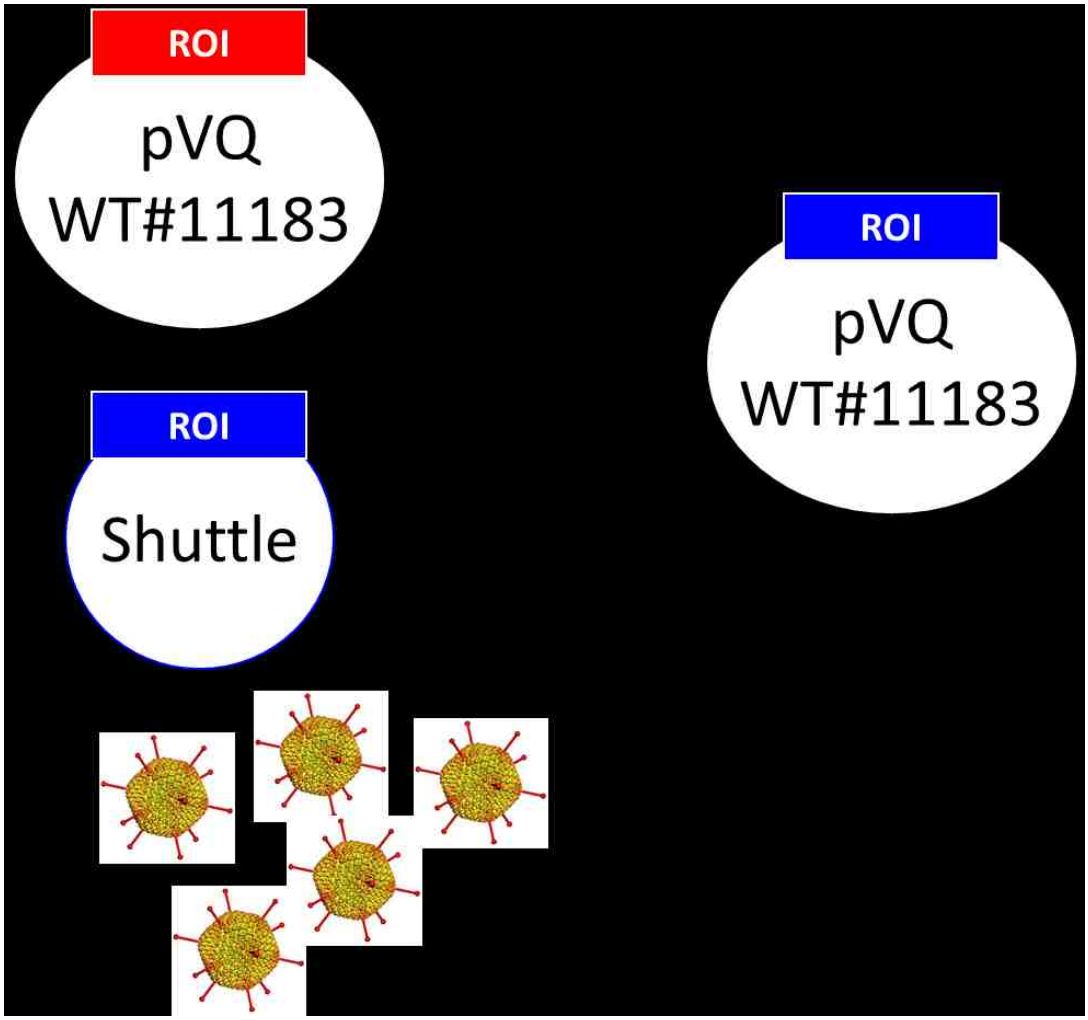

Figure 28: **Mutant HAdV-E4 construction strategy**
The PG I CL68578 genome is available in a genomic clone (pVQ WT#11183). A shuttle plasmid is constructed either using conventional cloning from purified PG II virus DNA or commercially synthesized and contains the PG II sequence for a region of interest (ROI). Homologous recombination is then performed using commercially available homologous recombination-competent E. coli cells to recombine the PG II ROI into the PG I backbone. The new mutant genomic clone is then linearized using the PacI restriction endonuclease to remove the bacterial plasmid sequence and transfected into A549 cells. After several passages in A549 cells, high titers of virus are produced.

5.4 Perspectives

This work provides novel insights into the magnitude and spectrum of HAdV-E4 intratypic genetic variability and reveals differences in phenotypes that are relevant to pathogenesis. HAdV-E4 genome variants, distinguishable by RFLP analysis or by comparison of WGS, cluster into two distinct evolutionary lineages which share approximately 95% sequence identity. Novel observations in sequence differences between PG I and PG II strains in the ITR, E1, L3, L4, and E3 regions distinguish these PGs. These phylogenetic groups are further distinguished by their *in vitro* growth, cell killing, and spread phenotypes and importantly by their *in vivo* pathogenic phenotypes. These variants are all neutralized with animal antiserum raised against the HAdV-E4 prototype strain, and thus have never been distinguishable as separate serotypes. The work in this dissertation clearly demonstrates that while they are serologically similar, their biological characteristics are different. Currently, biological characteristics (except for VN and HI) are not sufficient criteria for separating PG I and PG II strains into two separate genotypes as the genetic makeup at loci encoding the major capsid proteins (penton base, hexon, and fiber) has not been considered different enough to justify a distinction. Therefore, the use of the phylogroup designation to distinguish HAdV-E4 strains for epidemiology or pathogenesis studies would be helpful. PG I is defined as strains having a sequence identity of 99-100% to the RI-67 strain, large plaque sizes, faster replication kinetics, and low pathogenicity in the cotton rat model. PG II is defined as having 93-96% sequence identity to RI-67, small plaque sizes, slower replication kinetics, and

high pathogenicity in the cotton rat model. These new designations are more meaningful as they reflect the distinct genomic characteristics in addition to differences in *in vitro* and *in vivo* phenotypes. In the future, when molecular data are available (such as typing by RFLP, PCR, or NGS), reports should include the strain and phylogroup designation. Furthermore, as the diagnostic field has shifted to adopt molecular tools for typing clinical isolates, there are opportunities to develop assays that can distinguish PG I and PG II strains.

Appendices

Appendix A – Abbreviations

%G+C – Percentage of genomic guanine-cytosine content

ADP – Adenovirus death protein

AdV – Adenovirus

AICc – Akaike information criterion

ARD – Acute respiratory disease

CAR – Coxsackie and adenovirus receptor

CBP – p300/CREB-binding protein

CO_2 – Carbon dioxide

CPE – Cytopathic effect

CR – Conserved region.

CRLC – Cotton rat lung cell

DBP – DNA binding protein

dpi – Days post infection

E1 – Early region 1

E2 – Early region 2

E3 – Early region 3

E4 – Early region 4

ER – Endoplasmic reticulum

GI – gastrointestinal

H&E – Hematoxylin and eosin

HA – hemagglutinin

HAdV – Human adenovirus

HAdV-E – *Species Human mastadenovirus E*

HAdV-E4 – Human adenovirus type 4

HI – Hemagglutination inhibition

HI-NBCS – Heat-inactivated newborn calf serum

hpi – Hours post infection

HSCT – Human stem cell transplants

ICTV – International Committee on Taxonomy of Viruses

IFN – Interferon

INDEL – Insertion and deletion

ISG – Interferon-stimulated gene

ITR – Inverted terminal repeat

KO – Knock out

L1 – Late region 1

L2 – Late region 2

L3 – Late region 3

L4 – Late region 4

L5 – Late region 5

LDH – Lactate dehydrogenase

MEM – Minimum Essential Medium

MLP – Major late promoter

MOI – Multiplicity of infection

NBCS – Newborn calf serum

NGS – Next generation sequencing

NHP – Nonhuman primate

ORF – Open reading frame

PBS – Phosphate buffered saline

PBS++ – Phosphate buffered saline with magnesium and calcium

PCR – Polymerase chain reaction

PCRF – Percentage of comigrating restriction fragments

PFU – Plaque forming unit

PG – Phylogroup

PG I – Phylogroup I

PG II – Phylogroup II

PKR – Protein kinase R

PML – Promyelocytic leukemia protein

pol – Adenovirus DNA-dependent DNA polymerase

Pol III – RNA polymerase III

pTP – preterminal protein

RB – Retinoblastoma protein

RFLP – Restriction fragment length polymorphism

ROI – Region of interest

RT – Room temperature

RT-qPCR – Real-time quantitative PCR

SBI – Sigmovir Biosystems Inc.

SEM – Standard error of the mean

SOP – Standard operating procedure

TER – Transepithelial electrical resistance

tMRCA – Time to the most recent common ancestor

TP – Terminal protein

TPL – Tripartite leader

VA RNA – Virus-associated RNA

VA RNAI – Virus-associated RNA I

VA RNAII – Virus-associated RNA II

VN – Virus neutralization

WGS – Whole genome sequences

ybp – Year before the present

References

1. Rowe WP, Huebner RJ, Gilmore LK, Parrott RH, Ward TG. 1953. Isolation of a cytopathogenic agent from human adenoids undergoing spontaneous degeneration in tissue culture. Proc Soc Exp Biol Med 84:570–3.
2. Hilleman MR, Werner JH. 1954. Recovery of new agent from patients with acute respiratory illness. Proc Soc Exp Biol Med 85:183–8.
3. Echavarría M. 2008. Adenoviruses in immunocompromised hosts. Clin Microbiol Rev 21:704–15.
4. Berget SM, Moore C, Sharp PA. 1977. Spliced segments at the 5’ terminus of adenovirus 2 late mRNA. Proc Natl Acad Sci U S A 74:3171–5.
5. Chow LT, Gelinas RE, Broker TR, Roberts RJ. 1977. An amazing sequence arrangement at the 5’ ends of adenovirus 2 messenger RNA. Cell 12:1–8.
6. Sullivan NJ, Sanchez A, Rollin PE, Yang ZY, Nabel GJ. 2000. Development of a preventive vaccine for Ebola virus infection in primates. Nature 408:605–9.
7. Stanley DA, Honko AN, Asiedu C, Trefry JC, Lau-Kilby AW, Johnson JC, Hensley L, Ammendola V, Abbate A, Grazioli F, Foulds KE, Cheng C, Wang L, Donaldson MM, Colloca S, Folgori A, Roederer M, Nabel GJ, Mascola J, Nicosia A, Cortese R, Koup RA, Sullivan NJ. 2014. Chimpanzee adenovirus vaccine generates acute and durable protective immunity against ebolavirus challenge. Nat Med 20:1126–9.
8. Kennedy SB, Bolay F, Kieh M, Grandits G, Badio M, Ballou R, Eckes R,

Feinberg M, Follmann D, Grund B, Gupta S, Hensley L, Higgs E, Janosko K, Johnson M, Kateh F, Logue J, Marchand J, Monath T, Nason M, Nyenswah T, Roman F, Stavale E, Wolfson J, Neaton JD, Lane HC, PREVAIL I Study Group. 2017. Phase 2 Placebo-Controlled Trial of Two Vaccines to Prevent Ebola in Liberia. N Engl J Med 377:1438–1447.

9. Niemann J, Kühnel F. 2017. Oncolytic viruses: adenoviruses. Virus Genes 53:700–706.

10. Harrach B, Benko M, Both G, Brown M, Davison A, Echavarria M, Hess M, Jones M, Kajon A, Lehmkuhl H, Mautner V, Mittal S, Wadell G. 2012. Adenoviridae, p. 125–141. *In* King, AM, Adams, MJ, Carstens, EB, Lefkowitz, EJ (eds.), Virus Taxonomy: Ninth Report of the International Committee on Taxonomy of Viruses. Elsevier, San Diego.

11. Davison AJ, Benko M, Harrach B. 2003. Genetic content and evolution of adenoviruses. J Gen Virol 84:2895–908.

12. Robinson CM, Singh G, Lee JY, Dehghan S, Rajaiya J, Liu EB, Yousuf M a, Betensky R a, Jones MS, Dyer DW, Seto D, Chodosh J. 2013. Molecular evolution of human adenoviruses. Sci Rep 3:1812.

13. Lefkowitz EJ, Dempsey DM, Hendrickson RC, Orton RJ, Siddell SG, Smith DB. 2018. Virus taxonomy: the database of the International Committee on Taxonomy of Viruses (ICTV). Nucleic Acids Res 46:D708–D717.

14. Grayston JT, Johnston PB, Loosli CG, Smith ME. 1960. An improved technique for the neutralization test with adenoviruses in HeLa cell cultures. J Infect Dis 99:188–98.

15. Ginsberg HS. 1956. Characteristics of the new respiratory viruses (adenoviruses). I. Qualitative and quantitative aspects of the neutralization reaction. J Immunol 77:271–8.
16. Grayston JT, Johnston PB, Loosli CG, Smith ME. 1956. An improved technique for the neutralization test with adenoviruses in HeLa cell cultures. J Infect Dis 99:188–98.
17. Rowe WP, Hartley JW, Huebner RJ. 1956. Additional serotypes of the APC virus group. Proc Soc Exp Biol Med 91:260–2.
18. Seto D, Chodosh J, Brister JR, Jones MS, Members of the Adenovirus Research Community. 2011. Using the whole-genome sequence to characterize and name human adenoviruses. J Virol 85:5701–2.
19. Walsh MP, Seto J, Jones MS, Chodosh J, Xu W, Seto D. 2010. Computational analysis identifies human adenovirus type 55 as a re-emergent acute respiratory disease pathogen. J Clin Microbiol 48:991–3.
20. Kaján GL, Lipiec A, Bartha D, Allard A, Arnberg N. 2018. A multigene typing system for human adenoviruses reveals a new genotype in a collection of Swedish clinical isolates. PLoS One 13:e0209038.
21. Zhang Q, Dehghan S, Seto D. 2016. Pitfalls of restriction enzyme analysis in identifying, characterizing, typing, and naming viral pathogens in the era of whole genome data, as illustrated by HAdV type 55. Virol Sin 31:448–453.
22. Seto D, Jones MS, Dyer DW, Chodosh J. 2013. Characterizing, typing, and naming human adenovirus type 55 in the era of whole genome data. J Clin

Virol 58:741–2.

23. Reddy VS, Nemerow GR. 2014. Structures and organization of adenovirus cement proteins provide insights into the role of capsid maturation in virus entry and infection. Proc Natl Acad Sci U S A 111:11715–20.
24. San Martín C. 2012. Latest insights on adenovirus structure and assembly. Viruses 4:847–77.
25. Mangel WF, San Martín C. 2014. Structure, function and dynamics in adenovirus maturation. Viruses 6:4536–70.
26. Kidd AH, Chroboczek J, Cusack S, Ruigrok RW. 1993. Adenovirus type 40 virions contain two distinct fibers. Virology 192:73–84.
27. Jones MS, Harrach B, Ganac RD, Gozum MMA, Dela Cruz WP, Riedel B, Pan C, Delwart EL, Schnurr DP. 2007. New adenovirus species found in a patient presenting with gastroenteritis. J Virol 81:5978–84.
28. Pénzes JJ, Menéndez-Conejero R, Condezo GN, Ball I, Papp T, Doszpoly A, Paradela A, Pérez-Berná AJ, López-Sanz M, Nguyen TH, van Raaij MJ, Marschang RE, Harrach B, Benkő M, San Martín C. 2014. Molecular characterization of a lizard adenovirus reveals the first atadenovirus with two fiber genes and the first adenovirus with either one short or three long fibers per penton. J Virol 88:11304–14.
29. Marek A, Nolte V, Schachner A, Berger E, Schlötterer C, Hess M. 2012. Two fiber genes of nearly equal lengths are a common and distinctive feature of Fowl adenovirus C members. Vet Microbiol 156:411–7.
30. Hess M, Cuzange A, Ruigrok RWH, Chroboczek J, Jacrot B. 1995. The

avian adenovirus penton: two fibres and one base. J Mol Biol 252:379–85.

31. Kovács GM, Harrach B, Zakhartchouk AN, Davison AJ. 2005. Complete genome sequence of simian adenovirus 1: an Old World monkey adenovirus with two fiber genes. J Gen Virol 86:1681–6.

32. Yeh HY, Pieniazek N, Pieniazek D, Gelderblom H, Luftig RB. 1994. Human adenovirus type 41 contains two fibers. Virus Res 33:179–98.

33. Akusjarvi G. 2008. Temporal regulation of adenovirus major late alternative RNA splicing. Front Biosci 13:5006–15.

34. Arnberg N. 2012. Adenovirus receptors: implications for targeting of viral vectors. Trends Pharmacol Sci 33:442–8.

35. Varga MJ, Weibull C, Everitt E. 1991. Infectious entry pathway of adenovirus type 2. J Virol 65:6061–70.

36. Arnberg N. 2009. Adenovirus receptors: implications for tropism, treatment and targeting. Rev Med Virol 19:165–78.

37. Wiethoff CM, Wodrich H, Gerace L, Nemerow GR. 2005. Adenovirus protein VI mediates membrane disruption following capsid disassembly. J Virol 79:1992–2000.

38. Suomalainen M, Nakano MY, Keller S, Boucke K, Stidwill RP, Greber UF. 1999. Microtubule-dependent plus- and minus end-directed motilities are competing processes for nuclear targeting of adenovirus. J Cell Biol 144:657–72.

39. Fay N, Panté N. 2015. Nuclear entry of DNA viruses. Front Microbiol 6:1–19.

40. Frisch SM, Mymryk JS. 2002. Adenovirus-5 E1A: paradox and paradigm. Nat Rev Mol Cell Biol 3:441–52.

41. Jones N, Shenk T. 1979. An adenovirus type 5 early gene function regulates expression of other early viral genes. Proc Natl Acad Sci U S A 76:3665–9.

42. Berk AJ, Lee F, Harrison T, Williams J, Sharp PA. 1979. Pre-early adenovirus 5 gene product regulates synthesis of early viral messenger RNAs. Cell 17:935–44.

43. Moran E, Mathews MB. 1987. Multiple functional domains in the adenovirus E1A gene. Cell 48:177–8.

44. Avvakumov N, Kajon AE, Hoeben RC, Mymryk JS. 2004. Comprehensive sequence analysis of the E1A proteins of human and simian adenoviruses. Virology 329:477–92.

45. Berk AJ. 2005. Recent lessons in gene expression, cell cycle control, and cell biology from adenovirus. Oncogene 24:7673–85.

46. King CR, Zhang A, Tessier TM, Gameiro SF, Mymryk JS. 2018. Hacking the Cell: Network Intrusion and Exploitation by Adenovirus E1A. MBio 9:1–18.

47. White E. 2001. Regulation of the cell cycle and apoptosis by the oncogenes of adenovirus. Oncogene 20:7836–46.

48. Bos JL, Polder LJ, Bernards R, Schrier PI, van den Elsen PJ, van der Eb AJ, van Ormondt H. 1981. The 2.2 kb E1b mRNA of human Ad12 and Ad5 codes for two tumor antigens starting at different AUG triplets. Cell 27:121–

31.

49. Report of the international committee on taxonomy of viruses.pdf.

50. Cuconati A, White E. 2002. Viral homologs of BCL-2: role of apoptosis in the regulation of virus infection. Genes Dev 16:2465–78.

51. Han J, Sabbatini P, Perez D, Rao L, Modha D, White E. 1996. The E1B 19K protein blocks apoptosis by interacting with and inhibiting the p53-inducible and death-promoting Bax protein. Genes Dev 10:461–77.

52. Degenhardt K, Perez D, White E. 2000. Pathways used by adenovirus E1B 19K to inhibit apoptosis. Symp Soc Exp Biol 52:241–51.

53. Cheng CY, Gilson T, Dallaire F, Ketner G, Branton PE, Blanchette P. 2011. The E4orf6/E1B55K E3 ubiquitin ligase complexes of human adenoviruses exhibit heterogeneity in composition and substrate specificity. J Virol 85:765–75.

54. Bridge E, Ketner G. 1990. Interaction of adenoviral E4 and E1b products in late gene expression. Virology 174:345–53.

55. Hendrickx R, Stichling N, Koelen J, Kuryk L, Lipiec A, Greber UF. 2014. Innate immunity to adenovirus. Hum Gene Ther 25:265–84.

56. Winberg G, Shenk T. 1984. Dissection of overlapping functions within the adenovirus type 5 E1A gene. EMBO J 3:1907–12.

57. Montell C, Courtois G, Eng C, Berk A. 1984. Complete transformation by adenovirus 2 requires both E1A proteins. Cell 36:951–61.

58. Ullman AJ, Reich NC, Hearing P. 2007. Adenovirus E4 ORF3 protein inhibits the interferon-mediated antiviral response. J Virol 81:4744–52.

59. Burgert HG, Blusch JH. 2000. Immunomodulatory functions encoded by the E3 transcription unit of adenoviruses. Virus Genes 21:13–25.

60. Kelly TJ, Lewis AM. 1973. Use of nondefective adenovirus-simian virus 40 hybrids for mapping the simian virus 40 genome. J Virol 12:643–52.

61. Burgert HG, Maryanski JL, Kvist S. 1987. “E3/19K” protein of adenovirus type 2 inhibits lysis of cytolytic T lymphocytes by blocking cell-surface expression of histocompatibility class I antigens. Proc Natl Acad Sci U S A 84:1356–60.

62. Ginsberg HS, Lundholm-Beauchamp U, Horswood RL, Pernis B, Wold WS, Chanock RM, Prince GA. 1989. Role of early region 3 (E3) in pathogenesis of adenovirus disease. Proc Natl Acad Sci U S A 86:3823–3827.

63. Shisler J, Yang C, Walter B, Ware CF, Gooding LR. 1997. The adenovirus E3-10.4K/14.5K complex mediates loss of cell surface Fas (CD95) and resistance to Fas-induced apoptosis. J Virol 71:8299–8306.

64. Tollefson AE, Hermiston TW, Lichtenstein DL, Colle CF, Tripp RA, Dimitrov T, Toth K, Wells CE, Doherty PC, Wold WS. 1998. Forced degradation of Fas inhibits apoptosis in adenovirus-infected cells. Nature 392:726–30.

65. Elsing A, Burgert HG. 1998. The adenovirus E3/10.4K-14.5K proteins down-modulate the apoptosis receptor Fas/Apo-1 by inducing its internalization. Proc Natl Acad Sci U S A 95:10072–7.

66. Horton TM, Ranheim TS, Aquino L, Kusher DI, Saha SK, Ware CF, Wold WS, Gooding LR. 1991. Adenovirus E3 14.7K protein functions in the absence of other adenovirus proteins to protect transfected cells from

tumor necrosis factor cytolysis. J Virol 65:2629–39.

67. Krajcsi P, Dimitrov T, Hermiston TW, Tollefson a E, Ranheim TS, Vande Pol SB, Stephenson a H, Wold WS. 1996. The adenovirus E3-14.7K protein and the E3-10.4K/14.5K complex of proteins, which independently inhibit tumor necrosis factor (TNF)-induced apoptosis, also independently inhibit TNF-induced release of arachidonic acid. J Virol 70:4904–13.

68. Davison AJ, Akter P, Cunningham C, Dolan A, Addison C, Dargan DJ, Hassan-Walker AF, Emery VC, Griffiths PD, Wilkinson GWG. 2003. Homology between the human cytomegalovirus RL11 gene family and human adenovirus E3 genes. J Gen Virol 84:657–63.

69. Tollefson AE, Scaria A, Hermiston TW, Ryerse JS, Wold LJ, Wold WS. 1996. The adenovirus death protein (E3-11.6K) is required at very late stages of infection for efficient cell lysis and release of adenovirus from infected cells. J Virol 70:2296–306.

70. Windheim M, Southcombe JH, Kremmer E, Chaplin L, Urlaub D, Falk CS, Claus M, Mihm J, Braithwaite M, Dennehy K, Renz H, Sester M, Watzl C, Burgert H-G. 2013. A unique secreted adenovirus E3 protein binds to the leukocyte common antigen CD45 and modulates leukocyte functions. Proc Natl Acad Sci U S A 110:E4884-93.

71. Martinez-Martin N, Ramani SR, Hackney JA, Tom I, Wranik BJ, Chan M, Wu J, Paluch MT, Takeda K, Hass PE, Clark H, Gonzalez LC. 2016. The extracellular interactome of the human adenovirus family reveals diverse strategies for immunomodulation. Nat Commun 7:11473.

72. Thimmappaya B, Weinberger C, Schneider RJ, Shenk T. 1982. Adenovirus VAI RNA is required for efficient translation of viral mRNAs at late times after infection. Cell 31:543–51.

73. Ma Y, Mathews MB. 1996. Structure, function, and evolution of adenovirus-associated RNA: a phylogenetic approach. J Virol 70:5083–99.

74. Ma Y, Mathews MB. 1993. Comparative analysis of the structure and function of adenovirus virus-associated RNAs. J Virol 67:6605–17.

75. Andersson MG, Haasnoot PCJ, Xu N, Berenjian S, Berkhout B, Akusjärvi G. 2005. Suppression of RNA interference by adenovirus virus-associated RNA. J Virol 79:9556–65.

76. Mul YM, Verrijzer CP, van der Vliet PC. 1990. Transcription factors NFI and NFIII/oct-1 function independently, employing different mechanisms to enhance adenovirus DNA replication. J Virol 64:5510–8.

77. Harris MP, Hay RT. 1988. DNA sequences required for the initiation of adenovirus type 4 DNA replication in vitro. J Mol Biol 201:57–67.

78. Hay RT. 1985. Origin of adenovirus DNA replication. Role of the nuclear factor I binding site in vivo. J Mol Biol 186:129–36.

79. Lechner RL, Kelly TJ. 1977. The structure of replicating adenovirus 2 DNA molecules. Cell 12:1007–20.

80. Cuesta R, Xi Q, Schneider RJ. 2000. Adenovirus-specific translation by displacement of kinase Mnk1 from cap-initiation complex eIF4F. EMBO J 19:3465–74.

81. Cuesta R, Xi Q, Schneider RJ. 2004. Structural basis for competitive

inhibition of eIF4G-Mnk1 interaction by the adenovirus 100-kilodalton protein. J Virol 78:7707–16.

82. Dolph PJ, Racaniello V, Villamarin A, Palladino F, Schneider RJ. 1988. The adenovirus tripartite leader may eliminate the requirement for cap-binding protein complex during translation initiation. J Virol 62:2059–66.

83. Dolph PJ, Huang JT, Schneider RJ. 1990. Translation by the adenovirus tripartite leader: elements which determine independence from cap-binding protein complex. J Virol 64:2669–77.

84. Hong SS, Szolajska E, Schoehn G, Franqueville L, Myhre S, Lindholm L, Ruigrok RWH, Boulanger P, Chroboczek J. 2005. The 100K-chaperone protein from adenovirus serotype 2 (Subgroup C) assists in trimerization and nuclear localization of hexons from subgroups C and B adenoviruses. J Mol Biol 352:125–38.

85. Horwitz MS, Scharff MD, Maizel J V. 1969. Synthesis and assembly of adenovirus 2. I. Polypeptide synthesis, assembly of capsomeres, and morphogenesis of the virion. Virology 39:682–94.

86. Velicer LF, Ginsberg HS. 1970. Synthesis, transport, and morphogenesis of type adenovirus capsid proteins. J Virol 5:338–52.

87. Tollefson a E, Ryerse JS, Scaria A, Hermiston TW, Wold WS. 1996. The E3-11.6-kDa adenovirus death protein (ADP) is required for efficient cell death: characterization of cells infected with adp mutants. Virology 220:152–62.

88. Ying B, Wold WSM. 2003. Adenovirus ADP protein (E3-11.6K), which is

required for efficient cell lysis and virus release, interacts with human MAD2B. Virology 313:224–34.

89. Subramanian T, Vijayalingam S, Chinnadurai G. 2006. Genetic identification of adenovirus type 5 genes that influence viral spread. J Virol 80:2000–12.

90. Radke JR, Yong SL, Cook JL. 2016. Low-Level Expression of the E1B 20-Kilodalton Protein by Adenovirus 14p1 Enhances Viral Immunopathogenesis. J Virol 90:497–505.

91. Chen PH, Ornelles DA, Shenk T. 1993. The adenovirus L3 23-kilodalton proteinase cleaves the amino-terminal head domain from cytokeratin 18 and disrupts the cytokeratin network of HeLa cells. J Virol 67:3507–14.

92. Latorre IJ, Roh MH, Frese KK, Weiss RS, Margolis B, Javier RT. 2005. Viral oncoprotein-induced mislocalization of select PDZ proteins disrupts tight junctions and causes polarity defects in epithelial cells. J Cell Sci 118:4283–93.

93. Walters RW, Freimuth P, Moninger TO, Ganske I, Zabner J, Welsh MJ. 2002. Adenovirus fiber disrupts CAR-mediated intercellular adhesion allowing virus escape. Cell 110:789–99.

94. Lion T. 2014. Adenovirus infections in immunocompetent and immunocompromised patients. Clin Microbiol Rev 27:441–62.

95. Adhikary AK, Banik U. 2014. Human adenovirus type 8: the major agent of epidemic keratoconjunctivitis (EKC). J Clin Virol 61:477–86.

96. Itakura S, Aoki K, Sawada H, Ishiguro N, Shinagawa M. 1991. Changes in

subgenome types of adenovirus type 4 isolated from patients with ocular disease between 1985 and 1989 in Sapporo, Japan. J Clin Microbiol 29:1740–3.

97. Hoyle E, Erez JC, Kirk-Granger HR, Collins E, Tang JW. 2016. An adenovirus 4 outbreak amongst staff in a pediatric ward manifesting as keratoconjunctivitis-a possible failure of contact and aerosol infection control. Am J Infect Control 44:602–4.

98. Tebruegge M, Curtis N. 2010. Adenovirus infection in the immunocompromised host. Adv Exp Med Biol 659:153–74.

99. Kosulin K, Geiger E, Vécsei A, Huber W-D, Rauch M, Brenner E, Wrba F, Hammer K, Innerhofer A, Pötschger U, Lawitschka A, Matthes-Leodolter S, Fritsch G, Lion T. 2016. Persistence and reactivation of human adenoviruses in the gastrointestinal tract. Clin Microbiol Infect 22:381.e1–8.

100. Kosulin K, Berkowitsch B, Matthes S, Pichler H, Lawitschka A, Pötschger U, Fritsch G, Lion T. 2018. Intestinal Adenovirus Shedding Before Allogeneic Stem Cell Transplantation Is a Risk Factor for Invasive Infection Post-transplant. EBioMedicine 28:114–119.

101. Coughlan L, Alba R, Parker AL, Bradshaw AC, McNeish IA, Nicklin SA, Baker AH. 2010. Tropism-modification strategies for targeted gene delivery using adenoviral vectors. Viruses 2:2290–355.

102. Ginsberg HS, Moldawer LL, Sehgal PB, Redington M, Kilian PL, Chanock RM, Prince G a. 1991. A mouse model for investigating the molecular pathogenesis of adenovirus pneumonia. Proc Natl Acad Sci U S A

88:1651–5.

103. Kajon AE, Gigliotti AP, Harrod KS. 2003. Acute inflammatory response and remodeling of airway epithelium after subspecies B1 human adenovirus infection of the mouse lower respiratory tract. J Med Virol 71:233–44.

104. Rodríguez E, Ip WH, Kolbe V, Hartmann K, Pilnitz-Stolze G, Tekin N, Gómez-Medina S, Muñoz-Fontela C, Krasemann S, Dobner T. 2017. Humanized Mice Reproduce Acute and Persistent Human Adenovirus Infection. J Infect Dis 215:70–79.

105. Thomas MA, Spencer JF, La Regina MC, Dhar D, Tollefson AE, Toth K, Wold WSM. 2006. Syrian hamster as a permissive immunocompetent animal model for the study of oncolytic adenovirus vectors. Cancer Res 66:1270–6.

106. Tollefson AE, Ying B, Spencer JF, Sagartz JE, Wold WSM, Toth K. 2017. Pathology in Permissive Syrian Hamsters after Infection with Species C Human Adenovirus (HAdV-C) Is the Result of Virus Replication: HAdV-C6 Replicates More and Causes More Pathology than HAdV-C5. J Virol 91:JVI.00284-17.

107. Toth K, Spencer JF, Ying B, Tollefson AE, Wold WSM. 2017. HAdV-C6 Is a More Relevant Challenge Virus than HAdV-C5 for Testing Antiviral Drugs with the Immunosuppressed Syrian Hamster Model. Viruses 9.

108. Wold WS, Tollefson AE, Ying B, Spencer JF, Toth K. 2019. Drug development against human adenoviruses and its advancement by Syrian hamster models. FEMS Microbiol Rev 1–9.

109. Pacini DL, Dubovi EJ, Clyde W a. 1984. A new animal model for human respiratory tract disease due to adenovirus. J Infect Dis 150:92–7.

110. Prince GA, Porter DD, Jenson AB, Horswood RL, Chanock RM, Ginsberg HS. 1993. Pathogenesis of adenovirus type 5 pneumonia in cotton rats (Sigmodon hispidus). J Virol 67:101–11.

111. Ginsberg HS, Horswood RL, Chanock RM, Prince G a. 1990. Role of early genes in pathogenesis of adenovirus pneumonia. Proc Natl Acad Sci U S A 87:6191–5.

112. Ginsberg HS, Moldawer LL, Prince G a. 1999. Role of the type 5 adenovirus gene encoding the early region 1B 55-kDa protein in pulmonary pathogenesis. Proc Natl Acad Sci U S A 96:10409–11.

113. Roy S, Gao G, Clawson DS, Vandenberghe LH, Farina SF, Wilson JM. 2004. Complete nucleotide sequences and genome organization of four chimpanzee adenoviruses. Virology 324:361–72.

114. Roy S, Vandenberghe LH, Kryazhimskiy S, Grant R, Calcedo R, Yuan X, Keough M, Sandhu A, Wang Q, Medina-Jaszek CA, Plotkin JB, Wilson JM. 2009. Isolation and characterization of adenoviruses persistently shed from the gastrointestinal tract of non-human primates. PLoS Pathog 5:e1000503.

115. Dehghan S, Seto J, Liu EB, Walsh MP, Dyer DW, Chodosh J, Seto D. 2013. Computational analysis of four human adenovirus type 4 genomes reveals molecular evolution through two interspecies recombination events. Virology 443:197–207.

116. Robinson CM, Seto D, Jones MS, Dyer DW, Chodosh J. 2011. Molecular evolution of human species D adenoviruses. Infect Genet Evol 11:1208–17.

117. Dhingra A, Hage E, Ganzenmueller T, Böttcher S, Hofmann J, Hamprecht K, Obermeier P, Rath B, Hausmann F, Dobner T, Heim A. 2019. Molecular Evolution of Human Adenovirus (HAdV) Species C. Sci Rep 9:1–13.

118. Hilleman MR, Wwener JH, Dascomb HE, Butler RL. 1955. Epidemiologic investigations with respiratory disease virus RI-67. Am J Public Health Nations Health 45:203–10.

119. Kandel R, Srinivasan A, D'Agata EMC, Lu X, Erdman D, Jhung M. 2010. Outbreak of adenovirus type 4 infection in a long-term care facility for the elderly. Infect Control Hosp Epidemiol 31:755–7.

120. Narra R, Bono P, Zoccoli A, Orlandi A, Piconi S, Grasselli G, Crotti S, Girello A, Piralla A, Baldanti F, Lunghi G. 2016. Acute respiratory distress syndrome in adenovirus type 4 pneumonia: A case report. J Clin Virol 81:78–81.

121. D'Angelo LJ, Hierholzer JC, Keenlyside RA, Anderson LJ, Martone WJ. 1979. Pharyngoconjunctival fever caused by adenovirus type 4: report of a swimming pool-related outbreak with recovery of virus from pool water. J Infect Dis 140:42–7.

122. Artieda J, Pineiro L, Gonzalez M, Munoz M, Basterrechea M, Iturzaeta A, Cilla G. 2009. A swimming pool-related outbreak of pharyngoconjunctival fever in children due to adenovirus type 4, Gipuzkoa, Spain, 2008. Euro

Surveill 14:15–17.

123. Faden H, Gallagher M. 1980. Disseminated infection due to adenovirus type 4. Clin Pediatr (Phila) 19:427–9.

124. Levandowski RA, Rubenis M. 1981. Nosocomial conjunctivitis caused by adenovirus type 4. J Infect Dis 143:28–31.

125. Muzzi A, Rocchi G, Lumbroso B, Tosato G, Barbieri F. 1975. Acute haemorrhagic conjunctivitis during an epidemic outbreak of adenovirus-type-4 injection. Lancet (London, England) 2:822–3.

126. Aoki K, Kato M, Ohtsuka H, Ishii K, Nakazono N, Sawada H. 1982. Clinical and aetiological study of adenoviral conjunctivitis, with special reference to adenovirus types 4 and 19 infections. Br J Ophthalmol 66:776–80.

127. Ariga T, Shimada Y, Ohgami K, Tagawa Y, Ishiko H, Aoki K, Ohno S. 2004. New genome type of adenovirus serotype 4 caused nosocomial infections associated with epidemic conjunctivitis in Japan. J Clin Microbiol 42:3644–8.

128. Kajon AE, Lamson DM, Bair CR, Lu X, Landry ML, Menegus M, Erdman DD, St George K. 2018. Adenovirus Type 4 Respiratory Infections among Civilian Adults, Northeastern United States, 2011-20151. Emerg Infect Dis 24:201–209.

129. Hilleman MR. 1957. Epidemiology of adenovirus respiratory infections in military recruit populations. Ann N Y Acad Sci 67:262–72.

130. Gray GC, Callahan JD, Hawksworth AW, Fisher C a., Gaydos JC. 1999. Respiratory diseases among U.S. military personnel: countering emerging

threats. Emerg Infect Dis 5:379–85.

131. Couch RB, Chanock RM, Cate TR, Lang DJ, Knight V, Huebner RJ. 1963. Immunization with types 4 and 7 adenovirus by selective infection of the intestinal tract. Am Rev Respir Dis 88:SUPPL 394-403.

132. Pierce WE, Rosenbaum MJ, Edwards EA, Peckinpaugh RO, Jackson GG. 1968. Live and inactivated adenovirus vaccines for the prevention of acute respiratory illness in naval recruits. Am J Epidemiol 87:237–46.

133. Top FH, Buescher EL, Bancroft WH, Russell PK. 1971. Immunization with live types 7 and 4 adenovirus vaccines. II. Antibody response and protective effect against acute respiratory disease due to adenovirus type 7. J Infect Dis 124:155–60.

134. Top FH, Grossman RA, Bartelloni PJ, Segal HE, Dudding BA, Russell PK, Buescher EL. 1971. Immunization with live types 7 and 4 adenovirus vaccines. I. Safety, infectivity, antigenicity, and potency of adenovirus type 7 vaccine in humans. J Infect Dis 124:148–54.

135. Collis PB, Dudding BA, Winter PE, Russell PK, Buescher EL. 1973. Adenovirus vaccines in military recruit populations: a cost-benefit analysis. J Infect Dis 128:745–52.

136. Hoke CH, Snyder CE. 2013. History of the restoration of adenovirus type 4 and type 7 vaccine, live oral (Adenovirus Vaccine) in the context of the Department of Defense acquisition system. Vaccine 31:1623–32.

137. Barraza EM, Ludwig SL, Gaydos JC, Brundage JF. 1999. Reemergence of adenovirus type 4 acute respiratory disease in military trainees: report of

an outbreak during a lapse in vaccination. J Infect Dis 179:1531–3.

138. Hendrix RM, Lindner JL, Benton FR, Monteith SC, Tuchscherer MA, Gray GC, Gaydos JC. 1999. Large, persistent epidemic of adenovirus type 4-associated acute respiratory disease in U.S. army trainees. Emerg Infect Dis 5:798–801.

139. Kajon AE, Moseley JM, Metzgar D, Huong H-S, Wadleigh A, Ryan M a K, Russell KL. 2007. Molecular epidemiology of adenovirus type 4 infections in US military recruits in the postvaccination era (1997-2003). J Infect Dis 196:67–75.

140. Artenstein AW, Opal JM, Opal SM, Tramont EC, Peter G, Russell PK. 2005. History of U.S. military contributions to the study of vaccines against infectious diseases. Mil Med 170:3–11.

141. Russell KL, Hawksworth AW, Ryan M a K, Strickler J, Irvine M, Hansen CJ, Gray GC, Gaydos JC. 2006. Vaccine-preventable adenoviral respiratory illness in US military recruits, 1999-2004. Vaccine 24:2835–42.

142. Hoke CH, Hawksworth A, Snyder CE. 2012. Initial assessment of impact of adenovirus type 4 and type 7 vaccine on febrile respiratory illness and virus transmission in military basic trainees, March 2012. MSMR 19:2–4.

143. O'Donnell FL, Taubman SB. 2015. Follow-up analysis of the incidence of acute respiratory infections among enlisted service members during their first year of military service before and after the 2011 resumption of adenovirus vaccination of basic trainees. MSMR 22:2–7.

144. Alexander J, Ward S, Mendy J, Manayani DJ, Farness P, Avanzini JB,

Guenther B, Garduno F, Jow L, Snarsky V, Ishioka G, Dong X, Vang L, Newman MJ, Mayall T. 2012. Pre-clinical evaluation of a replication-competent recombinant adenovirus serotype 4 vaccine expressing influenza H5 hemagglutinin. PLoS One 7:e31177.

145. Weaver EA. 2014. Vaccines within vaccines: the use of adenovirus types 4 and 7 as influenza vaccine vectors. Hum Vaccin Immunother 10:544–56.
146. Wadell G, Hammarskjöld M -L, Winberg G, Varsanyi TM, Sundell G. 1980. Genetic variability of adenoviruses. Ann N Y Acad Sci 354:16–42.
147. Wadell G. 1984. Molecular epidemiology of human adenoviruses. Curr Top Microbiol Immunol 110:191–220.
148. Wadell G, Varsanyi TM. 1978. Demonstration of three different subtypes of adenovirus type 7 by DNA restriction site mapping. Infect Immun 21:238–46.
149. Li QG, Wadell G. 1988. The degree of genetic variability among adenovirus type 4 strains isolated from man and chimpanzee. Arch Virol 101:65–77.
150. Brůcková M, Wadell G, Sundell G, Syrůcek L, Kunzová L. 1980. An outbreak of respiratory disease due to a type 5 adenovirus identified as genome type 5a. Acta Virol 24:161–5.
151. Cooper RJ, Bailey AS, Killough R, Richmond SJ. 1993. Genome analysis of adenovirus 4 isolated over a six year period. J Med Virol 39:62–6.
152. Hang J, Vento TJ, Norby EA, Jarman RG, Keiser PB, Kuschner RA, Binn LN. 2017. Adenovirus type 4 respiratory infections with a concurrent outbreak of coxsackievirus A21 among United States Army Basic Trainees,

a retrospective viral etiology study using next-generation sequencing. J Med Virol 89:1387–1394.

153. Adrian T. 1992. Genome type analysis of adenovirus type 4. Intervirology 34:180–3.

154. Johansson ME, Andersson MA, Thörner PA. 1994. Adenoviruses isolated in the Stockholm area during 1987-1992: restriction endonuclease analysis and molecular epidemiology. Arch Virol 137:101–15.

155. Houng H-SH, Clavio S, Graham K, Kuschner R, Sun W, Russell KL, Binn LN. 2006. Emergence of a new human adenovirus type 4 (Ad4) genotype: identification of a novel inverted terminal repeated (ITR) sequence from majority of Ad4 isolates from US military recruits. J Clin Virol 35:381–7.

156. Kidd AH, Garwicz D, Oberg M. 1995. Human and simian adenoviruses: phylogenetic inferences from analysis of VA RNA genes. Virology 207:32–45.

157. Purkayastha A, Ditty SE, Su J, McGraw J, Hadfield TL, Tibbetts C, Seto D. 2005. Genomic and bioinformatics analysis of HAdV-4, a human adenovirus causing acute respiratory disease: implications for gene therapy and vaccine vector development. J Virol 79:2559–72.

158. Hilleman MR, Werner JH, Dascomb HE, Butler RL, Stewart MT. 1955. Epidemiology of RI(RI-67) group respiratory virus infections in recruit populations. Am J Hyg 62:29–42.

159. Sanchez JL, Binn LN, Innis BL, Reynolds RD, Lee T, Mitchell-Raymundo F, Craig SC, Marquez JP, Shepherd GA, Polyak CS, Conolly J, Kohlhase

KF. 2001. Epidemic of adenovirus-induced respiratory illness among US military recruits: epidemiologic and immunologic risk factors in healthy, young adults. J Med Virol 65:710–8.

160. Russell KL, Broderick MP, Franklin SE, Blyn LB, Freed NE, Moradi E, Ecker DJ, Kammerer PE, Osuna MA, Kajon AE, Morn CB, Ryan MAK. 2006. Transmission dynamics and prospective environmental sampling of adenovirus in a military recruit setting. J Infect Dis 194:877–85.

161. Dudding BA, Top FH, Winter PE, Buescher EL, Lamson TH, Leibovitz A. 1973. Acute respiratory disease in military trainees: the adenovirus surveillance program, 1966-1971. Am J Epidemiol 97:187–98.

162. Gray GC, Goswami PR, Malasig MD, Hawksworth AW, Trump DH, Ryan MA, Schnurr DP. 2000. Adult adenovirus infections: loss of orphaned vaccines precipitates military respiratory disease epidemics. For the Adenovirus Surveillance Group. Clin Infect Dis 31:663–70.

163. Aoki K, Tagawa Y. 2002. A twenty-one year surveillance of adenoviral conjunctivitis in Sapporo, Japan. Int Ophthalmol Clin 42:49–54.

164. Binder AM, Biggs HM, Haynes AK, Chommanard C, Lu X, Erdman DD, Watson JT, Gerber SI. 2017. Human Adenovirus Surveillance - United States, 2003-2016. MMWR Morb Mortal Wkly Rep 66:1039–1042.

165. GINSBERG HS, DIXON MK. 1961. Nucleuc acid synthesis in types 4 and 5 adenovirus-infected HeLa cells. J Exp Med 113:283–99.

166. Ginsberg HS. 1958. Characteristics on the adenoviruses. III. Reproductive cycle of types 1 to 4. J Exp Med 107:133–52.

167. Piña M, Green M. 1965. Biochemical studies on adenovirus multiplication. IX. Chemical and base composition analysis of 28 human adenoviruses. Proc Natl Acad Sci U S A 54:547–51.

168. Green M, Piña M, Kimes RC. 1967. Biochemical studies on adenovirus multiplication. XII. Plaquing efficiencies of purified human adenoviruses. Virology 31:562–5.

169. Crawford-Miksza LK, Nang RN, Schnurr DP. 1999. Strain variation in adenovirus serotypes 4 and 7a causing acute respiratory disease. J Clin Microbiol 37:1107–12.

170. Zhang Q, Jing S, Cheng Z, Yu Z, Dehghan S, Shamsaddini A, Yan Y, Li M, Seto D. 2017. Comparative genomic analysis of two emergent human adenovirus type 14 respiratory pathogen isolates in China reveals similar yet divergent genomes. Emerg Microbes Infect 6:e92.

171. Hillis WD, Goodman R. 1969. Serologic classification of chimpanzee adenoviruses by hemagglutination and hemagglutination inhibition. J Immunol 103:1089–95.

172. Kumar S, Stecher G, Li M, Knyaz C, Tamura K. 2018. MEGA X: Molecular Evolutionary Genetics Analysis across Computing Platforms. Mol Biol Evol 35:1547–1549.

173. Ronquist F, Teslenko M, van der Mark P, Ayres DL, Darling A, Höhna S, Larget B, Liu L, Suchard MA, Huelsenbeck JP. 2012. MrBayes 3.2: efficient Bayesian phylogenetic inference and model choice across a large model space. Syst Biol 61:539–42.

174. Lole KS, Bollinger RC, Paranjape RS, Gadkari D, Kulkarni SS, Novak NG, Ingersoll R, Sheppard HW, Ray SC. 1999. Full-length human immunodeficiency virus type 1 genomes from subtype C-infected seroconverters in India, with evidence of intersubtype recombination. J Virol 73:152–60.

175. Rambaut A, Lam TT, Max Carvalho L, Pybus OG. 2016. Exploring the temporal structure of heterochronous sequences using TempEst (formerly Path-O-Gen). Virus Evol 2:vew007.

176. Bouckaert R, Heled J, Kühnert D, Vaughan T, Wu C-H, Xie D, Suchard MA, Rambaut A, Drummond AJ. 2014. BEAST 2: a software platform for Bayesian evolutionary analysis. PLoS Comput Biol 10:e1003537.

177. Drummond AJ, Rambaut A, Shapiro B, Pybus OG. 2005. Bayesian coalescent inference of past population dynamics from molecular sequences. Mol Biol Evol 22:1185–92.

178. Drummond AJ, Ho SYW, Phillips MJ, Rambaut A. 2006. Relaxed phylogenetics and dating with confidence. PLoS Biol 4:e88.

179. Shinagawa M, Matsuda A, Ishiyama T, Goto H, Sato G. 1983. A rapid and simple method for preparation of adenovirus DNA from infected cells. Microbiol Immunol 27:817–22.

180. Blanco JCG, Pletneva L, Boukhvalova M, Richardson JY, Harris KA, Prince GA. 2004. The cotton rat: an underutilized animal model for human infectious diseases can now be exploited using specific reagents to cytokines, chemokines, and interferons. J Interferon Cytokine Res 24:21–8.

181. Blanco JCG, Richardson JY, Darnell MER, Rowzee A, Pletneva L, Porter DD, Prince GA. 2002. Cytokine and chemokine gene expression after primary and secondary respiratory syncytial virus infection in cotton rats. J Infect Dis 185:1780–5.

182. Pletneva LM, Haller O, Porter DD, Prince GA, Blanco JCG. 2008. Induction of type I interferons and interferon-inducible Mx genes during respiratory syncytial virus infection and reinfection in cotton rats. J Gen Virol 89:261–70.

183. Blanco JCG, Pletneva LM, McGinnes-Cullen L, Otoa RO, Patel MC, Fernando LR, Boukhvalova MS, Morrison TG. 2018. Efficacy of a respiratory syncytial virus vaccine candidate in a maternal immunization model. Nat Commun 9:1904.

184. Faul F, Erdfelder E, Lang A-G, Buchner A. 2007. G*Power 3: a flexible statistical power analysis program for the social, behavioral, and biomedical sciences. Behav Res Methods 39:175–91.

185. Dehghan S, Seto J, Jones MS, Dyer DW, Chodosh J, Seto D. 2013. Simian adenovirus type 35 has a recombinant genome comprising human and simian adenovirus sequences, which predicts its potential emergence as a human respiratory pathogen. Virology 447:265–73.

186. Jacobs SC, Davison AJ, Carr S, Bennett AM, Phillpotts R, Wilkinson GWG. 2004. Characterization and manipulation of the human adenovirus 4 genome. J Gen Virol 85:3361–6.

187. Blackford AN, Grand RJA. 2009. Adenovirus E1B 55-kilodalton protein:

multiple roles in viral infection and cell transformation. J Virol 83:4000–12.

188. Ablack JNG, Pelka P, Yousef AF, Turnell AS, Grand RJA, Mymryk JS. 2010. Comparison of E1A CR3-dependent transcriptional activation across six different human adenovirus subgroups. J Virol 84:12771–81.

189. King CR, Cohen MJ, Fonseca GJ, Dirk BS, Dikeakos JD, Mymryk JS. 2016. Functional and Structural Mimicry of Cellular Protein Kinase A Anchoring Proteins by a Viral Oncoprotein. PLoS Pathog 12:e1005621.

190. Bhat RA, Thimmappaya B. 1984. Adenovirus mutants with DNA sequence perturbations in the intragenic promoter of VAI RNA gene allow the enhanced transcription of VAII RNA gene in HeLa cells. Nucleic Acids Res 12:7377–88.

191. Rohan RM, Ketner G. 1987. A comprehensive collection of point mutations in the internal promoter of the adenoviral VAI gene. J Biol Chem 262:8500–7.

192. Crawford-Miksza LK, Schnurr DP. 1996. Adenovirus serotype evolution is driven by illegitimate recombination in the hypervariable regions of the hexon protein. Virology 224:357–67.

193. Thandapani P, O'Connor TR, Bailey TL, Richard S. 2013. Defining the RGG/RG Motif. Mol Cell 50:613–623.

194. Blanc RS, Richard S. 2017. Arginine Methylation: The Coming of Age. Mol Cell 65:8–24.

195. Iacovides DC, O'Shea CC, Oses-Prieto J, Burlingame A, McCormick F. 2007. Critical role for arginine methylation in adenovirus-infected cells. J

Virol 81:13209–17.

196. Koyuncu OO, Dobner T. 2009. Arginine methylation of human adenovirus type 5 L4 100-kilodalton protein is required for efficient virus production. J Virol 83:4778–90.

197. Li Y, Wold WS. 2000. Identification and characterization of a 30K protein (Ad4E3-30K) encoded by the E3 region of human adenovirus type 4. Virology 273:127–38.

198. Burgert HG, Ruzsics Z, Obermeier S, Hilgendorf A, Windheim M, Elsing A. 2002. Subversion of host defense mechanisms by adenoviruses. Curr Top Microbiol Immunol 269:273–318.

199. Zhang J, Kang J, Dehghan S, Sridhar S, Lau SKP, Ou J, Woo PCY, Zhang Q, Seto D. 2019. A Survey of Recent Adenoviral Respiratory Pathogens in Hong Kong Reveals Emergent and Recombinant Human Adenovirus Type 4 (HAdV-E4) Circulating in Civilian Populations. Viruses 11:129.

200. Arkin A, Ross J, McAdams HH. 1998. Stochastic kinetic analysis of developmental pathway bifurcation in phage lambda-infected Escherichia coli cells. Genetics 149:1633–48.

201. Weinberger LS, Burnett JC, Toettcher JE, Arkin AP, Schaffer D V. 2005. Stochastic gene expression in a lentiviral positive-feedback loop: HIV-1 Tat fluctuations drive phenotypic diversity. Cell 122:169–82.

202. Doronin K, Toth K, Kuppuswamy M, Ward P, Tollefson AE, Wold WS. 2000. Tumor-specific, replication-competent adenovirus vectors overexpressing the adenovirus death protein. J Virol 74:6147–55.

203. Doronin K, Toth K, Kuppuswamy M, Krajcsi P, Tollefson AE, Wold WSM. 2003. Overexpression of the ADP (E3-11.6K) protein increases cell lysis and spread of adenovirus. Virology 305:378–87.

204. Decker T, Lohmann-Matthes ML. 1988. A quick and simple method for the quantitation of lactate dehydrogenase release in measurements of cellular cytotoxicity and tumor necrosis factor (TNF) activity. J Immunol Methods 115:61–9.

205. Crouch SP, Kozlowski R, Slater KJ, Fletcher J. 1993. The use of ATP bioluminescence as a measure of cell proliferation and cytotoxicity. J Immunol Methods 160:81–8.

206. Ramirez RD, Sheridan S, Girard L, Sato M, Kim Y, Pollack J, Peyton M, Zou Y, Kurie JM, Dimaio JM, Milchgrub S, Smith AL, Souza RF, Gilbey L, Zhang X, Gandia K, Vaughan MB, Wright WE, Gazdar AF, Shay JW, Minna JD. 2004. Immortalization of human bronchial epithelial cells in the absence of viral oncoproteins. Cancer Res 64:9027–34.

207. Patterson LJ, Prince G a, Richardson E, Alvord WG, Kalyan N, Robert-Guroff M. 2002. Insertion of HIV-1 genes into Ad4DeltaE3 vector abrogates increased pathogenesis in cotton rats due to E3 deletion. Virology 292:107–13.

208. Kaneko H, Mori S, Suzuki O, Iida T, Shigeta S, Abe M, Ohno S, Aoki K, Suzutani T. 2004. The cotton rat model for adenovirus ocular infection: antiviral activity of cidofovir. Antiviral Res 61:63–6.

209. Kobayashi Y. 2008. The role of chemokines in neutrophil biology. Front

Biosci 13:2400–7.

210. Zsengellér Z, Otake K, Hossain SA, Berclaz PY, Trapnell BC. 2000. Internalization of adenovirus by alveolar macrophages initiates early proinflammatory signaling during acute respiratory tract infection. J Virol 74:9655–67.

211. Wunderlich K, van der Helm E, Spek D, Vermeulen M, Gecgel A, Pau MG, Vellinga J, Custers J. 2014. An alternative to the adenovirus inverted terminal repeat sequence increases the viral genome replication rate and provides a selective advantage in vitro. J Gen Virol 95:1574–84.

212. King AJ, van der Vliet PC. 1994. A precursor terminal protein-trinucleotide intermediate during initiation of adenovirus DNA replication: regeneration of molecular ends in vitro by a jumping back mechanism. EMBO J 13:5786–5792.

213. de Jong RN, van der Vliet PC, Brenkman AB. 2003. Adenovirus DNA replication: protein priming, jumping back and the role of the DNA binding protein DBP. Curr Top Microbiol Immunol 272:187–211.

214. Shenk T, Jones N, Colby W, Fowlkes D. 1980. Functional analysis of adenovirus-5 host-range deletion mutants defective for transformation of rat embryo cells. Cold Spring Harb Symp Quant Biol 44 Pt 1,:367–75.

215. Cohen MJ, Yousef AF, Massimi P, Fonseca GJ, Todorovic B, Pelka P, Turnell AS, Banks L, Mymryk JS. 2013. Dissection of the C-terminal region of E1A redefines the roles of CtBP and other cellular targets in oncogenic transformation. J Virol 87:10348–55.

216. Ablack JNG, Cohen M, Thillainadesan G, Fonseca GJ, Pelka P, Torchia J, Mymryk JS. 2012. Cellular GCN5 is a novel regulator of human adenovirus E1A-conserved region 3 transactivation. J Virol 86:8198–209.

217. White E, Sabbatini P, Debbas M, Wold WS, Kusher DI, Gooding LR. 1992. The 19-kilodalton adenovirus E1B transforming protein inhibits programmed cell death and prevents cytolysis by tumor necrosis factor alpha. Mol Cell Biol 12:2570–80.

218. Chiou SK, Tseng CC, Rao L, White E. 1994. Functional complementation of the adenovirus E1B 19-kilodalton protein with Bcl-2 in the inhibition of apoptosis in infected cells. J Virol 68:6553–66.

219. Mautner V, Bailey A, Steinthorsdottir V, Ullah R, Rinaldi A. 1999. Properties of the adenovirus type 40 E1B promoter that contribute to its low transcriptional activity. Virology 265:10–9.

220. Forrester NA, Sedgwick GG, Thomas A, Blackford AN, Speiseder T, Dobner T, Byrd PJ, Stewart GS, Turnell AS, Grand RJA. 2011. Serotype-specific inactivation of the cellular DNA damage response during adenovirus infection. J Virol 85:2201–11.

221. Chalabi Hagkarim N, Ryan EL, Byrd PJ, Hollingworth R, Shimwell NJ, Agathanggelou A, Vavasseur M, Kolbe V, Speiseder T, Dobner T, Stewart GS, Grand RJ. 2018. Degradation of a Novel DNA Damage Response Protein, Tankyrase 1 Binding Protein 1, following Adenovirus Infection. J Virol 92:1–24.

222. Cheng CY, Gilson T, Wimmer P, Schreiner S, Ketner G, Dobner T, Branton

PE, Blanchette P. 2013. Role of E1B55K in E4orf6/E1B55K E3 ligase complexes formed by different human adenovirus serotypes. J Virol 87:6232–45.

223. Toth K, Doronin K, Kuppuswamy M, Ward P, Tollefson AE, Wold WSM. 2005. Adenovirus immunoregulatory E3 proteins prolong transplants of human cells in immunocompetent mice. Virus Res 108:149–59.

224. Kalvakolanu D V., Bandyopadhyay SK, Harter ML, Sen GC. 1991. Inhibition of interferon-inducible gene expression by adenovirus E1A proteins: block in transcriptional complex formation. Proc Natl Acad Sci U S A 88:7459–63.

225. Chahal JS, Qi J, Flint SJ. 2012. The human adenovirus type 5 E1B 55 kDa protein obstructs inhibition of viral replication by type I interferon in normal human cells. PLoS Pathog 8:e1002853.

226. Chahal JS, Flint SJ. 2012. Timely Synthesis of the Adenovirus Type 5 E1B 55-Kilodalton Protein Is Required for Efficient Genome Replication in Normal Human Cells. J Virol 86:3064–3072.

227. Ullman AJ, Hearing P. 2008. Cellular proteins PML and Daxx mediate an innate antiviral defense antagonized by the adenovirus E4 ORF3 protein. J Virol 82:7325–35.

228. Zheng Y, Stamminger T, Hearing P. 2016. E2F/Rb Family Proteins Mediate Interferon Induced Repression of Adenovirus Immediate Early Transcription to Promote Persistent Viral Infection. PLoS Pathog 12:e1005415.

229. Vachon VK, Conn GL. 2016. Adenovirus VA RNA: An essential pro-viral non-coding RNA. Virus Res 212:39–52.

230. Gahéry-Ségard H, Farace F, Godfrin D, Gaston J, Lengagne R, Tursz T, Boulanger P, Guillet JG. 1998. Immune response to recombinant capsid proteins of adenovirus in humans: antifiber and anti-penton base antibodies have a synergistic effect on neutralizing activity. J Virol 72:2388–97.

231. Roy S, Clawson DS, Calcedo R, Lebherz C, Sanmiguel J, Wu D, Wilson JM. 2005. Use of chimeric adenoviral vectors to assess capsid neutralization determinants. Virology 333:207–14.

232. Sumida SM, Truitt DM, Lemckert AAC, Vogels R, Custers JHH V, Addo MM, Lockman S, Peter T, Peyerl FW, Kishko MG, Jackson SS, Gorgone DA, Lifton MA, Essex M, Walker BD, Goudsmit J, Havenga MJE, Barouch DH. 2005. Neutralizing antibodies to adenovirus serotype 5 vaccine vectors are directed primarily against the adenovirus hexon protein. J Immunol 174:7179–85.

233. Yu B, Dong J, Wang C, Zhan Y, Zhang H, Wu J, Kong W, Yu X. 2013. Characteristics of neutralizing antibodies to adenovirus capsid proteins in human and animal sera. Virology 437:118–23.

234. Tian X, Qiu H, Zhou Z, Wang S, Fan Y, Li X, Chu R, Li H, Zhou R, Wang H. 2018. Identification of a Critical and Conformational Neutralizing Epitope in Human Adenovirus Type 4 Hexon. J Virol 92:1–14.

235. Xi Q, Cuesta R, Schneider RJ. 2004. Tethering of eIF4G to adenoviral

mRNAs by viral 100k protein drives ribosome shunting. Genes Dev 18:1997–2009.

236. Hayes BW, Telling GC, Myat MM, Williams JF, Flint SJ. 1990. The adenovirus L4 100-kilodalton protein is necessary for efficient translation of viral late mRNA species. J Virol 64:2732–42.

237. Andrade F, Bull HG, Thornberry NA, Ketner GW, Casciola-Rosen LA, Rosen A. 2001. Adenovirus L4-100K assembly protein is a granzyme B substrate that potently inhibits granzyme B-mediated cell death. Immunity 14:751–61.

238. Kzhyshkowska J, Kremmer E, Hofmann M, Wolf H, Dobner T. 2004. Protein arginine methylation during lytic adenovirus infection. Biochem J 383:259–65.

239. Sester M, Burgert HG. 1994. Conserved cysteine residues within the E3/19K protein of adenovirus type 2 are essential for binding to major histocompatibility complex antigens. J Virol 68:5423–32.

240. Hatfield L, Hearing P. 1993. The NFIII/OCT-1 binding site stimulates adenovirus DNA replication in vivo and is functionally redundant with adjacent sequences. J Virol 67:3931–9.

241. Radke JR, Grigera F, Ucker DS, Cook JL. 2014. Adenovirus E1B 19-kilodalton protein modulates innate immunity through apoptotic mimicry. J Virol 88:2658–69.

242. Leonard GT, Sen GC. 1996. Effects of adenovirus E1A protein on interferon-signaling. Virology 224:25–33.

243. Mathews MB, Shenk T. 1991. Adenovirus virus-associated RNA and translation control. J Virol 65:5657–62.